ROCKET AND BALLOON STUDIES OF MIDDLE ATMOSPHERIC ELECTRODYNAMICS IN THE LOW LATITUDES

by

AMARENDRA NARAYAN

A THESIS

SUBMITTED FOR THE DEGREE OF

DOCTOR OF PHILOSOPHY

of the

GUJARAT UNIVERSITY

January 1988

PHYSICAL RESEARCH LABORATORY

AHMEDABAD 380 009

INDIA

Dedicated to

My Parents...

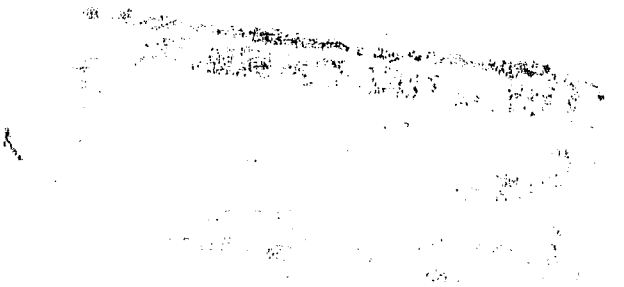

C E R T I F I C A T E

I hereby declare that the work presented in this thesis is original and has not formed the basis for the award of any degree or diploma by any University or Institution.

Amarendra Narayan

Amarendra Narayan

(Author)

Ceritfied by

B. H. Subbaraya

B.H.Subbaraya

(Professor in-charge)

S. P. Gupta

S.P.Gupta

(Associate Guide)

Date- 15 JAN 1988

ACKNOWLEDGEMENTS

I express with deep gratitude my indetedness to Dr. S.P. Gupta, who has guided me during all the stages of my work. Throughout my Ph.D. career he has been a great source of inspiration and encouragement for me.Working with him has been a great experience.

I am grateful to Prof. B. H. Subbaraya for the encouragement which he has provided throughout my Ph.D.work. He has painstakingly gone through this thesis and offered many useful suggestions. I shall ever be grateful for the guidance I have received from him.

I am thankful to Prof.S.P.Pandya,Senior Professor,PRL and Prof. R.K.Varma,Director,PRL for taking a keen interest in my work throughout the period of my Ph.D.work.

I am thankful to Prof.Satya Prakash,Prof.P.R.Pisharoty, Dr. D.K.Chakrabarty,Dr.G.Subamanyam and Prof.R.Raghavrao for the fruitful discussions I have had with them at a number of occasions which gradually helped me in understanding this subject better.

I want to thank my senior colleagues Dr.A.Jayraman,Dr. Shyam Lal, Dr.R.Pandey,Dr.H.Chand,Dr.H.S.S.Sinha and Dr.R. Sreedharan for the help they have given me at a number of

occasions in a number of ways.

Mr. S. G. Tikekar,Mr.D.Damle and Mr.N.R.Shah have worked with me throughout the stages of development,fabrication and testing of the different payloads.I am thankful for the help I have received from them in this project.

I am thankful to the staff of the PRL workshop,Mr.A.J. Shroff, Mr. C.K.Panchal,Mr.B.B.Panchal,Mr.S.C.Parmar,Mr.S.M. Shukla and others who have helped in the construction of the instruments.

Part of the data analysis has been done by Mr.K.S.Patel for which I acknowledge my thanks.I am also thankful to Mr. M. Nair for the typing assistance which he has provided at various occasions during my work.

I am thankful to Mr.R.N.Misra and Mr.Y.B.Acharya for the knowledge and experience in instumentation which they have shared and the help which they provided in this project.

I thank Mr. Ranpura of the photography section, Mrs.Kokilaben Bhatt of the PRL library and Mr.H.S.Panchal of the drafting section for their help in preparing the diagrams. I acknowledge my thanks to the staff of the computer centre and the staff of the PRL library for the help which they have provided during my Ph.D.work.

The funds for the present experiments were provided by the Indian Space Research Organisation under the Indian Middle Atmospheric Program(1982-1987). I acknowledge my thanks to the authorities for providing the funds for the experiments. I also thank Prof.R.R.Daniel,Senior Professor,

TIFR and Chairman, ADCOS (Advisory committee of Space Research in India), Prof. P.D.Bhavsar,Chairman,Program and Management Board of the Indian Middle Atmosphere Program, and Prof. A. P.Mitra,Director General,Council of Scientific and Industrial Research, New Delhi for taking a keen interest in the project.

I am thankful to Shree R. T. Redkar, Mr. Joshi, Mr, Sreenivasan, Mr. Chitre and all the staff of the Balloon Launching Facility, Hyderabad for the excellent facilities which they have provided for our balloon experiments.At the same time I acknowledge my thanks to Shree R.U.Kundapurkar and all the members of the Control Instrumentation group of the Tata Institute of Fundamental Research for the help which they provided during payload integration and flight.

I thank Mr.P.Rajratnam of MAP office,Bangalore and Dr.S. C. Chakravarty of ISRO Headquarters,Bangalore for their keen interest and for the help they have provided during the balloon launchings.

Thanks are due to the IMD (Indian Meteorology Department) for their help in providing wind data and balloon tracking facilities.

I am thankful to Dr.S.Sampath of CESS,Trivandrum,Dr.M.N. M. Rao and Dr. S. C. Garg of NPL, New Delhi for their suggestions regarding the gondola charging problem.I thank Prof. S.V.Damle of TIFR for his important suggestions during balloon launch.

I am thankful to my friends and colleagues who have always provided a friendly encouragement to me and have

helped me in numerous ways.My special thanks are for Dr.D. Sengupta,Dr.B.R.Sitaram,Dr.K.P.Subramanyam,Dr.B.S.Kotlia,Mr. B. Pandey,Mr.G.Beig,Mr.S.Deshpande,Mr.Venkatramani and Mr.M. Ahmed. They have helped me through various phases of my work and illuminated me through numerous scientific discussions. I also thank all the people who have directly or indirectly helped me in completing this work.

The members of my family have been a constant source of moral support, emcouragement and inspiration.A special debt of gratitude is due to them.I am grateful to my wife who has ungrudgingly supported and encouraged me throughout my work with a lot of understanding and patience.

Amarendra Narayan

Amarenda Narayan

STATEMENT

The work presented in this thesis was carried out by the author at the Physical Research Laboratory, Ahmedabad under the guidance of Dr.S.P.Gupta and Prof.B.H.Subbaraya.

The studies presented in this thesis deal with various aspects of the electrodynamics of the middle atmosphere at low latitudes.

The author has been involved in the design and construction of instruments for measuring conductivity and electric field at stratospheric altitudes. These instruments were flown from the low latitude station Hyderabad (India) on balloon-borne platforms at a number of occasions in order to make in-situ measurements of atmospheric conductivity and vertical electric field in the stratosphere. The results of these measurements are presented and discussed in this thesis.

The first chapter forms the introduction to this thesis. Various concepts which are important for the study of middle atmospheric electrodynamics have been reviewed briefly in this chapter.

The second chapter deals with the physics of conductivity and electric field measurement. In this chapter, an attempt has been made by the author to discuss different

theoretical aspects of the measurement process.A simple model for the probe behaviour has been presented in this chapter and various possibilities encountered during realistic measurement situations are discussed in detail. The relaxation technique for conductivity measurement and the double probe technique for electric field measurement are described in this chapter(These techniques have been used by the author for conducting balloon-borne measurements). This chapter also contains a discussion on the author's investigations on the nature and extent of charging of the balloon-borne gondola during its ascent and float periods.

A discussion of the use of rocket-borne Langmuir probes for measuring ion and electron conductivity in the mesosphere is given in the second chapter. Using the electron and ion currents obtained from Langmuir probe measurements, the conductivities at these altitudes were derived. Ion conductivity for the mesosphere has been obtained using rocket-borne Langmuir probe data.This has been presented in chapter four.

Chapter three describes in detail the instruments constructed by the author for conducting in-situ measurements. This chapter also describes various support instruments that go with the payload during balloon flight. A discussion of the instrument testing procedure and the balloon launch procedure has been included in this chapter.

The results of measurement of polar conductivity and electric field in the stratosphere and mesosphere

constitute the contents of the fourth chapter of this thesis.

The fifth chapter of this thesis contains discussions of the results and the new findings obtained during the present work.

A comparison of the conductivity measurements done by the author has been made with measurements done elsewhere by other groups.The positive ion conductivity was observed to be higher than the negative ion conductivity by a factor of four and half.This aspect has been discussed in chapter five where a comparison has been made between theoretically expected ratio between the two polar conductivities with the observed ratio.

A comparison of stratospheric and mesospheric conductivities has also been done in this chapter. A discussion of the rocket body potential in the mesosphere as observed during several rocket flights is given. A suggestion has been made that the existence of such potentials might be indicating a presence of large vertical electric field in the mesosphere.

The effects of volcanic eruptions on conductivity has also been discussed in chapter five. The positive ion conductivity has been found to be affected much more drastically than the negative ion conductivity by volcanic activity.The implications of this observation are discussed.

The sixth chapter contains a summay of the important results. This chapter also contains suggestions for further work.

TABLE OF CONTENTS

CHAPTER III : INSTRUMENTATION AND DATA ANALYSIS

CHAPTER I

INTRODUCTION

1.1 The Atmosphere

The earth is surrounded by a gaseous envelope known as the atmosphere. This atmosphere is held to the earth by the force of gravity and balanced by hydrostatic pressure. There are numerous phenomena taking place in the atmosphere which make its study interesting and important. We study the atmosphere in the branch of science known as aeronomy. ("Aero" means pertaining to air, and "nomy" means the study of.) Although the study of the atmosphere has been going on since a long time, this field is still very much active today and a number of interesting features related to the atmosphere are being investigated.

The major constituents in the atmosphere are the following: Nitrogen constitutes about 78.09 percent of air,

Oxygen constitutes 20.95 percent, Argon constitutes 0.93 percent and Carbon dioxide constitutes 0.033 percent of dry air by volume. The proportion of water in air varies widely from place to place as well as at different altitudes and with time. In addition to these there are a number of species(trace constituents) which occur in minute quantities-parts per million or less, but which play an important role in the chemistry and physics of the atmosphere.

Air also contains ions and aerosols. Different types of ions are predominant at different altitudes. Large cluster-ions are predominant from ground level upto about 40-45 km altitude. At higher altitudes monoatomic and diatomic ions are predominant[Mitra, 1981]. Aerosols of different sizes varying from 0.001 micron to 1 micron are present in the atmosphere mainly at altitudes ranging from ground upto 40 km altitude. These particles are mostly dust, water vapour and sulfuric acid globules [Turco et al., 1982].

1.2 Regions of the Atmosphere

The atmosphere has been classified into different regions for the purpose of reference. The temperature profile of the atmosphere provides an important basis for classification of the different regions in the atmosphere. Fig 1.1 shows this classification. The temperature of air near the earth's surface is around 300°K. There is a large variation in this temperature from place to place and

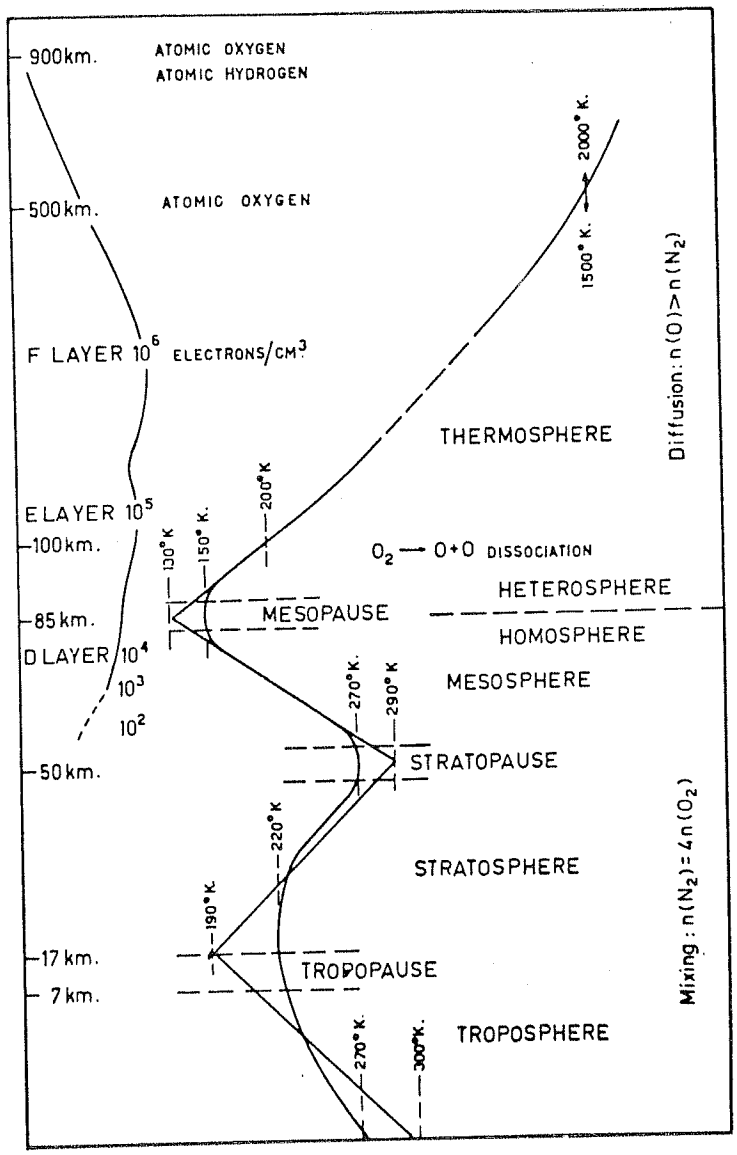

Fig 1.1 ATMOSPHERIC NOMENCLATURE

between different seasons. But as one goes higher up, the temperature decreases at the rate of roughly 5 to 7 degrees celsius per kilometer of altitude[Iribarne and Cho, 1980, p3]. This continues upto an altitude of 12 to 18 km. This region is known as the troposphere and its upper limit is known as the tropopause. Most of the weather related phenomena, e.g. cloud formation, thunderstorm and lightning activity, etc. take place in the troposphere. Above tropopause, the temperature increases with altitude and reaches nearly $-10^{o}c$ at an altitude of 45 km. This region is known as the stratosphere and its upper limit is known as the stratopause. The main reason why temperature increases in the stratosphere is the presence of the gas ozone in air which absorbs incoming solar ultravoilet radiation and consequently heats the air [Rishbeth and Garriott, 1969, p2, Mitra, 1952, p143]. Above stratopause the temperature again decreases rapidly with altitude. It reaches almost $-90^{o}c$ at around 85 to 90 km. This region is known as the mesosphere and its upper limit is called the mesopause. Above the mesopause the temperature increases to a value of $1000^{o}c$ to $1500^{o}c$ in the region known as the thermosphere. Above an altitude of around 500 km the atmosphere becomes so much rarefied that collisions between the air molecules are very infrequent. The molecules of air in such a situation follow almost ballistic trajectories[Mitra, 1952, p17, Rishbeth and Garriott, p3]. The exosphere is defined as that region where the mean free path of the air molecules is greater than one scale height. This region extends from around 500 km

altitude right upto the upper limit of the earth's atmosphere.

The stratosphere and the mesosphere are together known as the middle atmosphere,and they cover an altitude region of 20 to 100 km.

Although ions exist in the atmosphere at all levels, ionisation effects are particularly strong in the altitude range between 60 km and 500 km.This region is known as the Ionosphere. The main sources of ionisation in this region are the solar ultravoilet radiation and the x-rays.These are absorbed by the air molecules which get ionised and form positive ions and electrons.At lower altitudes many of these electrons get attached to neutral molecules and form negative ions.

Fig 1.1 shows the electron density as a function of height. This electron density profile has a number of maxima or peaks. The regions where these peaks occur have been given different names.The lowermost peak occurs between 60 and 90 km. This peak is formed only during daytime.The region where it is formed is called the D region.The next peak occurs at somewhere around 105 km.The region between 90 km and 140 km altitude(in which this peak occurs) is known as the E region.The portion of the ionosphere above the E region is known as the F region.Often during daytime, two peaks appear in the F region.These peaks are called the F1 and the F2 peaks.At night these peaks merge and there is only one F layer peak.

1.3 Middle Atmospheric Electrodynamics

The field of atmospheric electrodynamics covers a broad range of phenomena. These include a study of the global electric circuit, thunderstorm electrification and lightning, sferics, ionisation in the lower, middle and upper atmosphere, ionospheric dynamo and solar wind interaction with geomagnetic fields[Volland, 1984]. Goldberg[1984] and Maynard et al.[1984] have discussed the current status of Middle Atmospheric Electrodynamics(MAE). MAE incorporates various phenomena like global electric circuit, sun-weather relation, vertical and horizontal electric fields and currents, ionospheric potentials and the recently observed mesospheric electric fields, etc. The present study is restricted to a few of the above mentioned topics in the electrodynamics of the middle atmosphere. The author has conducted balloon-borne measurement of electrical conductivity and vertical electric field in the stratosphere[Gupta and Narayan, 1987]. The author has also studied some of the features of mesospheric electrodynamics using data from several rocket-borne experiments conducted earlier from Thumba, India[Subbaraya et al., 1985].

1.3.1 Ionisation in the Middle Atmosphere

The basic sources of ion production in the atmosphere are high energy cosmic ray particles and solar ultravoilet photons[Rishbeth and Garriott, 1969]. Different ionising

sources play the dominant roles in this process at different altitudes. Near the earth's surface within a few hundred meters height, radioactive materials present in the earth's crust as well as the radioactive radon gas produced by them are the main agents for the ionisation of air. As one goes higher up, the ionisation rate decreases a little, and then increases upto 10-12 km altitude[Cole and Pierce, 1965, Goldberg, 1984]. The cosmic rays play a dominant role in ion production in this region. In fact, they are the principal source of ionisation in the upper troposphere, the stratosphere and the lower mesosphere[Goldberg, 1984]. Ion production by meteoric source has also been proposed by Aikin[1981]. Fig 1.2 shows the relative contribution to ion production by various sources. The two curves marked q(NaOH) and q(CaOH) show the contributions of meteoric sources as proposed by Aikin. In the mesosphere, as one can see in Fig 1.2, the solar emission at Hydrogen Lyman α (wavelength 121.6 nm) which ionises the Nitric Oxide takes over as the principal ionising source. Further up, in the E region and above(not shown), the solar ultravoilet radiation and the hard X-rays constitute the main source of ionisation[Rishbeth and Garriott, 1969].

In the middle atmosphere, the most important contribution to the ionisation is due to the cosmic rays. Cosmic rays are very high energy( )BeV) particles of extraterrestrial origin. These particles consist mainly of Protons, but a small number of heavier nuclei are also present[Pomerantz, 1971]. These particles on entering the

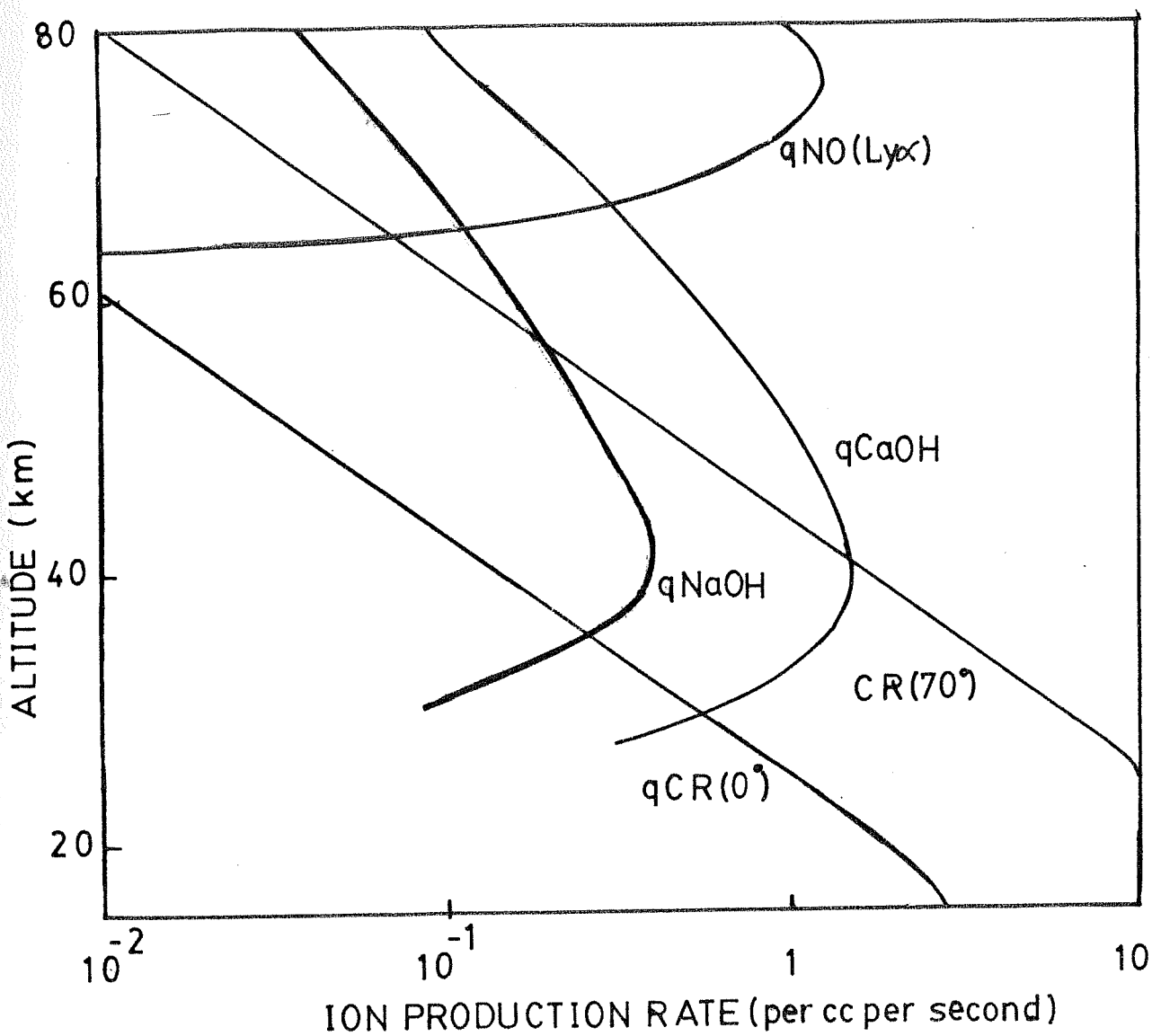

FIG 1.2: Sources of ionisation at different altitudes

atmosphere collide with the molecules present in the atmosphere and generate a large number of secondary particles. These secondary particles are mainly electrons, protons, mesons and gamma photons[Daniel and Stephens, 1974]. The number of secondary particles produced is a function of the energy of the primary cosmic ray particle. An average energy of 35 eV is required for the production of one ion pair[Velinov, 1968]. Thus each CR(Cosmic ray) particle which has energy of the order of BeV can produce millions of secondary particles depending on its energy. These secondary particles react with the constituent molecules of air and form the ions present in the atmosphere. Thus the total ion production rate depends on the cosmic ray flux and energy spectrum.

Since cosmic rays consist of atomic nuclei, they are deflected by magnetic fields. This results in two important effects. The incoming CR flux is observed to have a dependence on the solar activity cycle. The primary CR flux is higher during the solar minima as compared to the solar maxima. This variation is roughly by a factor of 2 at 36 km altitude[Heaps, 1978]. The latitude effect occurs because of the variation of the direction of the geomagnetic field lines with latitude[Pomerantz, 1971]. The earth's magnetic field is nearly vertical at polar latitudes. Towards the equator, the horizontal component of the earth's magnetic field is higher. The motion of a CR particle incident on earth is guided by magnetic field lines, and it requires a much higher initial energy for the CR particle to reach the

earth's atmosphere at the equator than at the poles. Thus the resulting flux of cosmic rays at low latitudes is lower than that at high latitudes. Heaps [1978] has given a semiemperical formula for the ion production rate at different latitudes and covering the altitude range between 18 and 40 km altitudes. Theoretically, ion production rates have been calculated on basis of measured flux and energy spectrum of cosmic rays. Datta et al. [1984] have tabulated the ion production rates due to primary CR flux for different latitudes and altitudes. The contributions due to re-entrant and albeido CR have been calculated by Verma and Bhatnagar [1987] and Verma and Kothari [1987] for Hyderabad (Latitude 18° north). Actual ionisation rates at low latitudes have been measured only upto 34 km altitude [Neher, 1967].

The relative contribution to ionisation in the stratosphere by sources other than CR is not certain. Theoretically sources of meteoric origin have been proposed which can explain experimentally observed ion densities [Aikin, 1981], but direct measurements are not available. In the mesosphere, the Hydrogen Lyman α emission line in the solar ultravoilet radiation becomes important. At still higher altitudes, the solar ultravoilet radiation at other wavelengths also become important (These are not shown in fig 1.2).

1.3.2 The small ion number density

The number density of small ions in the atmosphere (i.e. those ions having mass < 400 amu.), is a function of their production and loss mechanisms. In the previous section the mechanism for ion production was discussed. In this section the expression for the number density of small ions will be discussed. The loss of ions takes place primarily through ionic recombination and through ion-aerosol attachment processes[Gringel et al. 1978]. Ionic recombination takes place when through collision, positive and negative ions react and form neutral products of reaction[Bates, 1985]. In attachment process, an ion on colliding with aerosol particle gets attached to it physically. Aerosols are much larger than small ions and their mobility is proportionately much smaller. Thus attachment of ion to aerosols results in its mobility decreasing by a factor of more than 1000 which in effect removes them from the scene of electrical conduction. The small ion number density is governed by the following equation of continuity[Volland, 1984, p5]:

$$\frac{dN\pm}{dt} = q - \alpha N_+ N_- - \beta N\pm N_a \qquad ..(1.1)$$

Here, $N_\pm$ denotes the number density of the positive and the negative small ions respectively, q denotes the ion pair production rate, α is the ionic recombination

coefficient, β is the average attachment coefficient to the aerosols, and N_a denotes the number density of aerosols.

Under steady state conditions, we can consider dN/dt as 0 so that we have an equation quadratic in $N_{\pm}$. The solution of this equation is:

$$N_{\pm} = \frac{\beta N_a \pm \sqrt{(\beta N_a)^2 + 4\alpha q}}{2\alpha} \qquad ..(1.2)$$

This is a useful expression relating several important parameters.

The number density of ions in the stratosphere has been experimentally measured [Paltridge, 1965, Morita, 1983, Rosen and Hofmann, 1981B, 1985] as well as theoretically calculated using the above equation [Gringel et al., 1978]. Typical values are shown in fig 1.3 which has been taken from Arijs[1983]. In the diagram, P64 refers to measurements by Paltridge[1965], B66: Bragin[1967], Ro68: Rose et al.[1972], W75: Widdel et al. [1977] and R79 is a model calculation by Reid[1979]. The number density is generally estimated to be of the order of 2×10^9 per m^3 at an altitude of about 35 km.

The average lifetime of ions is given by its number density divided by its production rate. This is of the order of 1000 seconds at 35 km altitude in the stratosphere[Nevejans et al. 1985].

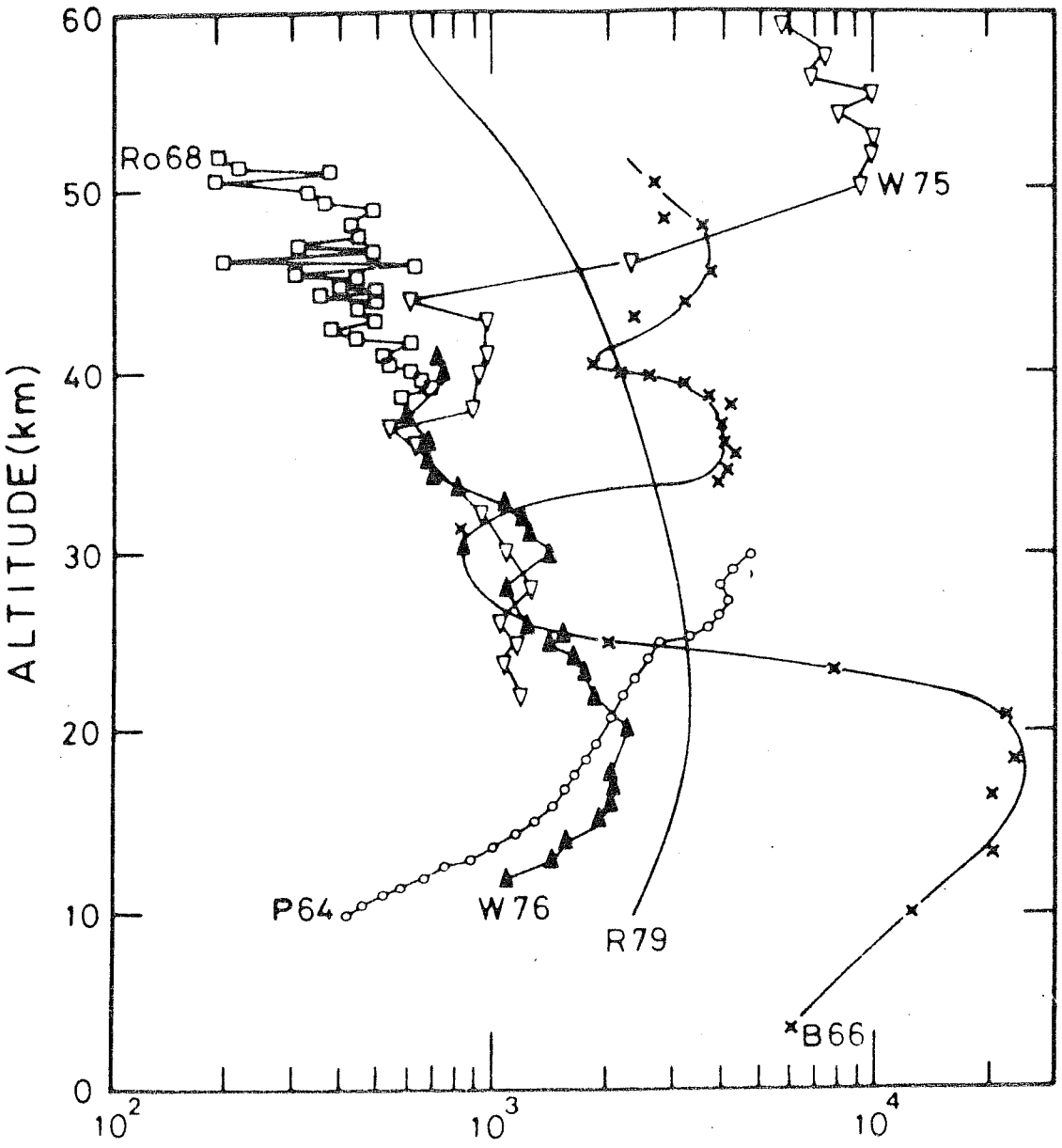
60
50
40
30
20
10
0
ALTITUDE(km)
Ro68
W75
P64
W76
R79
B66
10^2
10^3
10^4
ION NUMBER DENSITY (cm^{-3})

FIG 1.3

1.3.3 Ionic Recombination

Ionic recombination is one of the two major loss processes for the atmospheric small ions. Ionic recombination involves those chemical reactions in which ions of opposite polarity react and form neutral molecules. Several such recombination reactions are known which take place in the atmosphere. Recombination reactions have been classified into dissociative recombination, radiative recombination, and so on[Bates, 1985, Mitra, 1981].

The recombination coefficient α is the weighted average of the rate constants of different recombination reactions that take part in a given situation. Most of the recombination reactions that take place in the atmosphere are either two body recombination reactions or three body recombination reactions[Smith and Adams, 1982].

At higher pressures which exist in the lower stratosphere, the dominant recombination processes are three body type. Three body recombination processes can be represented by the following equation:

$$A^+ + B^- + M \xrightarrow{\alpha_3} AB + M \qquad ..(1.3)$$

Here, A^+ and B^- are the two reactant ions, M is a third body which is necessary for taking care of the extra energy of reaction, but which otherwise does not participate in this reaction. α_3 is the three body recombination coefficient. AB

represents the product of this reaction. Since three body collisions are less frequent as compared to binary collisions, such recombination reactions are dominant at altitudes < 20 to 25 km where pressure is relatively high [Gringel et al., 1978].

At higher altitudes, where collisional processes are less frequent, probability of three body collisions decreases rapidly. Under these circumstances, binary recombination takes over as the dominant recombination process. Binary recombination processes can be represented by the following general equation:

$$A^+ + B^- \xrightarrow{\alpha_2} AB\ (+\epsilon) \qquad ..(1.4)$$

α_2 is the two body recombination coefficient. ϵ represents an amount of energy released through photon emission or some other means.

Several calculations of the recombination coefficient have been done for the ions present in the stratosphere and mesosphere[Bates, 1982, 1985, Gringel et al., 1978, Smith and Adams, 1982]. Experimentally measured values have also been provided by Rosen and Hofmann[1981]. The recombination coefficient values given by Smith and Adams [1982] appear to be the most realistic ones and these values (see Fig 1.4) will be mainly referred to in further discussions.

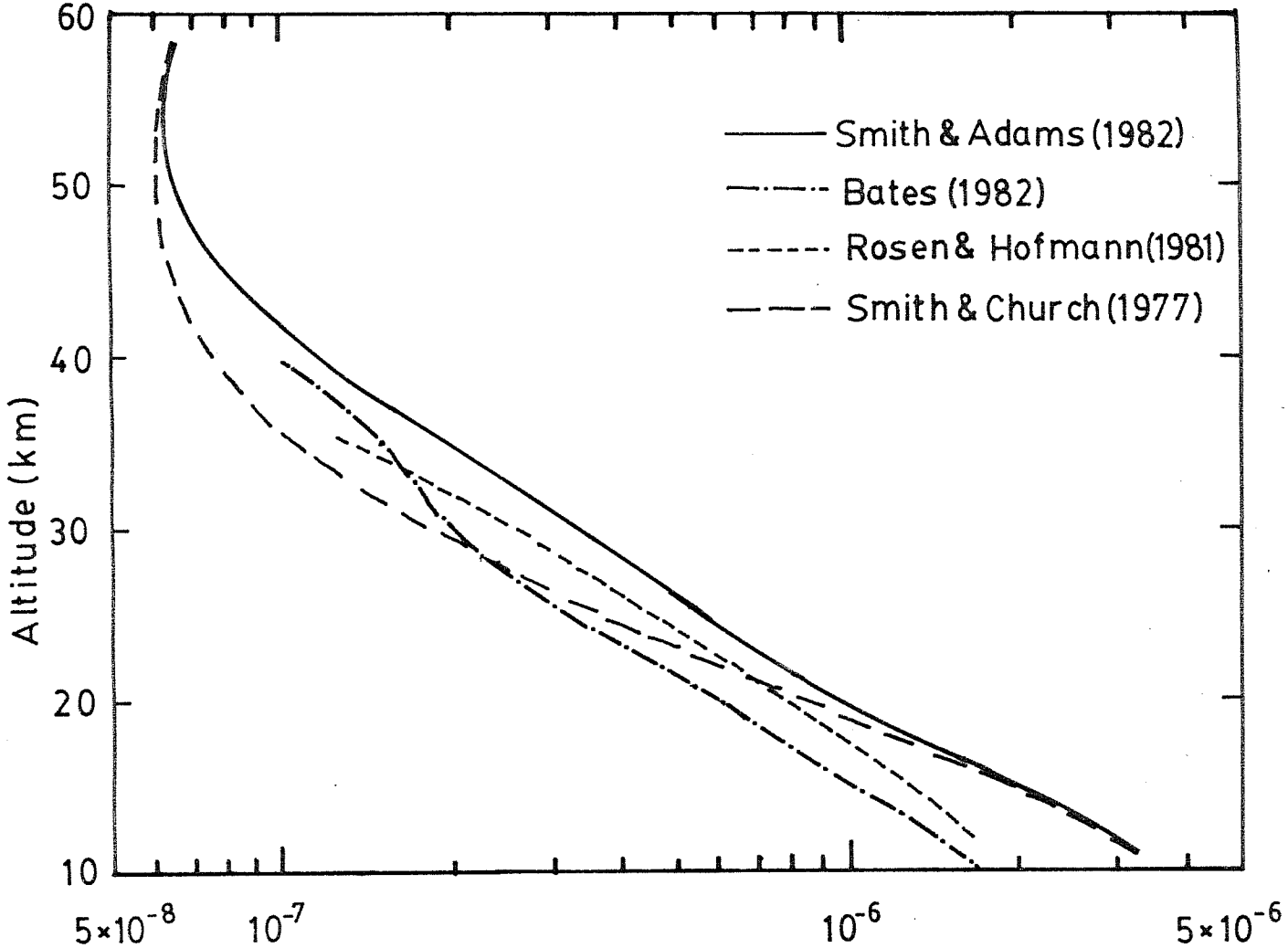

FIG 1.4 RECOMBINATION COEFFICIENT $\alpha_T (cm^3 s^{-1})$

1.3.4 Attachment process

The other method by which small ions get removed from the atmosphere is through the ion-aerosol attachment. Aerosols are particulate matter in solid and liquid phases which are dispersed in air. They appear in a wide range of size distribution right from 0.01 micron to 100 micron size[Twomey, 1977, p3]. When an ion collides with an aerosol particle, it attaches itself to the particle. The attachment coefficient β is the number of ion-aerosol attachments taking place per unit volume per unit time for a unit number density of the particles. Actually, this is an average over the different sizes, and βN_a gives the fractional loss of small ions due to aerosols[Twomey, 1977, p263, Kondo et al., 1982A, Gringel et al., 1978]. Under normal conditions, this quantity is small as compared to the recombination loss term[Kondo et al., 1982A, 1982B]. But when conditions like volcanic eruptions take place, the aerosol number density can get enhanced to several thousands per cc[Cadle et al., 1976] and the attachment process becomes important in the overall ion loss mechanism[Mitra, 1981, Volland, 1984, p18].

Aerosols play an important part in ion chemistry[Arnold et al., 1982, Mitra, 1981, Datta et al., 1987B]. Its role in positive ion chemistry was proposed by Mitra[1981] and was experimentally observed by Takagi and Morita[1980], Hofmann and Rosen[1982, 1983]. Arnold [1982] has discussed about the possible effect of metallic ions on aerosol production. But

the effect of aerosols on ionisation in the stratosphere is still not fully understood.

1.3.5 Ion chemistry

The ionisation process is intimately related to ion chemistry. Soon after its production, an ion in the atmosphere undergoes a series of reactions. The steady state concentrations of various ionic species in the atmosphere depends on the rate constants of the numerous reactions taking place in the atmosphere. The positive ions and the negative ions follow different schemes of reaction[Brasseur and Chatel , 1983]. The problem of ion chemistry is to make models of ion reactions and to find out the concentrations of different ionic species from them which would explain the actually observed concentrations.

In recent years, it has become technically feasible to put mass spectrometers on balloon-borne gondolas and measure the ion compositions at stratospheric altitudes. Arnold et al.[1982], Arijs et al.[1983, 1985], Schlager and Arnold[1987], Ingels et al.[1987] have identified the different ionic species present in the stratosphere. The relative concentrations of different ionic species have been measured by them at altitudes ranging from 17 to 45 km. Two families of positive ions have been observed. Ions known as Proton Hydrates(PH) have the general formula $H^+(H_2O)_n$, while those known as Non-Proton Hydrates(NPH) have the general formula $H^+(CH_3CN)_m(H_2O)_n$. At altitudes below 35 km,

NPH are the dominant positive ion species while at higher altitudes, the proton hydrates are dominant[Brasseur and Chatel , 1983, Arijs and Brasseur, 1986]. There are two main families for the negative ions also. The negative ions form sulfate $(HSO_4)^-$ and nitrate $(NO_3)^-$ cluster ions. (H_2SO_4) and (HNO_3) molecules attach to these ions to form these species of negative ions. Nitrate cluster ions are dominant at altitudes below 35 km while sulfate cluster ions are dominant above this altitude[Arijs, 1983].

Because of availability of good ion composition data in the stratosphere and improved laboratory techniques for studying the reaction rates [Smith and Church, 1977, Albritton, 1978, Smith et al., 1981, Viggiano et al., 1982, Alge et al., 1983], it has now been possible to model the complex behaviour pattern of stratospheric ions. Brasseur and Chatel [1983] did the first elaborate modelling of the stratospheric ions. Several other models have been given [Fergusen et al., 1979, Mitra, 1981, Beig and Chakrabarty, 1987], which deal with different features of the ionisation behaviour in the stratosphere.

Ion chemistry models help in getting a consolidated picture of what happens at these altitudes. Laboratory measurements such as those by Smith et al.[1981] and others provide the input information to these studies. Other input information such as ionisation rate, ion density, conductivity and mobility, come from the study of the atmospheric electric parameters.

1.4 Conductivity in the middle atmosphere

Air in the stratosphere is weakly conducting. Its conductivity increases roughly exponentially with altitude (fig 1.5) in the troposphere, stratosphere and mesosphere. This conductivity exists because of the presence of ions which act as carriers of electric charge in the atmosphere. The polar conductivity is the conductivity because of charge transport by ions of a particular polarity.

The following equation relates the conductivity with the number density and masses of the ions.

$$\sigma\pm = \frac{n\pm e^2}{m\pm \nu} \qquad ..(1.5)$$

Mobility is given by the following expression:

$$\mu = \frac{e}{M\nu} \qquad ..(1.6)$$

The average polar mobility is thus,

$$\mu\pm = \frac{e}{N\pm} \sum_{\pm} \frac{ni}{mi\,\nu i} \qquad ..(1.7)$$

In terms of mobility the conductivity can be written as

$$\sigma\pm = n\pm\, e\, \mu\pm \qquad ..(1.8)$$

In the stratosphere $n_+ \simeq n_-$ and we get

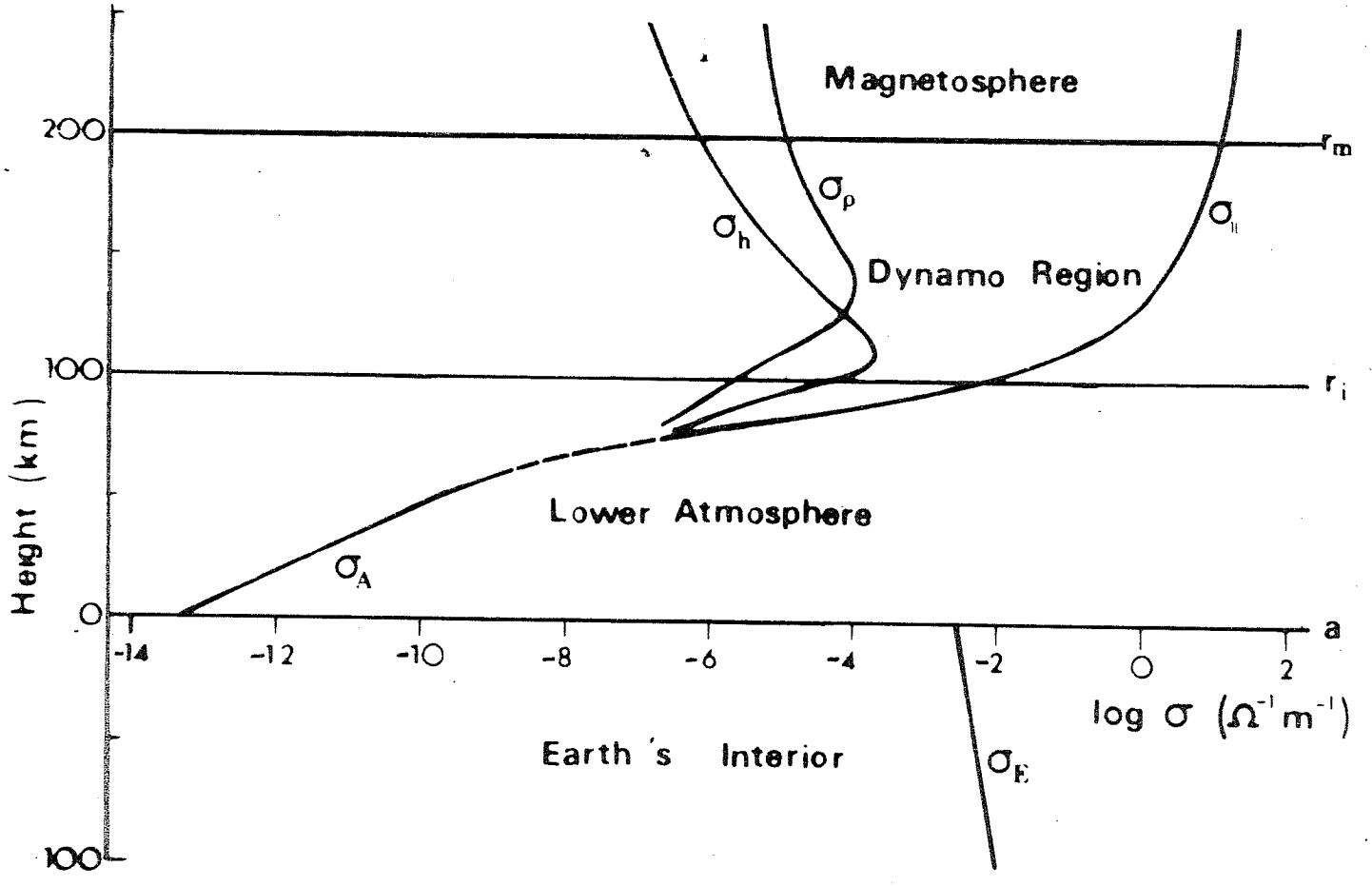

FIG 1.5 Mean altitude profile of electric conductivity.

$$\sigma\pm = n\ e\ \mu\pm \qquad ..(1.9)$$

The ratio of conductivities gives the ratio of average polar mobilities:

$$\frac{\sigma+}{\sigma-} = \frac{\mu+}{\mu-} \qquad ..(1.10)$$

This is related to collision frequency and the mass of the ions via equation 1.8.

Meyerott et al.[1980] have given a curve showing the dependence of ionic mobility on ionic mass. This curve is based on the measurements done by Kilpatric[1971], Huertas et al.[1974] and Dotan et al.[1974]. One can also obtain the ionic masses from mobility by using the well known relation between the two quantities. Mobility is related to mass and collision frequency via equation 1.6. The main problem with using this equation is that the mass dependent collision frequencies for most of the cluster ions is not known at present. However if appropreate form of this dependence is assumed (using proper models) then with independent knowledge of either the number density or mobility the other quantity could be estimated.

Equation 1.8 gives the polar conductivity in terms of number densities of small ions and their mobilities. The number density of small ions decreases after occurance of major volcanic eruptions because large amounts of aerosols

are thrown into the atmosphere. These aerosols deplete the air of ions through attachment process(Equation 1.1). Measurement of ratio of polar conductivities before and after volcanic eruptions can give important clues regarding the nature of the ionised medium after volcanic eruptions[Kondo et al., 1982B].

Conductivity measurements are being done since the beginning of this century. During a balloon flight in 1905, Gerdien obtained the first measurements of atmospheric conductivity[Israel, 1970]. Later, Wigand[1914] performed similar measurements during balloon ascents upto 9 km altitude. Numerous measurements of conductivity have been done since then. Some of the results have been summarised by Hake Pierce and Viezee[1973], Rosen and Hofmann[1981A], Rosen et al.[1982]. In earlier measurements ratio of polar conductivity was measured only upto around 28 km and this ratio was found to be $\simeq 1$[Woessner et al., 1958, Kraakevick, 1958, Paltridge, 1965, Hake, Pierce and Viezee, 1973]. Recent measurements have concentrated on positive conductivity[Rosen et al., 1982] or total conductivity and related phenomena[Bering et al., 1980, Holzworth et al., 1984]. We have conducted polar conductivity measurements from Hyderabad(India) during the period 1984 to 1987. We have studied the effect of volcanic aerosols on conductivity.

1.5 The Global Electric circuit

There exists a vertical electric field in the atmosphere having a magnitude of the order of 120 volts per meter in fair weather near the ground[Volland,1984]. This electric field is in the downward direction. If we sum this electric field between the earth and the ionosphere (upto 50 km altitude) we obtain a potential difference of the order of 3×10^5 volts. Air is a weak conductor in the region between the ionosphere and the earth's surface. Because of the potential difference between the ionosphere and the earth, a weak current flows down from the ionosphere to the earth all the time. The current density is roughly 10^{-12} amp/m^2. In order to maintain this current system, a source is required which can replenish it.

C.T.R. Wilson [1920] proposed a hypothesis in order to explain this air-earth current phenomenon. This hypothesis envisages a global electric circuit as is depicted in fig 1.6. Several other people like Whipple[1929], Reiter[1972], Kasemir[1977], Hill[1971], and Hays and Roble[1979] have also worked on this hypothesis and have progressively refined and evolved it. To date, this is the best explanation we have for understanding this phenomenon.

According to this hypothesis[Israel, 1970, Muhleson, 1977, Hays and Roble, 1979], the earth's atmosphere can be divided into two regions. They are, the fair weather region, and the disturbed weather region. By fair weather regions, one means

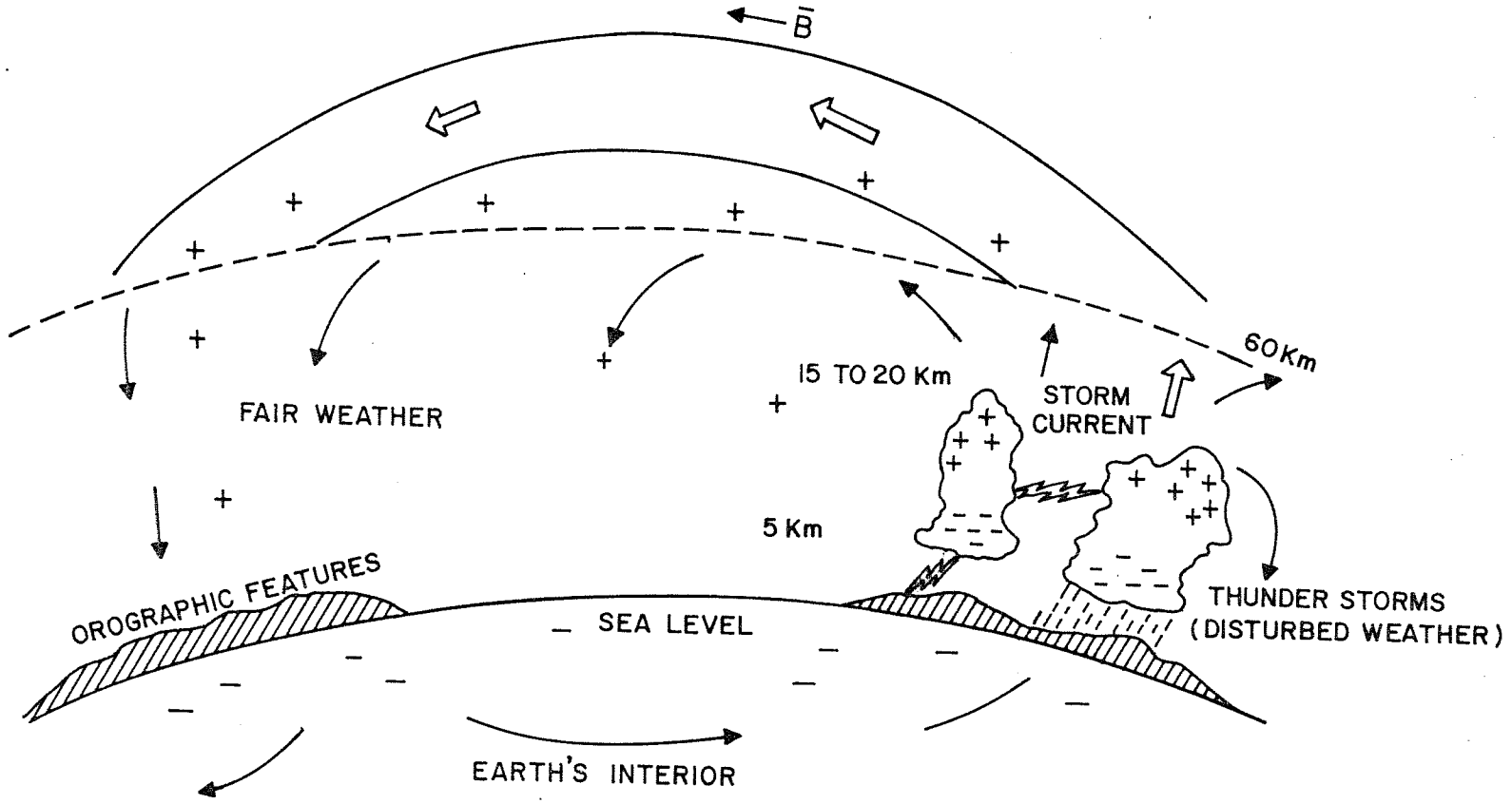

fig1.6: THE GLOBAL ELECTRIC CIRCUIT

those regions which do not have any cloud cover, or have a minimal quantity of it. By disturbed weather regions, we mean those regions which are partially or heavily clouded, or are having rain or thunderstorms. During disturbed weather (when there is rain and thunderstorms), the electric field reverses its direction and can increase ten times in magnitude [Gish and Wait, 1950, Stergis et al., 1957, Holzworth et al., 1986].

Almost eighty percent of the earth's surface at any time is included in the fair weather region. In this region there is an air-earth current flowing downwards. This current is a function of the ionosphere-earth potential and the total resistance between the ionosphere and the earth. This resistance, calculated over unit surface area of earth is known as the columnar resistance Λ and is given by

$$\Lambda = \int_0^H \frac{dh}{\sigma} \qquad ..(1.11)$$

where σ is the conductivity of air and dh is an element of height h. H is the total height upto the ionosphere (H ~ 50 km).

The values of Λ are typically around 1.3×10^{17} ohms-m at the sea level [Gish, 1944]. Λ is also a function of the earth's orography. Since the resistivity at low altitudes is much higher than that at high altitudes, major contribution (upto 70 percent) to the columnar resistance comes from the lowermost 2 km of the atmosphere from the sea level [Muhleson, 1977]. This is why the columnar resistance is

strongly dependent on the altitude of the place of measurement above the sea level.

The Ionosphere-earth potential is calculated by summing the vertical electric field E_v over height.

$$V = \int_0^H E_v dh \qquad ..(1.12)$$

The ionosphere-earth potential difference and the columnar resistance are two important parameters in the fair weather region of the global electric circuit. The product $E(h) \times \sigma(h)$ which is also equal to V/Λ gives the air earth current. The air earth current is nearly constant over the height range between the earth and the ionosphere[Goldberg, 1984]. This potential difference is of the order of 290000 volts [Muhleson, 1977] and varies over the period of a day by almost $\pm$ 60 percent. The maxima occurs at 1800 hrs. U.T. and the minima occurs at 0600 hrs. U.T.[Goldberg, 1984].

The principal sources which maintain the ionosphere earth potential are thunderstorms. They act as generators for this global current. About 1800 to 2000 thunderstorms are taking place around the globe at any time. Each thunderstorm pumps a current of 0.5 to 1 ampere on average into the ionosphere, thus maintaining the charge on the global capacitor[Muhleson, 1977]. If this charging process stops then it will take about 12 minutes time for the global capacitor to discharge(τ = 100 seconds)[Volland, 1984]. Around 100 lightning flashes take place per second around the globe[Orville and Spencer, 1979]. As a result the

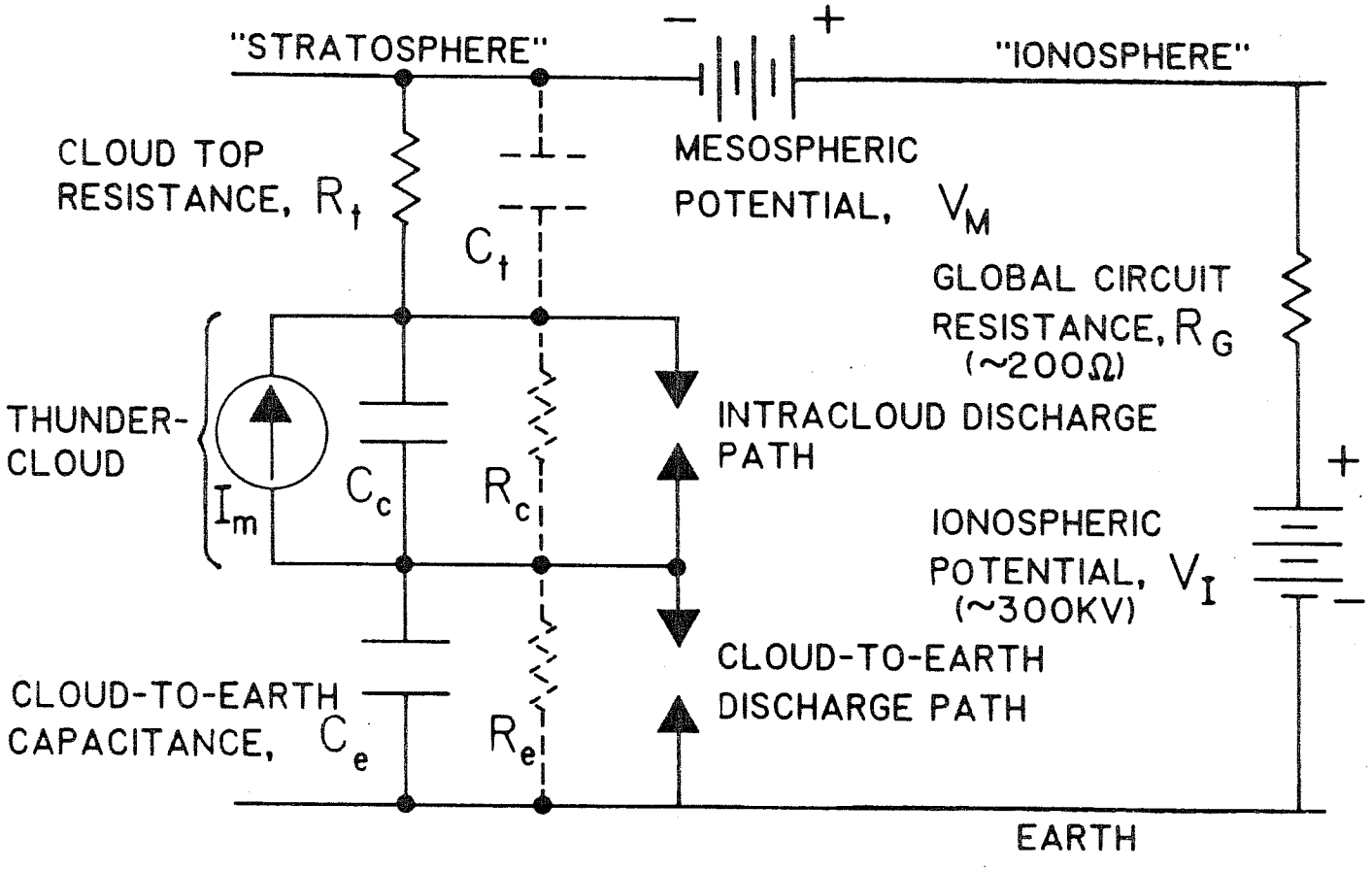

FIG 1.7 EQUIVALENT CIRCUIT FOR GEC.

global capacitor carries a charge of 550000 coulombs which resides at its two concentric plates. Fig 1.7 depicts the global circuit.

Fig 1.8 shows a thunderstorm cell and the air currents inside it. Thunderstorms are the main generators in the global current system. Electric fields of the order of several hundred kilovolts per meter develop inside thunderstorm cells [Levin et al., 1977]. The thunderstorm cells act as dipole current sources[Kasemir, 1977, Hays and Roble, 1979] for the global circuit.

Several mechanisms of charge seperation have been identified within thunderstorms. The most common one[Moore, 1977] is described below. Water droplets and ice particles of various sizes are suspended in air within a thunderstorm cell. Because of the presence of a vertical electric field within the cell, which is directed downwards, these droplets get electrically polarised. Larger droplets fall faster than smaller droplets. In this process, they collide with the smaller droplets below them. The bottom side being positively polarised, the droplets that brush past take away positive charge leaving a net negative charge on the drop. Because of a higher falling rate, the larger droplets shift the overall negative charge further downwards, thus building up the existing vertical electric field.

Whenever a large enough potential gradient of the order of 400kilovolts per meter builds up through this or some other charging process, an electrical breakdown takes place resulting in a lightning discharge. Lightning discharges of

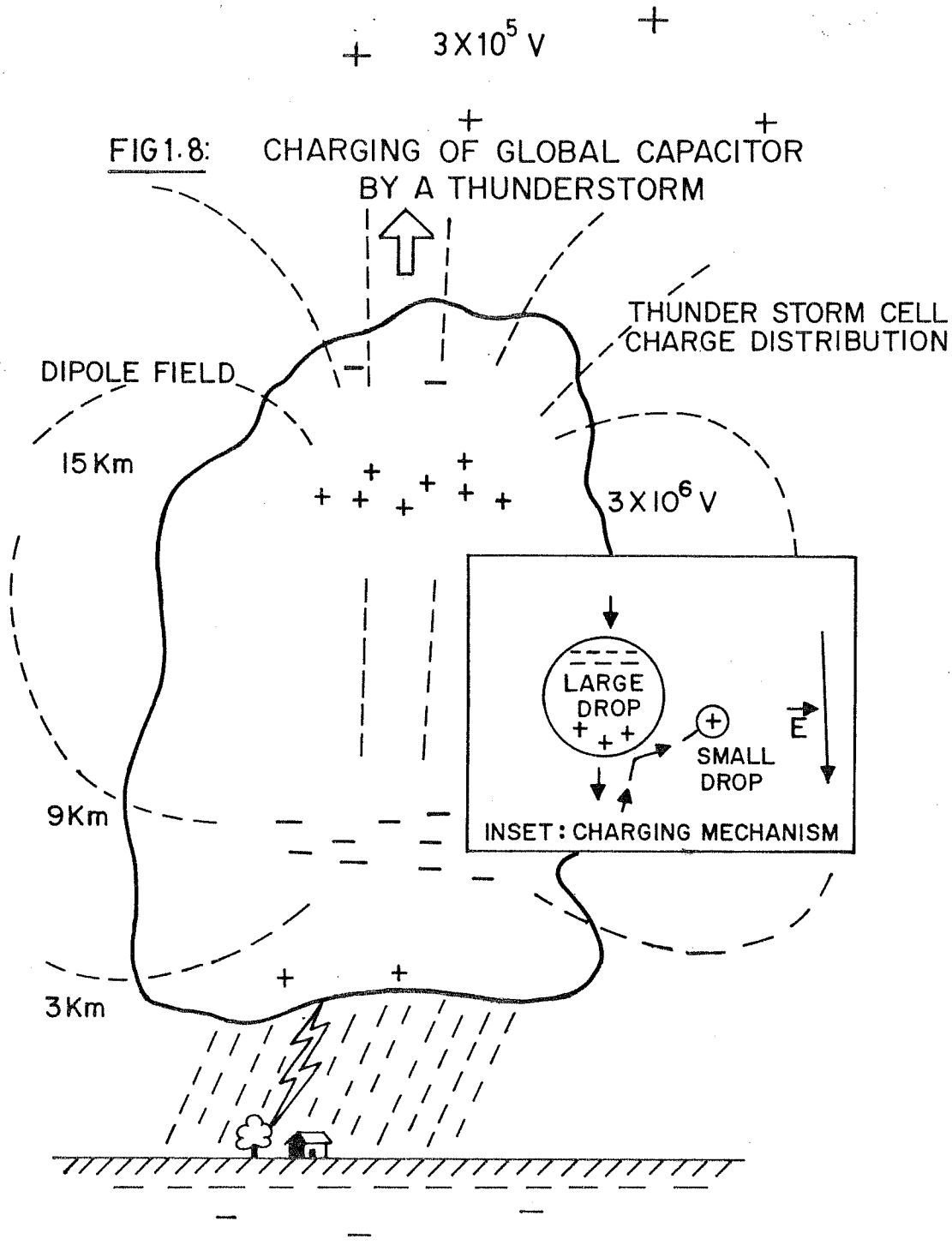

FIG 1.8: CHARGING OF GLOBAL CAPACITOR BY A THUNDERSTORM

the kind cloud to cloud or cloud to ground and vice versa or cloud to ionosphere have been observed. It is the cloud-ground and the cloud-ionosphere discharges that are major contributors to the global circuit.There are other sources also which contribute to this. Among them are Convective generators[Markson, 1975], Austasch generators[Kasemir, 1977], and non-thunderstorm clouds and precipitation[Chalmers and Little,1960].

Some of our measurements relate to the global circuit and have been discussed in chapters 4 and 5.Table 1.1 [from Muhleson, 1977] shows the different parameters of the global electric circuit and their estimated magnitudes.

1.6 Mesospheric electric fields

Recently, there have been several measurements of the vertical electric field in the mesosphere[Hale et al.,1981, Maynard et al., 1981, 1984, Kelley et al.,1983] which have indicated that there exist electric fields in the mesosphere whose magnitudes are of the order of several volts per meter. In fig 1.7, which shows an equivalent circuit of the global electric circuit,these fields are included in the form of mesospheric voltage sources.Several rocket-borne measurements had been carried out from Andoya, Norway under MAE(Middle Atmospheric Electrodynamics) campaign to study this problem in detail[Maynard et al., 1984]. The main observations were that the large vertical electric fields are present in the mesosphere only at

TABLE 1.1

Parameters of the Global Electric Circuit

Number of Thunderstorms	1500-1800
Mean Current Intensity over one Thunderstorm cell	0.5-1.0 Amp.
Global Current	800-1800 Amp.
Ionosphere Potential	180-400 kV(range)
Columnar Resistance	1.3×10^{17} Ohm m^2
Total Resistance	230 Ohms

certain times. A necessary but not sufficient condition for their existence was that the mesospheric conductivity should be relatively low. Some of our rocket borne langmuir probe measurements show indirect evidence of such V/m electric fields. The mechanism of generation of this electric field is not yet understood fully and experimental as well as theoretical study of this problem is required.

1.7 Scope of this thesis

Numerous measurements of electrical conductivity and electric field have been done in the stratosphere. But they have all been done in the high- and mid-latitude regions. Upto now, very few measurements have been done over low latitudes

The conditions at low latitudes are somewhat different from those at high latitudes. The ion production in the stratosphere at low latitudes is much less as compared to that at high latitudes because of the low CR flux reaching the atmosphere at these latitudes.

The ion composition at mid latitudes is known and there exists a model of the ion chemistry corresponding to those measurements. But no model information of ion chemistry of the stratosphere exists for low latitudes. Although drastic differences from the mid-latitude ion chemistry are not expected, the latitude dependent factors like CR flux can make some difference in the ion chemistry. Measurement of

conductivity at low latitude was thus expected to bring out some new information of this region.

The measurements of polar conductivity done in the fifties and sixties show that their ratio was of the order of one upto 30 km altitudes. Recent measurements of ion composition suggest that the ratios between polar conductivities should be as high as three to five times at around 30 to 35 km altitude. This ratio is the ratio of the average masses of the positive and the negative ionic species, and is a useful parameter which tells about the kinds of ions to be expected at these altitudes. The measurement of this ratio which was done from Hyderabad has been discussed in chapters 4 and 5. As we shall see, this measurement has given some very useful information about the nature of stratospheric ions.

We have measured polar conductivity before and after two major volcanic eruptions and found that the ratio of the polar conductivities undergoes drastic change after the eruption. The results are given in chapter 4 and discussed in chapter 5.

Measurement of vertical electric field has been done just after volcanic eruption. This has been higher than the expected values under normal conditions. The results are discussed in chapter 5.

The electrical charging behaviour of balloon-borne gondola has been studied during ascent and float periods. The charging of the gondola is one of the nagging problems for the experimenters involved in ionisation measurements.

described in chapter 2.

A peculear behaviour of langmuir probes in the mesosphere has been investigated. The possibility of existance of large mesospheric electric fields on the basis of this anomalous behaviour of the probe is discussed in chapters 2,4,and5.

Since Middle Atmospheric Electrodynamics involves a large variety of phenomena,it is beyond the scope of this thesis to cover all or even most of them. I have attempted to study some of the phenomena which occur in middle atmospheric electrodynamics using experimental technique and have presented them in this thesis. It is expected that this work will help towards a better understanding of the middle atmosphere at low latitudes.

CHAPTER II

PROBE THEORY AND PHYSICS OF CONDUCTIVITY AND ELECTRIC FIELD MEASUREMENT

The present chapter deals with the principles of measurement of conductivity and electric field in the middle atmosphere. Various practical and theoretical aspects of the measurement technique are discussed in this chapter.

Conductivity measurement involves measuring the current collected by a sensor immersed in the ambient medium. Alternately, conductivity measurement is done by charging a sensor and allowing its potential to decay to the ambient value. In the latter case the time constant of decay gives the conductivity. For electric field measurement, two techniques are generally employed. The double probe technique is based on measuring potential difference between probes seperated by a given distance in the ambient medium. The field mill uses an inductive method for direct determination of electric field. The author has used the

relaxation probe technique for conductivity measurement and double probe technique for the measurement of electric field.

In section 2.1 and 2.5 of this chapter, the principles of measurement of conductivity and electric field in the stratosphere are explained. The basic expression for current collection by an electrostatic probe has been derived using the Gauss's theorem in sections 2.1.1 and 2.1.2. Some of the problems encountered during actual measurements and possible measures for rectifying them are discussed in sections 2.2 and 2.3. The techniques for conductivity measurement are described in section 2.2. The author has conducted a study of the variation of floating potential of the balloon-borne gondola during the balloon ascent and float periods. This has been described in section 2.4 of this chapter. The double probe technique which has been used for electric field measurement in the stratosphere has been described in section 2.5. In sections 2.6 the principles involved in measurement of mesospheric conductivity are discussed. A discussion of possible effect of presence of large electric field on current collection by a d.c. probe is given in section 2.6.3. This has been used in chapter 5 for explaining some of the features observed during rocket-borne mesospheric measurements.

2.1 Principle of conductivity measurement

The conductivity of a medium is the current which passes through a unit cross section of the medium when unit electric field is applied across it. Conductivity is thus the inverse of resistivity. The unit of conductivity in the MKS system is Ohm^{-1} per meter, also known popularly as mhos per meter or Siemens per meter(S/m). If E is the electric field and j is the current density then the conductivity σ is given by the following expression.

$$\sigma = \frac{j}{E} \qquad ..(2.1)$$

Conductivity measurement in the atmosphere is done with help of electrodes which collect ions from the ambient medium. Basically two methods are used for this purpose. In attracting potential method a probe is kept at a fixed or a swept voltage bias and the current collected by it is measured. In the transient response method the probe is initially charged to some given voltage and its potential is continuously monitored as it discharges through the medium. The conductivity of the medium is obtained from the time constant for this discharge. The basic principles of these two methods are described below.

2.1.1 Transient response method

In the transient response method, a metallic conductor of suitable shape is used for the sensor. Fig 2.1 illustrates this method schematically.

In the beginning, the sensor is charged to a suitable voltage and is allowed to discharge through the medium. The sensor potential decays exponentially with time. The voltage decay with respect to time is recorded and the time constant is measured. Conductivity is obtained using equation 2.2.

$$\sigma = \frac{\epsilon_o}{\tau} \qquad ..(2.2)$$

where ϵ_o is the permittivity of the ambient medium and τ is the time constant of decay of the sensor potential. A derivation of this expression from basic electrostatic equations is given below.

Consider a capacitor formed by a pair of conductors A and B. Let an amount of charge +Q reside on the conductor A and -Q reside on the conductor B. The medium in-between A and B is weakly conducting and has a conductivity σ. Let us consider an arbitrary gaussian surface S enclosing the conductor A in such a way that B lies fully outside S. Then for the surface S, using Gauss theorem, we have

$$\oint_S E.dS = \frac{Q}{\epsilon_o} \qquad ..(2.3)$$

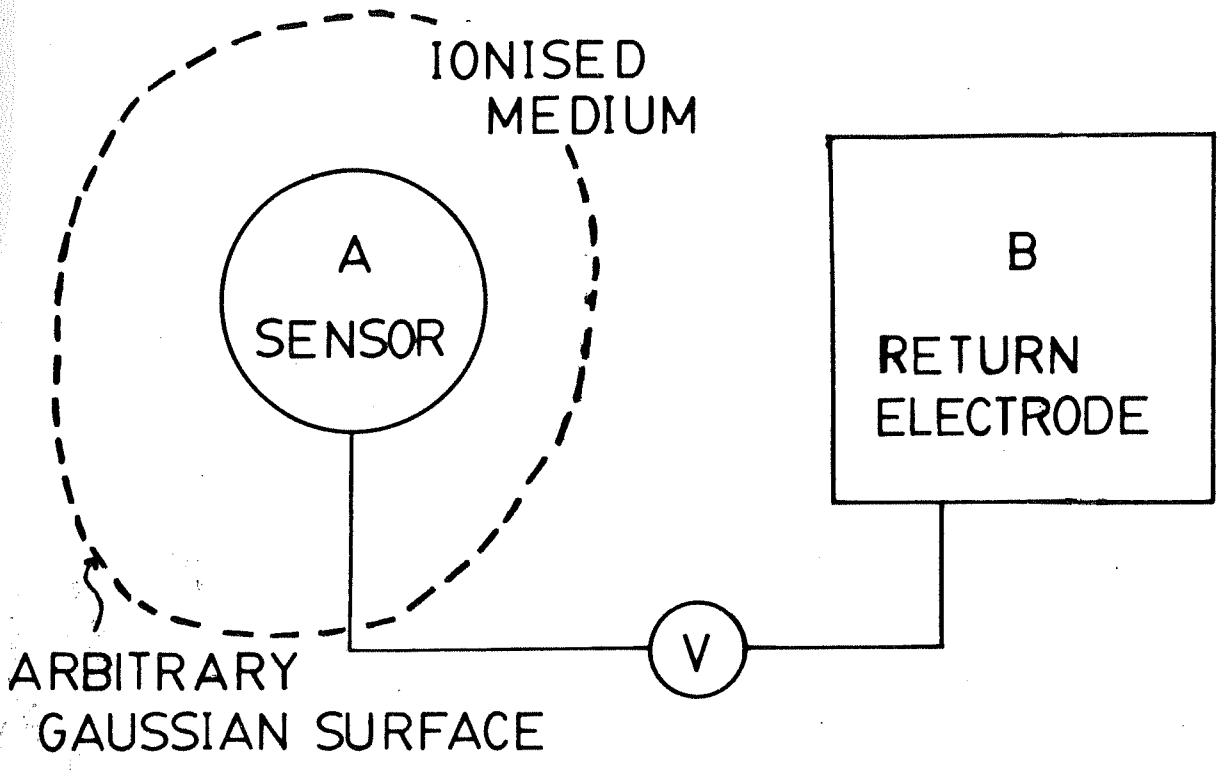

Fig 2.1 Principle of Conductivity measurement

We use $j=\sigma E$ with this and get

$$\frac{1}{\sigma}\oint J.dS = \frac{Q}{\epsilon_o} \qquad ..(2.4)$$

The total current I is given by

$$I = \oint J.dS = \frac{V}{R} \qquad ..(2.5)$$

where V is the potential difference between the two conductors and R is the resistance between them. Using equations 2.4 and 2.5 we get

$$\frac{1}{\sigma}\frac{V}{R} = \frac{Q}{\epsilon_o}$$

or

$$R = \frac{\epsilon_o}{\sigma(Q/V)}$$

or

$$R = \frac{\epsilon_o}{\sigma C} \qquad ..(2.6)$$

If this system of two conductors is charged and allowed to discharge through the medium, the potential at the conductor decays exponentially according to the following expression:

$$V = Vo\ \exp(-t/\tau) \qquad ..(2.7)$$

The conductivity σ is expressible using equation 2.6 in terms of the decay constant τ which is equal to R X C as

$$\sigma = \frac{\epsilon_o}{\tau}$$

Thus we get equation 2.2. This is the principle which we have employed in our measurement of conductivity. In the actual measurement, the sensor B has been taken as a conducting surface at infinity. The voltage decay is monitored by attaching a high impedance voltmeter to the conductor A. The sensor is charged to a suitable voltage and allowed to discharge through the medium. The variation of

the sensor voltage with time is measured and recorded. The voltage-time curve obtained in this way is later analysed to get the conductivity. The instrument will be described in detail in chapter 3. But some of the important aspects of the measurement process will be discussed in section 2.2, 2.3 and 2.4. We shall see that some of the assumptions involved in the above expression are not strictly true.

2.1.2 Attracting potential method

In this method the sensor potential is varied by applying a voltage sweep, and the current collected by the sensor is measured. The slope $\frac{dI}{dV}$ gives the conductivity.
We use $R=\frac{dV}{dI}$ and eq. 2.6 to get

$$\frac{dV}{dI} = \frac{\epsilon_o}{\sigma C}$$

or

$$\sigma = \frac{\epsilon_o}{C(dV/dI)} \qquad ..(2.8)$$

For making the measurements, a sweeping voltage is applied to a sensor kept in the ambient medium and the current collected by the probe is measured. The slope $\frac{dI}{dV}$ is derived from the measured current-voltage characteristics. The conductivity is then obtained by using equation 2.8.

2.2 Instruments for conductivity measurement

Two types of instruments have been generally used by

experimenters for measuring conductivity in the atmosphere. These are known as (1) the relaxation time probe, and (2) the Gerdien condenser. Some experimenters have also used current collecting Langmuir probes for conductivity measurement. In this section I will describe the relaxation time probe and the Gerdien condenser, which are the more popular ones amongst the techniques being used. The technique that we have used for our measurements is the relaxation time technique and its method will be described in more detail in this section.

2.2.1 Relaxation time probe

The relaxation time probe consists of a metallic sensor which is put in the ambient medium whose conductivity is to be measured. The probe is connected to a high sensitivity voltmeter which continuously measures its potential with reference to the payload ground potential. The probe is charged to a suitable potential and is then allowed to discharge through the surrounding medium. Ions present in the surrounding medium which have similar polarity as the sensor are repelled from the probe while ions having opposite polarity are attracted by it. The probe collects these charges and as a result its potential decays with time. This decay of the probe potential is given by equation 2.7 in Section 2.1.1. One should note that the equation 2.7 describes the voltage decay of the probe with respect to the surrounding ambient medium while the measurement done

by the voltmeter connected to the probe is with respect to the payload ground potential. This potential is different from the ambient potential and it is important to know the relation between them. This will be discussed in section 2.3. and section 2.4.

Theory (given in section 2.1.1) allows for the probe to have any shape and dimention. Probes of spherical[Mozer and Serlin, 1969, Holzworth and Chiu, 1982] and disc shapes [Ogawa et al., 1975] have been used for similar measurements. Thin long wires have also been used by several experimenters[Rosen et al., 1982]. We have used probes having a spherical geometry. The probes were carried on balloon-borne gondolas and the measurements were carried out at the stratospheric altitudes of around 35 km. In order to do the measurements the probes were charged to +5 volts and -5 volts with respect to the payload ground potential and were then allowed to discharge through the medium. Details of instrumentation and the procedure for data analysis are given in chapter 3.

2.2.2 Gerdien Condenser

The Gerdien Condenser is an instrument which works on the principle described in section 2.1.2 as the attracting potential method. The instrument has two concentric cylinders which act as electrodes. The electrodes are biased by external electric circuit so that an electric field exists between them. Air is made to flow longitudinally in

the space between the two electrodes. The ions which are present in this air are attracted to the electrodes which have opposite polarity and are collected by them. The current collected by the electrodes is measured while the biasing potential of the electrode is varied in a linear fashion. This gives the quantity $\frac{dV}{dI}$ which is used in equation 2.8 for calculating the conductivity σ [Paltridge, 1965, Leiden, 1976].

2.3 Factors involved in realistic measurement situation

In the derivation of the expression for conductivity which was given in section 2.1.1 and 2.1.2, it was implicitly assumed that the number density of ions in the vicinity of the probe is not affected as a result of current collection. In reality, when the probe collects ions, the air in its neighbourhood gets depleted of charge. The loss of ions due to collection by the probe disturbs the state of dynamic balance of ions existing in air as a result of their production and recombination. If the depletion rate due to collection by probe becomes comparable to the ion production rate, the measurement process will affect the ion number density and the measurements will not be true. Let us see what happens during actual measurement situation.

In the following subsections, I will discuss the following topics: (1) Depletion of charges in still air and the importance as well as effect of air flow around the

probe, (2) Size of the gondola and the return electrode, and their effect on current collection process, (3) Photoelectric emission from the probe surface, and (4) Choice of the size of the probe.

2.3.1 Need for air flow around the probe

When an isolated charged body is kept in an ionised medium, it is surrounded by ions of the opposite polarity. The accumulated charge partially shields the body from outside fields. This effect is known as the Debye shielding effect. The thickness of the charge cloud surrounding the conductor is a basic parameter of the medium and is known as the Debye shielding distance. For balloon-borne probes in stratosphere, this distance is of the order of 2 cm. Chang and Kodera [1985] have discussed the effect of variation of probe size (compared to the Debye length) on current collection in case of stationary porobes. For probe potentials of the order of $\frac{kT}{e}$ they have shown that current collection gets appreciably affected due to Debye shielding and the voltage decay curve gets distorted.

The situations we encounter during our balloon experiments are different from this case in two respects: (1) The probe potentials are nearly hundred times larger than $\frac{kT}{e}$, which is of the order of 0.02 volts, and (2) the probe is not stationary.

The problem of current collection by a spherical probe in a weakly ionised stationary plasma for probe potentials $\gg \frac{kT}{e}$ might be more relevant for the present case. The problem was attempted by the author. The basic equations used are same as those used by Chang and Kodera[1985]. They are given below:

$$J_+ = -\mu_+ N_+ \nabla V - D_+ \nabla N_+ \qquad \nabla . J_+ + \frac{dN+}{dt} = 0 \quad ..(2.9)$$

$$J_- = +\mu_- N_- \nabla V - D_- \nabla N_- \qquad \nabla . J_- + \frac{dN-}{dt} = 0 \quad ..(2.10)$$

$$\nabla^2 V = -\frac{e}{\epsilon_o}(N_+ - N_-) \qquad ..(2.11)$$

where $N\pm$ is the number density, $\mu\pm$ and $D\pm$ are the mobility and diffusion coefficients and the subscripts refer to the positive and the negative species respectively.

The current collected by the probe is

$$Ip = -e \oint (J_+ - J_-) . dS \qquad ..(2.12)$$

The boundary conditions are

$N_+ = N_- = 0$ $\qquad$ $V = Vp$ at the probe surface

$N_+ = N_- = N$ $\qquad$ $V = 0$ at infinity.

The dimensionless forms of these equations are more convenient to work with. The following dimensionless variables can be introduced:

$$j = \frac{Rp Jp}{N_\infty D_+} \qquad n = \frac{N}{N_\infty}$$

$$r = \frac{R}{Rp} \qquad \Phi p = \frac{eVp}{kT}$$

$$\tilde{\nabla} = Rp\nabla \qquad \tau = \frac{tD+}{Rp^2}$$

$$ds = \frac{dS}{Rp^2}$$

The Debye Length is given by $\lambda_D^2 = \frac{\epsilon_o kT}{N_\infty e^2}$

The Einstein's relation has been assumed to hold in the present case ($\mu = \frac{eD}{kT}$).

Using the above substitutions, the following dimensionless equations were obtained:

$$j_+ = -\tilde{\nabla}n_+ - n_+\tilde{\nabla}\Phi \qquad \tilde{\nabla}.j_+ + \frac{\partial n+}{\partial \tau} = 0 \quad ..(2.13)$$

$$j_- = -\alpha\tilde{\nabla}n_- + \alpha n_-\tilde{\nabla}\Phi \qquad \tilde{\nabla}.j_- + \frac{\partial n-}{\partial \tau} = 0 \quad ..(2.14)$$

$$\tilde{\nabla}^2\Phi = -(Rp/\lambda_D)^2 (n_+ - n_-) \quad ..(2.15)$$

The boundary conditions are now

$$n_+ = n_- = 0 \qquad \Phi = \Phi p \quad \text{at the probe surface}$$

$$n_+ = n_- = n \qquad \Phi = 0 \quad \text{at infinity.}$$

We first consider the case of current collection by the probe at a steady probe voltage. This corresponds to the case in the attracting potential method when the probe is kept at a fixed bias potential. Under such a case $\frac{\Phi p}{\tau} = 0$. If the solution is to be meaningful and representative of a

steady state condition, one will require that

$$\frac{\partial n+}{\partial \tau} = \frac{\partial n-}{\partial \tau} = 0 \qquad ..(2.16)$$

Under such a condition equations 2.13 and 2.14 become

$$\tilde{\nabla}.(\tilde{\nabla} n_+ + n_+ \tilde{\nabla}\Phi) = 0 \qquad ..(2.17)$$

$$\tilde{\nabla}.(\tilde{\nabla} n_- - \alpha n_- \tilde{\nabla}\Phi) = 0 \qquad ..(2.18)$$

One can assume characteristic lengths in gradients of V and n to be same. Then $\tilde{\nabla}n$ term goes as $\frac{n}{L}$ while the other term $n\tilde{\nabla}\Phi$ goes as $\frac{n\Phi}{L}$ where L is the characteristic length. Since $n \sim 1$ and $\Phi >> 1$, we have $\tilde{\nabla}n << n\tilde{\nabla}\Phi$ and thus we can ignore the first term in the above equations 2.17 and 2.18.

The three equations become

$$\tilde{\nabla}.(n_+ \tilde{\nabla}\Phi) = 0 \qquad ..(2.19)$$

$$\tilde{\nabla}.(n_- \tilde{\nabla}\Phi) = 0 \qquad ..(2.20)$$

$$\tilde{\nabla}^2 \Phi = \beta^2 (n_+ - n_-) \qquad ..(2.21)$$

where $\beta = \frac{R_D}{\lambda_D}$.

Since this problem of current collection by a spherical probe has a spherical symmetry, we shall choose spherical co-ordinates. Also, for convenience, we shall use the co-ordinate system $x = \frac{1}{r}, \theta, \Phi$. Due to spherical symmetry, the problem reduces to a one-dimensional one.

Using $\tilde{\nabla} = x^2 \frac{\partial}{\partial x}$, the equations 2.19-2.21 become

$$x^2 \frac{\partial}{\partial x} \left(n_+ x^2 \frac{\partial \Phi}{\partial x} \right) = 0 \qquad ..(2.22)$$

$$x^2 \frac{\partial}{\partial x} \left(n_- x^2 \frac{\partial \Phi}{\partial x} \right) = 0 \qquad ..(2.23)$$

$$x^2 \frac{\partial}{\partial x} \left(x^2 \frac{\partial \Phi}{\partial x} \right) = \beta^2 (n_+ - n_-) \qquad ..(2.24)$$

Integrating equations 2.22 and 2.23 once, we get

$$n_+ x^2 \Phi' = C1 \qquad ..(2.25)$$

$$n_- x^2 \Phi' = C2 \qquad ..(2.26)$$

This gives at $x = 1$

$$n_+(x=1) = \frac{C1}{\Phi'} = 0;$$

$$n_-(x=1) = \frac{C2}{\Phi'} = 0 \qquad ..(2.27)$$

which means that either $\Phi' = 0$ at $x = 1$, which is non-physical, or else, $C1 = C2 = 0$ and consequently $n_+ = n_- = 0$ everywhere. This is not consistent with the boundary conditions except for the trivial case when $N = 0$. Thus there are no steady state solutions to equations 2.22-2.24 which are practical (i.e. which satisfy the given boundary conditions non-trivially).

The non-existence of a steady state solution in a stationary plasma is not surprising. It means that if the ambient medium is stationary, current collection cannot go on without depleting the medium(The steady state solution

which does exist for stationary plasma predicts both the number densities as zero). Thus one must have a flowing medium for current collection to take place properly.

A spherical sensor for measuring conductivity having a diameter of 20 cm will have a capacitance of 10 pf. When it is charged to 5 volts and is left to discharge, it will collect a charge of 5×10^{-11} coulombs during its discharge. Stratospheric air contains around 2×10^{9} ions per cu. m. Therefore one requires 0.115 cu. m. of fresh air to provide this charge. Israel[1970] has discussed the aspect of charge depletion by the probe in detail. According to Israel, a minimum air flow rate of 20 cm per second is required for proper current collection by the probe.

During measurement using balloons, some air flow always exists around the gondola. Even when the balloon is floating at its ceiling altitude, there is a certain amount of air flow and turbulence present near the gondola which makes it possible to make the measurement without much difficulty.

2.3.2 Probe in flowing air

In section 2.3.1 it was shown that flow of air around the probe is necessary for making conductivity measurement by relaxation technique. In this section I will describe the behaviour of the probe in presence of air-flow.

A simple model for the behaviour of the probe in flowing air was given in Israel[1970, page 39]. The model considers a probe in air which has a uniform velocity v.

Using this model Israel has shown that current collected by the probe is independent of the shape and dimension of the probe and is given by the usual expression (equation 2.2) as long as the probe is smaller than a particular size which depends on the air flow speed and potential of the probe. For typical balloon measurements at ceiling altiude it is of the order of 0.05m. This is of the same order in size as the probe used during the experiment which has a radius of 0.1 m. But the flow around the probe is not a simple uniform flow as considered by Israel. At Reynolds number $\simeq$ 100 which is typical of the situation, the flow corresponds to a laminar to turbulent wake condition at the rear of the probe. A study of the probe behaviour under these conditions requires a numerical simulation which is beyond the scope of the present work. However some ideas regarding the behaviour of the probe can be obtained by using simplistic models.

Let us consider the case of a spherical probe kept in flowing air. We have to make some assumption of the rate of air flow around the probe. Let us take it as 2 m/s which is roughly the balloon ascent velocity. The probe dimension is taken as 0.1m. Reynold's number is an important parameter which determines what will be the nature of air flow around the probe. $Re = \frac{uL}{\nu}$ where u is the flow velocity around the probe, L is the probe dimension and ν is the kinematic viscosity of the ambient air. The values of ν was taken from US Standard Atmosphere[1962]. For air at 35 km $\nu = 2 \times 10^{-3} m^2$ per second. Thus Re at 35 km is of the order of

100 and it is higher at low altitudes. For air flowing around spherical bodies, a wake developes at the rear side of the body for flow Reynolds number greater than 10 [Batchelor, 1967]. The above mentioned rate of air flow past the probe is thus well within the regime of occurance of wake. We can safely assume that a wake is present and see whether its presence alters the current collection rate by the probe in any way.

Fig 2.2 which has been taken from Son and Hanratty[1969] shows a spherical probe in flowing air. The boundary of the wake formed by the movement of air past the body is also shown. Basic conservation laws of fluid dynamics demand that the fluid inside the wake remains inside and the fluid outside the wake remains outside[Landau and Lifshitz, 1959]. The wake itself can be considered as a cylindrical or semi-ellipsoidal body of fluid co-moving with the body. Under such circumstances, if the wake is stable and the probe is having some charge then the fluid trapped inside the wake will soon get depleted of ions of opposite polarity which will be collected by the probe. If such a situation is reached and is stable(for a length of time larger than one measurement cycle) then the only ion collected at the wake side will be those ions which cross the wake boundary and enter it due to Coulombic attraction.

Those ions that cross the wake boundary are eventually collected. The number of ions collected at the wake side by a probe was calculated for a flow velocity of 2 m/s and

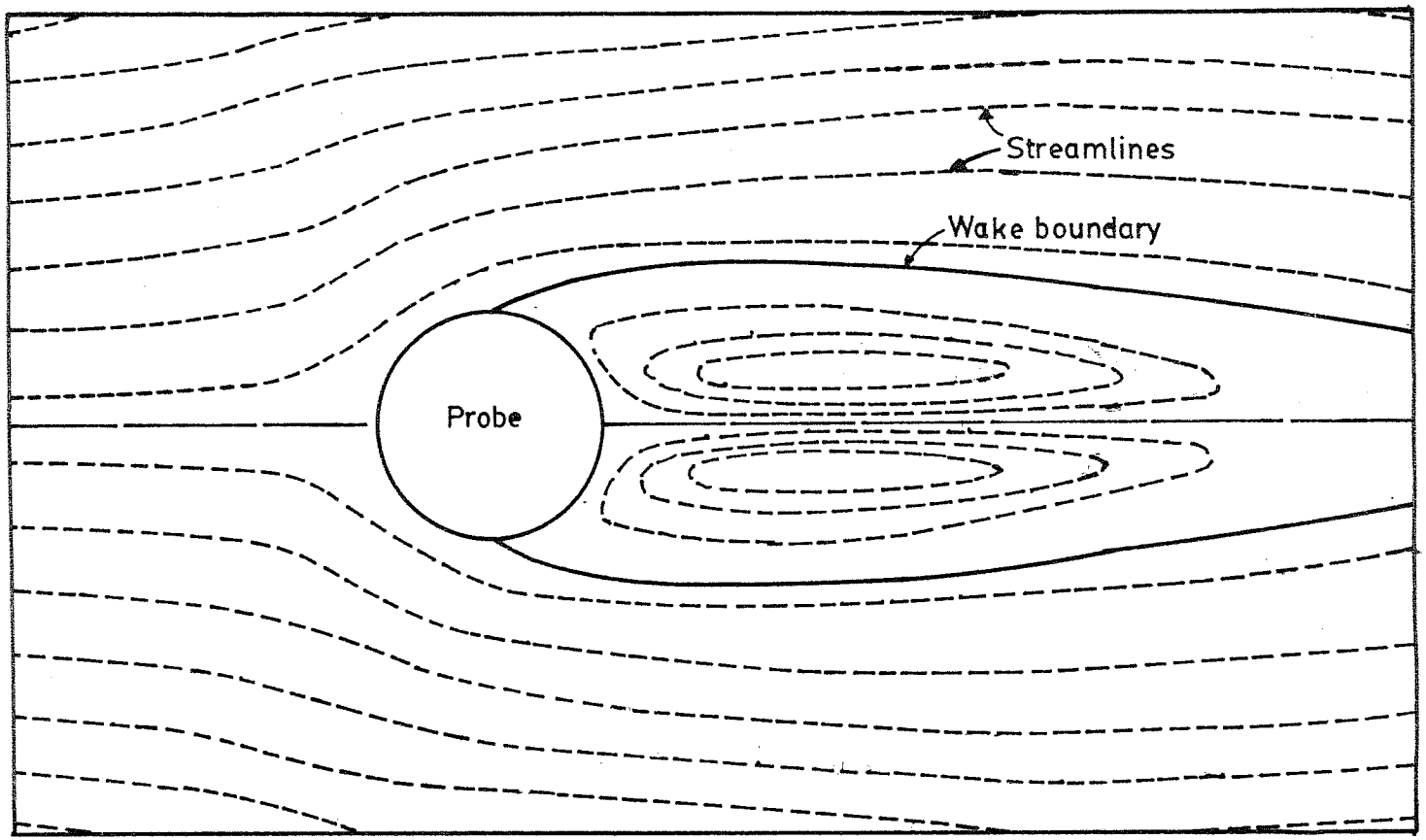

FIG 2·2 SPHERICAL PROBE IN FLOWING AIR (R=40)

conditions at 30-35 km altitude, assuming a spheroidal shaped wake. It was found to be roughly ten times less than the situation when there is no wake. This quantity has been found to decrease to very small values at high flow velocities. If one includes a wake in the calculation of current collected by the probe it will mean that most of the current will be collected by the front half of the probe. The rear half of the probe will collect a relatively small amount of current. Thus a wake-if it is formed and is stable in time, will reduce the total current collected by the probe by a factor of two. If relaxation time method is used then the resistance R of the air mass around the probe is doubled while the capacitance of the probe, C remains unchanged. The product RC is thus twice compared to its value when there is no wake. In other words, the measured σ will have a factor of two lower value.

However, one should apply this model with a caution. The balloon movement with respect to the ambient is not very well known. The velocity during ascent is fairly stable and relatively high. But during float the relative velocity between the air mass and the balloon depends on a number of parameters(e.g. gondola rotation) and this problem is not very well understood. This velocity is much smaller than the balloon ascent velocity. Moreover, its direction keeps on changing due to various gondola motions. There have been no direct measurements of this velocity but it appears that the conditions are not suitable for forming a strong steady wake during float period(meaning, a wake which remains

steady for period of time more than one measurement cycle). If however measurements are taken during ascent, the wake effect should be noticable. Rosen et al.[1982] have reported such an effect during an intercomparison campaign.

However a more accurate simulation supported by careful measurement of the air flow around the probe is necessary before arriving at any definite conclusion regarding the magnitude of error induced by air flow around the probe.

2.3.3 Effect of gondola and of return electrode

In our experiment the voltage decay of the conductivity probe takes place with respect to the ambient potential while the measurement is done with respect to the payload ground potential. This section deals with the relation between the ambient potential and the payload ground potential. In this section, only one aspect-the way in which the finite size of the gondola and return electrode affects conductivity measurement-will be discussed. Other aspects will be discussed later in this chapter in section 3.4.

The probe draws current from the surrounding ambient medium. In order to complete the electric circuit, the instrument should replenish this current to the medium. The return electrode performs this function. At any time one can assume that the amount of charge transfer from the medium to the gondola is the same as that from the gondola to the medium. We shall assume for the present discussion that there is no gondola charging effect(Actually there is, and

it will be discussed in the following section).

When a probe is charged to a potential V with respect to the payload ground potential, the average potential of the system is not changed as a result of this process. The potential difference V between the probe and the gondola is distributed into two parts: Vp, the potential difference between the probe and the ambient, and Vg, the potential difference between the gondola and the ambient. If Cp and Cg be the capacitances of the probe and the gondola respectively, then

$$V = \frac{CpVp + CgVg}{Cp + Cg} \qquad ..(2.28)$$

If the net charge on the gondola is zero then

$$CpVp + CgVg = 0 \qquad ..(2.29)$$

and Vp and Vg are of opposite polarities.

As a result of this, the probe and the gondola potentials will decay with different time constants, τp and τg. The time constant τp will be given by equation 2.2. The value of τg will depend on Cg as well as Rg which is the resistance corresponding to the discharging of the gondola. This is smaller than the resistance corresponding to a fully conducting body (mentioned in section 2.1.1) by a factor which is roughly equal to the ratio of the area of the return electrode and that of the gondola. If this ratio is α, then

$$\tau_g = \alpha \tau_{\pm} \qquad ..(2.30)$$

where $\tau_{\pm}$ is the decay time constant for a conductor in

contact with the surrounding medium on all sides. The measured potential at time t, Vt is then given by

$$V(t)^{\pm} = Vp \exp(-t/\tau p) + Vr \exp(-t/\tau r)$$

or $$V(t)^{\pm} = \frac{V(t=0)^{\pm}}{Cp+Cg} \left(Cg \exp\left(\frac{-t}{\tau^{\pm}}\right) + Cp \exp\left(\frac{-t}{\alpha\tau^{\pm}}\right)\right) \quad ..(2.31)$$

In our instruments the ratio Cg/Cp was between 10 and 20 so that the net decay curve was a (weighted) superposition of two decay curves, the weighting factor being of the order of 10: 1. This superposition introduces a distortion in the decay curve and the measured conductivity can have a typical error of 5 percent and a maximum of 10 percent as a result of this distortion.

2.3.4 Photoelectron emission from probe surface

Photoelectrons are emitted by metallic or carbon coated surfaces when photons having energy greater than the work function of the surface material are incident on them. For aquadag (amorphous carbon) coated surfaces the work function is 4.8 volts[CRC Handbook of Phys. & Chem. 1984-85] and the threshold wavelength is 260 nm. Photoelectron emission occurs when photons having wavelength smaller than 260 nm are incident on the surface.

At stratospheric altitudes, the ultravoilet component of the incoming solar radiation is substantially higher than that at the ground level. With increased ultravoilet flux it is quite possible that the probe starts emitting electrons when exposed to sunlight. Such a situation occurs during

daytime measurements. Nighttime measurements of conductivity are free from any possible contamination due to photoelectron emission from the probe. In the present section the possibility of contamination of conductivity measurement due to photoemission from probe surface during daytime is discussed.

Most of the UV components of solar radiation get absorbed by the atmosphere before they reach the stratosphere. The intensity of solar radiation reaching down to 35 km is negligibly small for wavelengths less than 190 nm. The probes which have been used were aquadag coated. As has been mentioned earlier, wavelengths greater than 260 nm will not contribute to photoelectron emission from aquadag surfaces. The wavelengths between 190 nm and 260 nm are also strongly attenuated, but a small portion of it does reach down to 35 km.

A theoretical calculation was done to estimate the magnitude of photoelectron emission to be expected at stratospheric altitudes. For this estimate, the amount of solar radiation reaching the given altitude was first calculated for various wavelengths. These were multiplied by photoelectron yields for the corresponding wavelengths to get the photoelectric current density. The incoming flux of solar radiation for this calculation was taken from Whitten and Popoff[1965, p22]. The spectral cross sections of O_2 and O_3 were taken from the data compiled by Deshpande and Mitra[1983]. O_3 number density was based on thumba model[Subbaraya and Jayraman, 1987] while the O_2 number

TABLE 2.1

Estimated magnitude of Photoemission from the Conductivity Probe (Radius 10 cm.)

Month	Time (A.M.)	Alt. (km)	Solar Zenith Angle(Deg)	Probe Current ($X10^{-8}$amp)
April	9.15	35	43	3.375
April	12.00	35	10	4.695
October	9.30	32	40	1.855
October	11.45	32	27	2.334
December	8.40	34	62	1.326
April	7.30	34	70	0.522
April	8.00	29	68	0.082

density was based on Thumba air density[Sasi and Sengupta, 1979]. The extinction coefficients of Ozone and Oxygen were calculated and Beer Lambert's Law was used to get the attenuated values of solar UV flux. The photoelectron yield values given by Feuerbacher and Fitton[1972] were used for this calculation. The results of this calculation which are tabulated in table 2.1 are quite interesting. According to this calculation, the photoelectric current is orders of magnitude higher than those expected during conductivity measurement. Before coming to any conclusion about this result, let us also see in what way will photoelectron emission manifest during conductivity measurement.

Figure 2.3, 2.4 and 2.5 depict three hypothetical situations. In each case, the current voltage characteristics are given on the left side and the corresponding voltage decay curves are given on the right side.

Figure 2.3a shows the current voltage characteristics of the probe when there is no photoelectron emission. A linear dependence of the probe current on probe voltage exists as given by equation 2.3a. The current voltage characteristic curve is thus a straight line. The decay curve on the right is obtained with help of the following integral:

$$V(t) = V(t=0) - \frac{1}{C} \int I(t')dt' \qquad ..(2.32)$$

For fig 2.3b, the decay curve is exponential.

CASE-1

Photoelectric effect not present

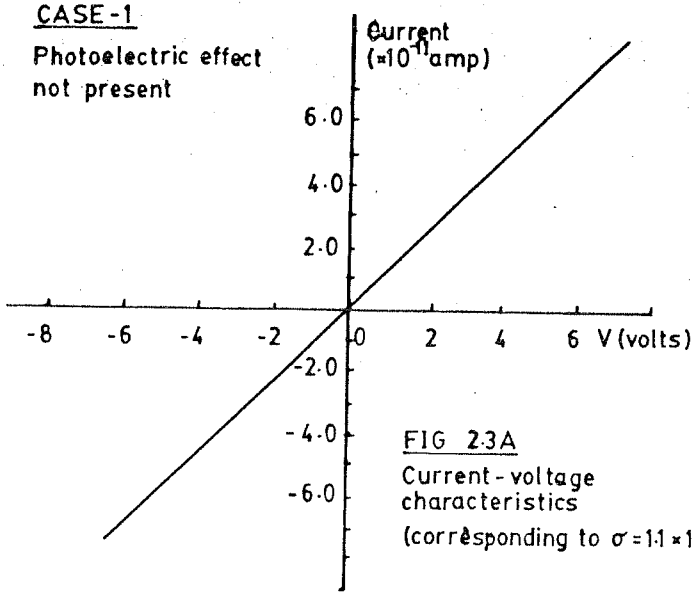

FIG 2·3A
Current-voltage characteristics
(corresponding to $\sigma = 1.1 \times 10^{-11}$ s/m)

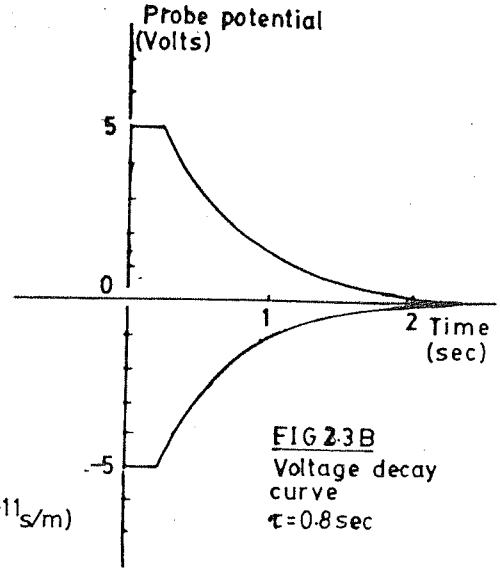

FIG 2·3B
Voltage decay curve
$\tau = 0.8$ sec

CASE-2

Photoelectric current of the order of typical probe currents

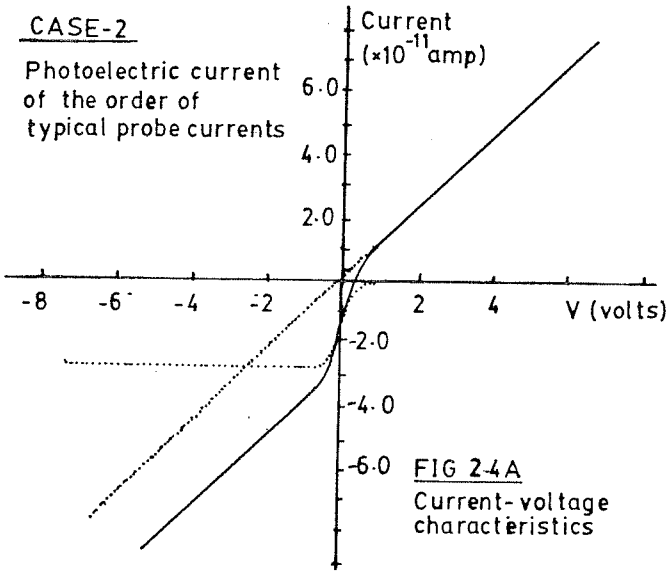

FIG 2·4A
Current-voltage characteristics

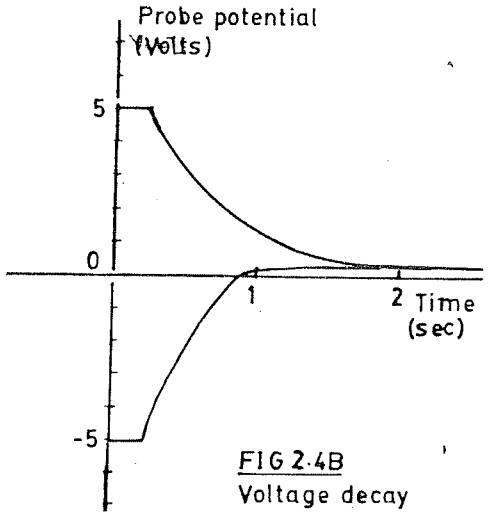

FIG 2·4B
Voltage decay curve

CASE-3

Photoelectric current larger than typical probe currents

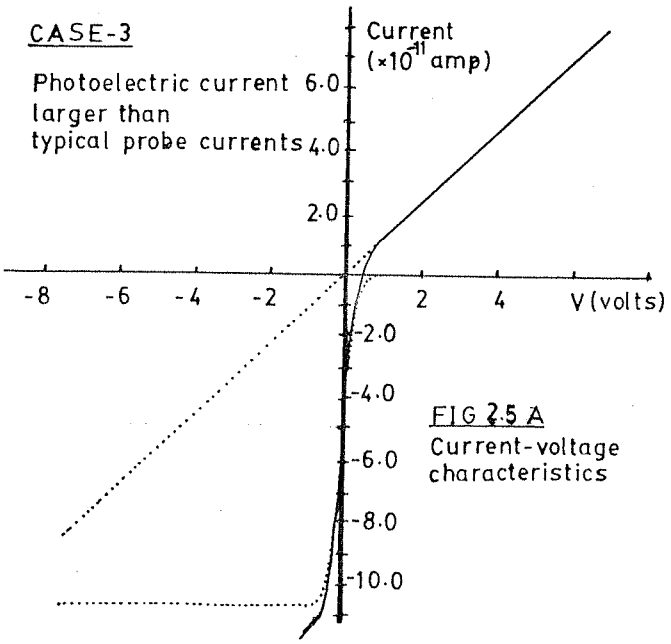

FIG 2·5A
Current-voltage characteristics

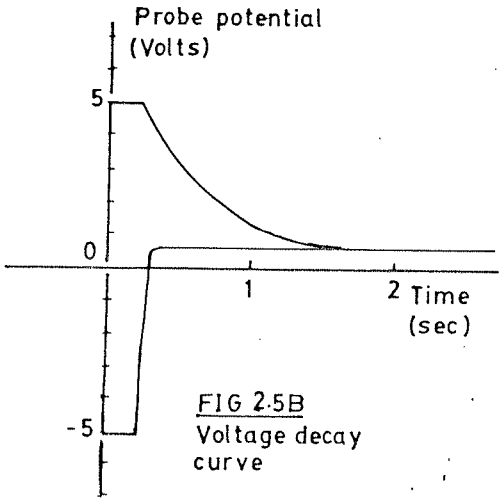

FIG 2·5B
Voltage decay curve

The next figure depicts a situation when photoelectron emission currents are of the same order of magnitude as those involved in the measurement. The shape of actual voltage-current characteristic for photoemission due to a single wavelength of incoming radiation has been discussed by Derberwick et al.[1974]. Since there is a finite bandwidth of the incoming radiation in the present case, a number of such characteristic curves have to be integrated in order to obtain the overall effect. For our purpose, however, an approximation will be enough. In the present case, the current-voltage characteristic for photoemission has been approximated by the dotted curve in figure 2.4a. The solid curve gives the sum of conductivity current and photoelectric current. The voltage decay curve corresponding to it has been calculated using equation 2.32 and is shown in fig 2.4b. The figure shows that the voltage decay curve corresponding to negative ions is not affected. But the decay curve corresponding to positive ions is distorted and is steeper than the exponential curve of fig 2.3b. The degree of distortion from the exponential will give the extent of contamination of the positive conductivity due to photoemission.

Fig 2.5a shows current voltage characteristics similar to the previous one, only, the photoelectric current here is assumed to be higher than typical probe currents by a factor of two. Fig 2.5b shows the voltage decay curve corresponding to it. It is clearly demonstrated that it is not possible to retrieve any positive ion conductivity

value under these conditions,or under conditions when the photoemission is still more.

In our balloon flights,we obtained voltage decay curves which were only slightly distorted from true exponential shapes (Fig 3.16). Thus the possibility of photoelectric emission to be orders of magnitude higher than typical conductivity currents, which was predicted by theoretical considerations earlier in this section has been ruled out. The reason for this kind of behaviour of the probe is not clear. One possible reason is that the photoelectric efficiency of the probe surface materials as measured by Feuerbacher and Fitton under laboratory conditions are too large compared to the values under in-situ flight conditions. Due to surface contaminations during the actual flight, the photoelectric efficiency might be getting drastically reduced. There is also a possibility that the intensity of the solar ultravoilet radiation reaching the balloon altitude is less than the calculated value(which considers extinction by O_2 and O_3),but this is not expected to add more than 50 percent to the total extinction. Considering the small magnitude of shape distortion in the decay curve, one can say that the effect of photoelectric emission on measured conductivity at this altitude,if any, is small. There is a little distortion present in the decay curves and the curves corresponding to positive ion conductivity are a little steeper than exponential.But it is not possible by examining the data obtained during the daytime flights to ascertain whether this is an effect of

photoemission, or of finite gondola size(section 2.3.3). Looking at the decay curves obtained experimentally(Fig 3.16), one can say safely that the overall error due to the photoelectric emission as well as the gondola effect(section 2.3.3) is within 10 percent.

2.3.5 Size and placement of sensor in instrument design

Optimum probe size: In the relaxation time technique for conductivity measurement it was shown in section 2.1.1 that the decay time constant does not depend on dimensions of the sensor. But when one makes measurements, one connects a voltmeter to the sensor which requires a small but finite current for making the measurement. We have used preamplifiers which require about 0.15 pico-ampere current for making proper measurement. The sensor should be large enough to provide this current without the probe getting appreciably loaded. The loading effect by the probe has been discussed by Slamanig [1981] who has given the following expression to estimate the error involved in electric field measurement:

$$\frac{\Delta V}{V} = \frac{1}{4\pi r_o R_i \sigma} \qquad ..(2.32)$$

where ro is the probe radius and Ri is the internal resistance of the instrument. This comes out to be 8×10^{-4} in the present case, and can be neglected.

In a similar way the error in conductivity can be

evaluated. The error in the measured voltage is given by the following equation:

$$\Delta V = Ri * Ii \qquad ..(2.33)$$

The input current of the instrument, Ii, as mentioned above is 0.15 picoampere while Ri is given as $1/(4\pi r_p \sigma)$. The value of ΔV comes out to be less than 0.2 volts, which is negligible in the present case.

If necessary, one can increase the sensor size to reduce the above mentioned error. But again, the upper limit is governed by the fact that a larger sensor will load the overall measuring system resulting in distortion of the voltage decay curve (section 2.3.3). For larger sensors one requires larger return electrodes. But a too large return electrode might be a source of other problems which will be discussd in section 2.4.1. A consideration was made of all these points and a spherical sensor having 20 cm diameter was chosen. Typical gondola dimensions are between 1 and 2.5 meters (section 3.2.2).

In order to make measurements in-situ, a boom of approximately 1m. length was employed. The boom was deployed from the gondola. The sensor was connected at the end of the boom. This ensured two things: (1) The stray capacitance effect due to presence of other bodies near the sensor was small, and (2) the air near the sensor was less affected by the presence of gondola. The gondola can contaminate the air

through degassing. Also, since the gondola is a large body, it will deplete the surrounding air of ions when it gets charged due to air friction(section 2.4.1).

2.4 The problem of gondola charging

The gondola which carries the instruments during balloon flight, has been found to get charged during balloon ascent, and remain so for some time after the balloon has reached the floating altitude. We observed this problem of charging of the gondola during our balloon flights when we were unable to get conductivity data during the ascent period of the balloon[Gupta, 1987]. In the present section some of the investigations done by the author regarding the behaviour of the balloon-borne gondola are reported.

2.4.1 The gondola charging during balloon ascent

During the balloon ascent, the telemetry channels in the conductivity and the electric field experiments were found to get saturated. These channels correspond to the measurement of the probe potential with reference to the payload ground potential and their getting saturated means that the potential difference between the probe and the gondola is greater than the payload supply voltage, which was ± 12 volts. This state has been found to be present throughout the balloon ascent period and continue upto 2

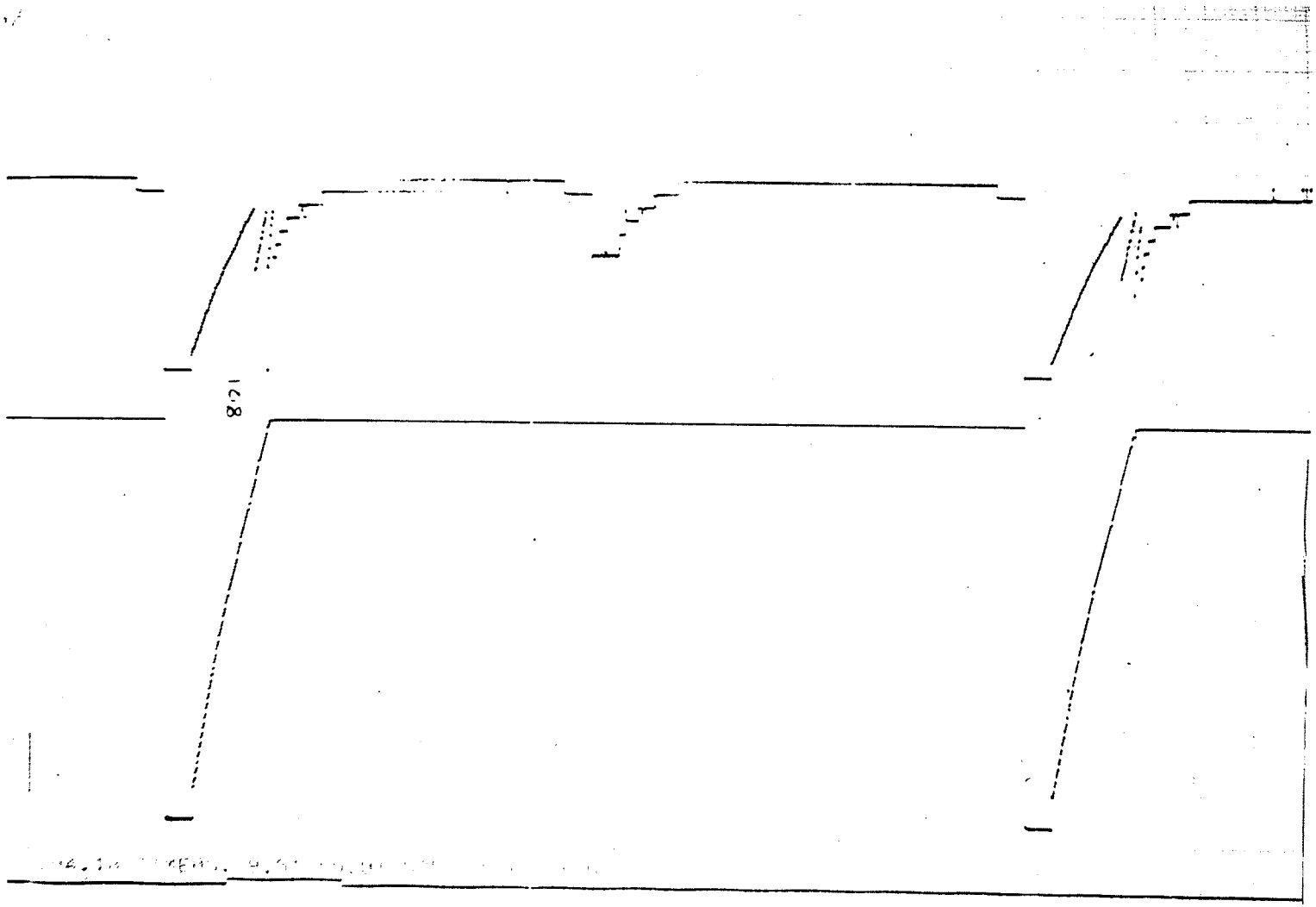

FIG 2.6 TELEMETRY OUTPUT DURING BALLOON ASCENT

hours, after the balloon has reached the float altitude. Fig 2.6 shows how the telemetry outputs appear during ascent. One can compare it with fig 3.16 which shows telemetry output at a time when it was possible to make measurement. The asymptotic voltage level in the decay curve has shifted out of range in fig 2.6 thus making it impossible to measure the time constant. The direction of shift of the asymptotic voltage level in fig 2.6 corresponds to a situation where the gondola is positively charged with reference to the ambient medium. In this subsection, some of the observations related to this effect which were made in course of our balloon experiments are presented. The following points were observed:

1. After the balloon was launched, the voltage output of the conductivity channel in the instrument (which also gives the potential difference between the probe and the gondola) was found to fluctuate in a random manner with amplitudes which were apparantly much larger than the telemetry output range.

2. When the balloon ascended to higher altitudes, fluctuations were still present in the voltage discharge curve, but the probe potential tended to settle at the negative side.

3. Above 13 km altitude, the discharge curve became smoother, and it used to quickly settle to the saturation value at the negative voltage limit of the

telemetry channel.

4. This state continued for some time after the balloon reached ceiling altitude. It took a period of time between about 15 minutes to 2 hours before the asymptotic voltage of the decay curves gradually came down to values within the telemetry range of ± 5 volts.

5. In one of the balloons (IMAP-C2), an 'APEX' valve was used. Using this valve the balloon was made to float at two different altitudes. It was observed that the gondola potential remained small during the float period, but shifted towards the positive side, both during balloon ascent as well as descent. Thus it appears that the polarity of the gondola charging does not depend on the direction of motion of the gondola, i.e. whether the gondola ascends or descends the effect is same.

From these observations, it appears that the gondola charging process takes place when there is a relative motion between the surrounding air mass and the gondola. Frictional forces are velocity dependent and the cause of charging in the present case also appears to be frictional.

For a better understanding of the problem an estimate of the extent of this charging is desirable. Since the telemetry channels get saturated during the balloon ascent it is not possible to make a direct measurement of the potential of the gondola. An estimation of this quantity was

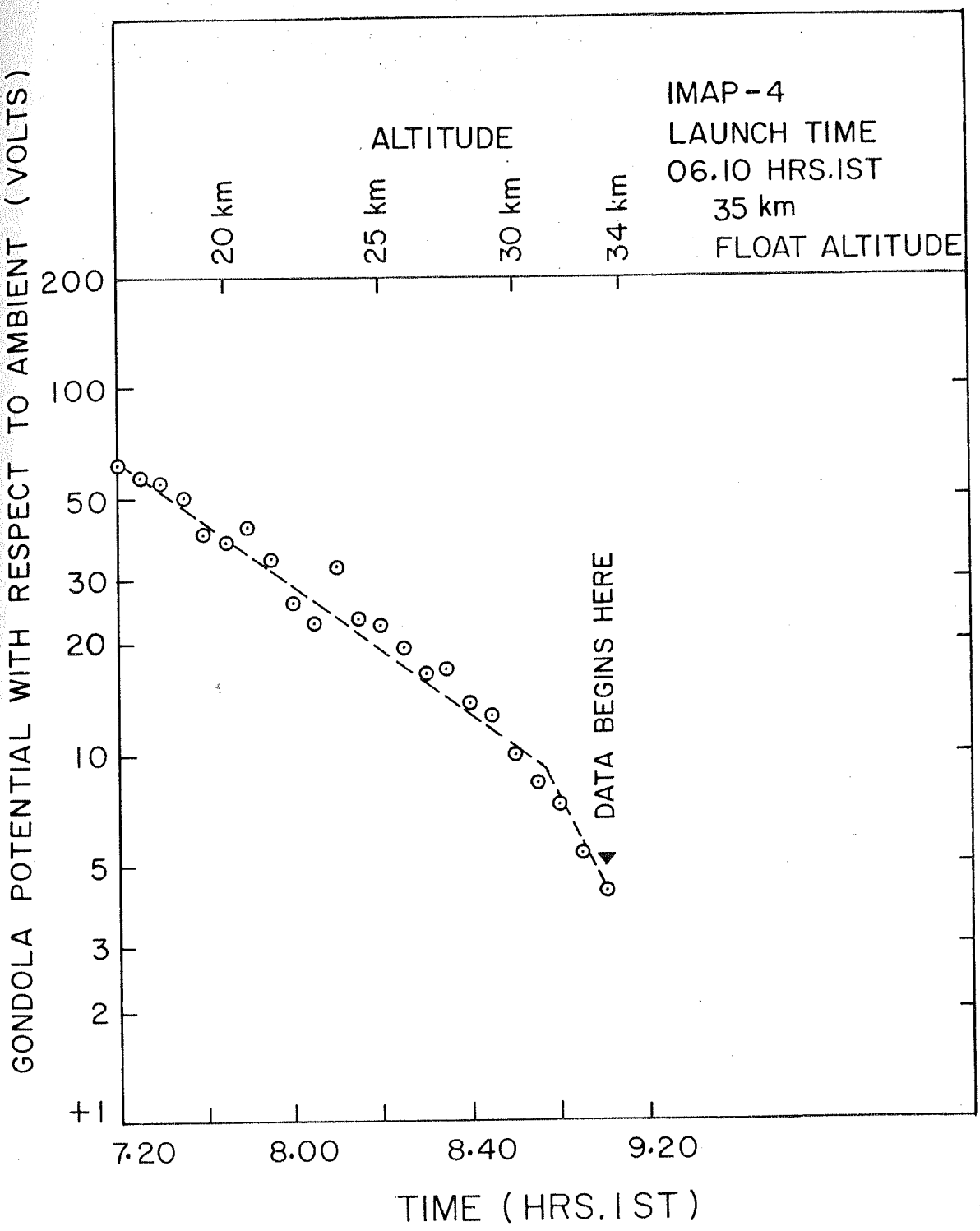

FIG 2.7 IMAP-4 Gondola potential variation

done using the method described below.

The current collected by the probe at any given stage of its voltage decay can be written as following:

$$I = \frac{dQ}{dt} = C \frac{dV}{dt}$$

$$V = IR = RC \frac{dV}{dt}$$

$$\text{or,} \quad V = \tau \frac{dV}{dt} = \frac{\epsilon o}{\sigma} \frac{dV}{dt} \qquad ..(2.34)$$

The only problem wih using this expression for estimating V is that σ is not known at all the altitudes. The slope $\frac{dV}{dt}$ can be measured directly on strip chart data.

For the sake of calculation, the conductivity was assumed to increase exponentially with height[Volland, 1984]. The measured conductivity at float altitude was used as a reference for this and the conductivity values at other altitudes were calculated using the expression given below, with scale height H as 7.5 km:

$$\sigma = \sigma o \exp(h/H) \qquad ..(2.35)$$

Here, h is the altitude above the reference level and σo is the conductivity at the reference altitude.

This estimation was done for one daytime flight (IMAP-4) and one nighttime flight(IMAP-7).(Details of these flights are given in table 4.1). The values of floating potentials observed during these flights are given in fig 2.7 and fig 2.8. In this section the floating potentials of these flights as observed during ascent time will be

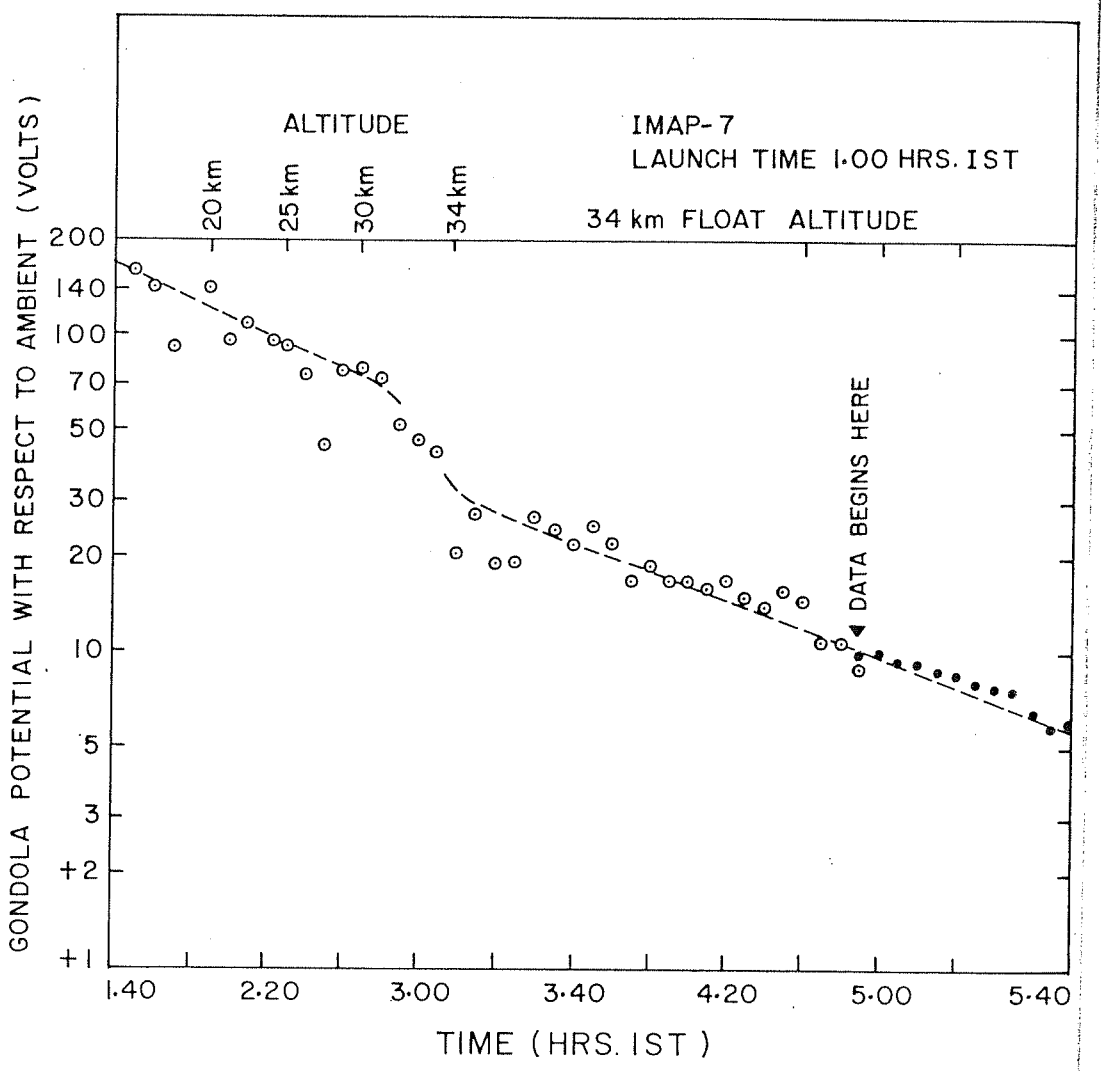

FIG 2.8 IMAP-7 GONDOLA POTENTIAL VARIATION

discussed. The following observations can be made regarding these floating potential values

1. During IMAP-7(night) flight, the gondola potential at 15-20 km was between 100 V and 160 V. These values are probably on the higher side because the conductivity measured at the ceiling altitude during that flight are smaller than the normally occuring values.(This is due to presence of volcanic aerosols in the stratosphere).

2. The ascent velocity of IMAP-4 was around 2.6m/sec while that of IMAP-7 was 4.7m/sec. The gondola potential in the latter case at 15-20 km was about twice that for IMAP-4. At higher altitudes, this ratio was still higher.

There have been no measurement of the balloon gondola potential to date in the knowledge of the author. Some measurements of potentials developed on rocket bodies exist [e.g. Raja et al., 1981] which show that rocket bodies get charged to several kilovolts during flight. Similar measurements for balloon borne gondolas are also necessary.

2.4.2 Floating potential at ceiling altitude

It takes some time for the gondola to dissipate its charge after it has reached floating altitude. This period can be as small as 15 minutes(for IMAP-4) or as large as 2

hours(for IMAP-7) or more. Only after this time has elapsed, does it become possible to make conductivity measurement. This subsection describes the different factors which might be influencing the gondola potential.

In section 2.3.3 I have discussed the way in which the gondola size and the size of the return electrode affect the potential of the gondola. The gondola charging effect points to at least one more factor which is important in determining the gondola potential.

That such a source of charging also exists during the float period of the balloon can be said because it takes upto 2 hours time (during a night-time flight) for the gondola to discharge from typically 20-25 volts down to less than 10 volts(Fig 2.7). The conductivity of air being greater than 10^{-12} s/m at 34 km altitude(float altitude), it should not take more than about 10 seconds time to dissipate this much charge. The time constant is given by $\epsilon o/\sigma$, where ϵo is equal to 8.85 X 10^{-12} farad per meter while σ is of the order of 10^{-11} s/m. Actually it took more than 2 hours time during the float for the potential to come down. This points to the existence of a source of charging which is active even during the float period (although to a lesser extent).

The most probable source of this charging is the airflow around the gondola. The large amount of charging during ascent might be attributed to the bulk flow of air past the gondola as the balloon ascends, while the smaller amount of charging during float might be caused by a

smaller amount of (horizontal) air-flow past the gondola as it is carried about by the wind.

During daytime the gondola potential is less(Fig 2.8). The reason for this appears to be connected with either photoelectric effect or heating of the return electrode by sunlight. But the mechanism is still to be explained.

2.5 Electric Field Measurement

Vertical electric fields exist in the stratosphere which have magnitudes of the order of a fraction of volts per meter. Instruments that measure electric fields in the atmosphere employ either of the two techniques described below. These two techniques are: (1) the double probe technique and(2) the electric field mill technique. The author has used the double probe technique whose principle of measurement will be described in this section. Some considerations involved in the measurement technique used will also be discussed. The field mill technique, although an important technique[Israel, 1973] will not be described here.

2.5.1 The Double Probe Method

The double probe technique for electric field measurement consists of using two probes which are kept at their respective floating potentials. The potential difference between them is measured. When two conducting bodies are seperated by a distance d in a weakly conducting

medium having an ambient electric field, and allowed to float, they eventually acquire potentials whose difference is related to the potential difference corresponding to their locations in the ambient medium. This potential difference divided by the distance of seperation between them gives the electric field component in the direction along the seperation of the two bodies.

Fahleson [1967] has described the theory of electric field measurement in detail. Although this theory deals with electric fields in the ionosphere, a more or less similar mechanism is involved in stratospheric measurement process.

Fig 2.9 depicts the relationship between the measured electric field and the ambient electric field for measurements in the stratosphere. The following equation gives the relation between the measured potential difference between the probes and the ambient electric field which exists at the location.

$$Vm = E.d + \Delta W + \Delta V' + \Delta Vf \qquad ..(2.36)$$

where Vm is the measured voltage, ΔW is the difference in work function of the surfaces of the two probes, ΔV is the error in voltage measurement due to finite current drawn by the instrument(section 2.3.5), and ΔVf is the error due to frictional charging effect mentioned in section 2.4.2. E is the electric field we are trying to measure and d is the vector seperation between the two probes.

The presence of the gondola distorts the electric field

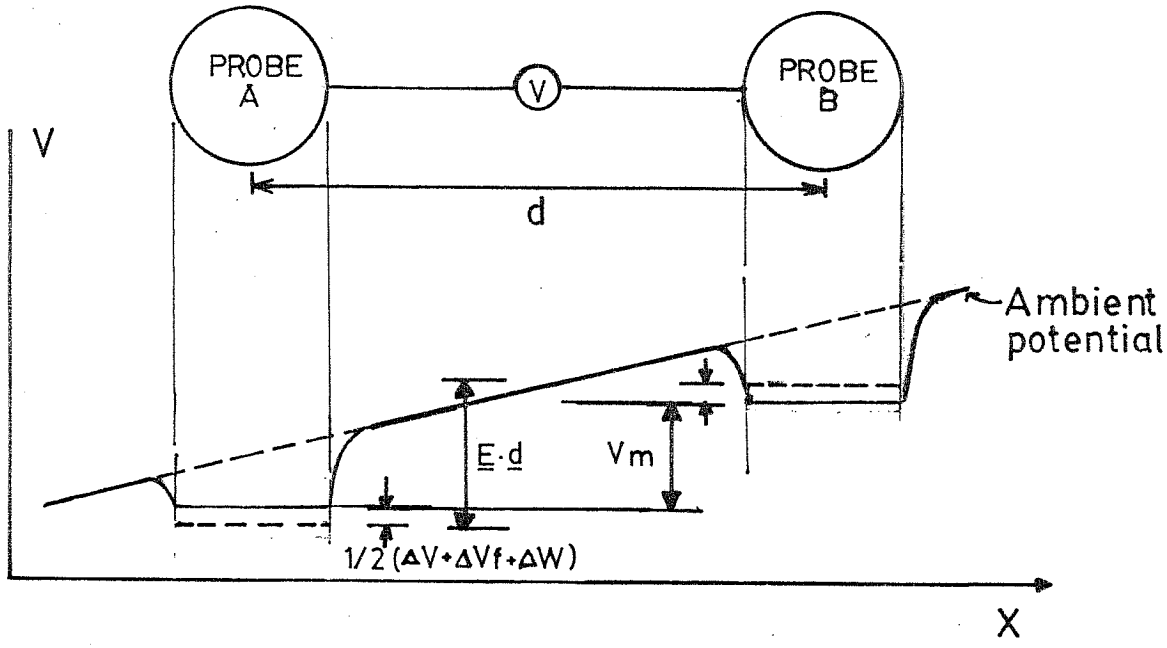

FIG 2.9 MEASUREMENT OF ELECTRIC FIELD USING DOUBLE PROBE

lines appreciably. A correction has to be applied to compensate for this distortion of field lines. This aspect will be dealt with in section 2.5.2. In the present subsection, the different terms in equation 2.36 will be discussed.

The work function of the surface of a conductor is the potential difference which exists between a point inside the conductor and a point outside it. The work function expressed in electron volts is the energy required for an electron inside the conductor to be ejected out of its surface. This quantity depends on the material of the surface as well as the way in which it is prepared. We have used aquadag coated probes which has workfunction 4.8 volts. All the probes were prepared in identical manner so as to ensure that work function differences between the probes are minimum. This difference is expected to be less than 50 mV.

The third term in equation 2.36 is ΔV, the error due to measurement process. ΔV is given by equation 2.32. The error due to this term has already been discussed in section 2.3.5 and has been shown to be small.

The fourth term ΔVf is the difference of the probe potentials due to the frictional mechanism which charges the gondola. Since the probes are identical, the only difference that can occur in their potentials will be because of differences in flow velocities past the probes. The exact dependence on various parameters is not known and all we can say is that ΔVf is some function of $(u1-u2)$.

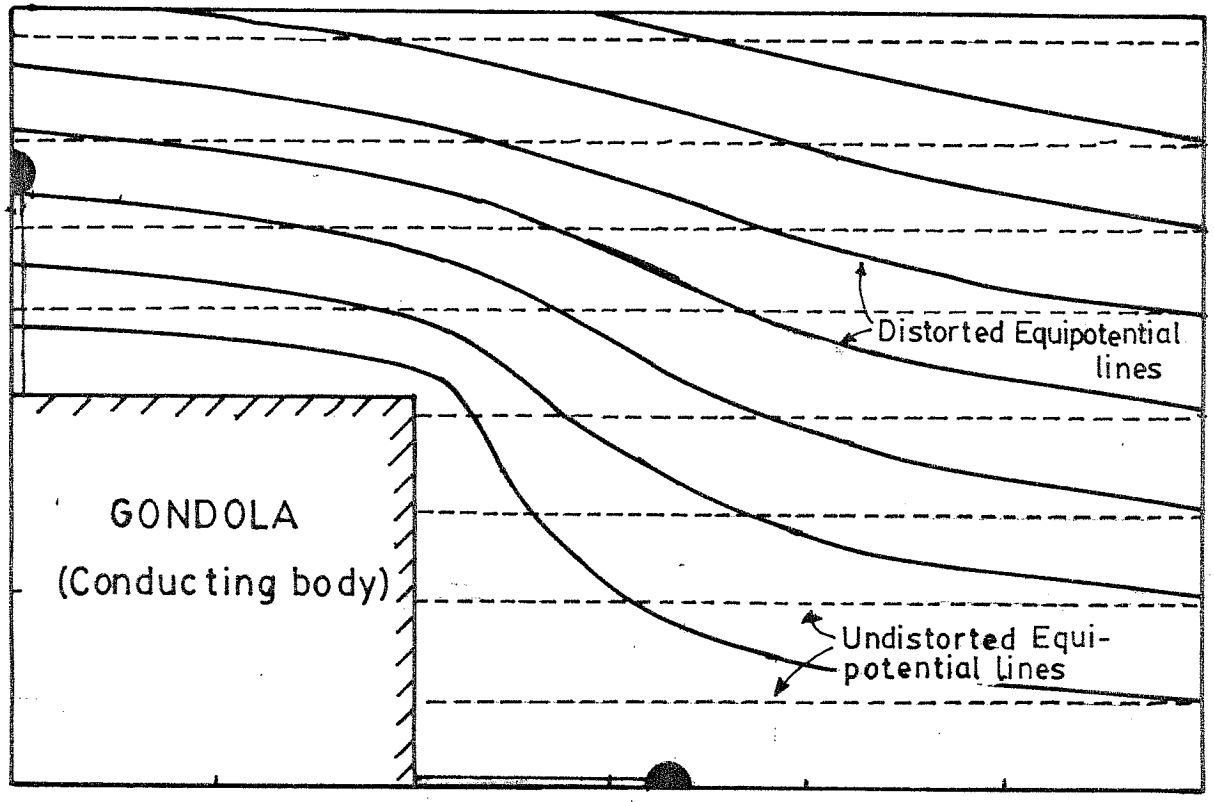

FIG 2·10 DISTORTION OF EQUIPOTENTIAL CURVES DUE TO PRESENCE OF GONDOLA

Although symmetry is maintained to the extent possible in the size and placement of the probes, it is quite possible that the difference between u1 and u2 is non-zero, for example when the gondola rotates. At present this quantity is difficult to estimate theoretically. Unless it is measured, the contribution due to this term is difficult to establish and estimate. The large almost random fluctuations in the electric field raw data(fig 4.10) of IMAP-7 might be partly attributed to this source of error.

2.5.2 Field distortion due to presence of gondola

In the double probe technique described in section 2.5.1, it was implicitly assumed that the presence of the measuring instrument does not distort the ambient electric field. Actually the situation is not so. The size of the gondola in the present experiment is comparable to the vertical distance between the probes. The effective distance between the probes in such case is different from the physical distance, because the electric field lines near the gondola get distorted by its presence and a correction has to be applied.

Fig 2.10 depicts distortion of equipotential contours in an ambient vertical electric field, around a conducting body such as a balloon-borne gondola. The dotted lines show the corresponding undistorted equipotential lines. This diagram has been adapted from Kirchoff[1985, p88] which gives a solution for Laplace's equation for the case of an

unbounded step function in two dimensions. For the three dimensional case, the field lines over the body get compressed roughly, by a factor of 0.66. This factor has been estimated by making a comparison between the spherical and cylindrical cases for which exact solutions exist. This ratio for rectangular (2-d) and rectilinear (3-d) boundary conditions is expected to be within 15 percent of this ratio. The effective distance between the probes for IMAP-7 payload is thus about 1 meter(for the configuration depicted in fig 3.2c).

2.6 Measurement technique for Mesosphere

Mesospheric conductivity measurement is done using rocket and parachute borne probes. The technique used as well as the nature of data that one obtains in the mesosphere are different from those in the stratosphere where the balloon-borne techniques are used. While balloon-borne techniques make long duration measurements at single altitude, rocket and parachute borne techniques give a height profile at a given time. Techniques which have been successfully used in the mesosphere are Gerdien condensers[Leiden, 1976], Langmuir Probes[Prakash et al., 1967, 1974, Subbaraya et al. 1985], and Blunt probes[York et al., 1982]. Langmuir probes have been used for a long time in our laboratory for measurement of the plasma parameters in the Ionosphere[Subbaraya et al., 1985]. In this section the use of Langmuir probes for measurement of ion and electron

conductivity in the mesosphere is described.

2.6.1 Conductivity measurement using Langmuir Probe

Langmuir probes are used for measuring plasma parameters in a given ionised medium. The principle was first given by Mott Smith and Langmuir[1926] in their classic paper. Several scientists have used Langmuir probes for measurement of ionospheric parameters since then[Ichimaya et al., 1960, Spencer et al. 1962, Boyd and Willmore, 1963, Prakash et al., 1967]. Smith [1969] has given an adaptation of the original theory for ionospheric measurements. Langmuir probes have been used with success at altitudes above 100 km[Subbaraya et al., 1985]. But in the mesosphere, the behaviour of Langmuir probe is not understood very well because this is a transition region below which air behaves as a viscous fluid while above it air molecules display kinetic behaviour. Thus, any measurement done in this region has to be interpreted carefully. In the present section the applicability of Langmuir probe theory in this region has been discussed.

Langmuir probes are current collecting probes. The probe consists of a conductor of spherical or some other shape. In the present work an ogive shaped probe was used[Prakash and Subbaraya, 1967]. This probe was biased at a potential of 4 volts (with respect to its return electrode potential) using electronic technique and the current collected by it was measured. A positive and negative(sawtooth shaped)

voltage sweep was also applied for a part of the time. The measured current I under such a situation is related to the conductivity σ by the following relation:

$$I = \frac{\sigma A V}{L} \qquad ..(2.37)$$

where V is the probe biasing potential, A is its effective area of current collection and L is its effective size parameter(~ radius). As mentioned above, the behaviour of the Langmuir probe is different in the collision dominated stratosphere and the collisionless upper atmosphere. In the uper atmosphere, the current collected by a positively biased spherical Langmuir probe is given by the following equation[Smith, 1969]:

$$I = Io\ (1 + \frac{eV}{kT}) \qquad ..(2.38)$$

Here Io is the current collected at the floating potential and is given by the following equation[Subbaraya et al.(1983)]:

$$Io \simeq Ae(\frac{kTe}{2\pi m_e})^{\frac{1}{2}} n_e \qquad ..(2.39)$$

The equations will also hold for small probes which have shapes that are not exactly spherical, but nearly so, for example, an Ogive shape.

The current collected by a negatively biased probe will depend on ion conductivity according to the equation 2.37 above. This equation can thus be used for measurement of ion

conductivity. The effective area A can be either calculated theoretically, or a calibration can be done. The latter method was used for getting the effective area in the present case. This method is described in section 2.6.2. The effective area obtained was 3.7 sq.cm. Equation 2.37 was then used for calculating the ion conductivity.

The ion conductivities obtained in this way are given in Figure 4.11.

2.6.2 Method of Calibration of Langmuir Probe

The expressions (equations 2.38 and 2.39) for electron density obtained from Langmuir probe current provides a means for getting the effective collection area for the Langmuir Probe in the mesosphere. Electron density measurements can be done by several in-situ techniques. Langmuir probes are good for studying fluctuations in electron density. But they do not give the absolute electron density values that accurately. For good absolute values they have to be calibrated using other techniques like radio propagation technique.

Two rockets were launched on 16th February 1980 and 17th February 1980 These rockets carried a Langmuir Probe payload from PRL and a radio propagation receiver from NPL(New Delhi). The radio propagation technique involves measurement of attenuation of radio waves propagated through the atmosphere between the ground and the rocket for obtaining the absolute electron density[Somayajulu,

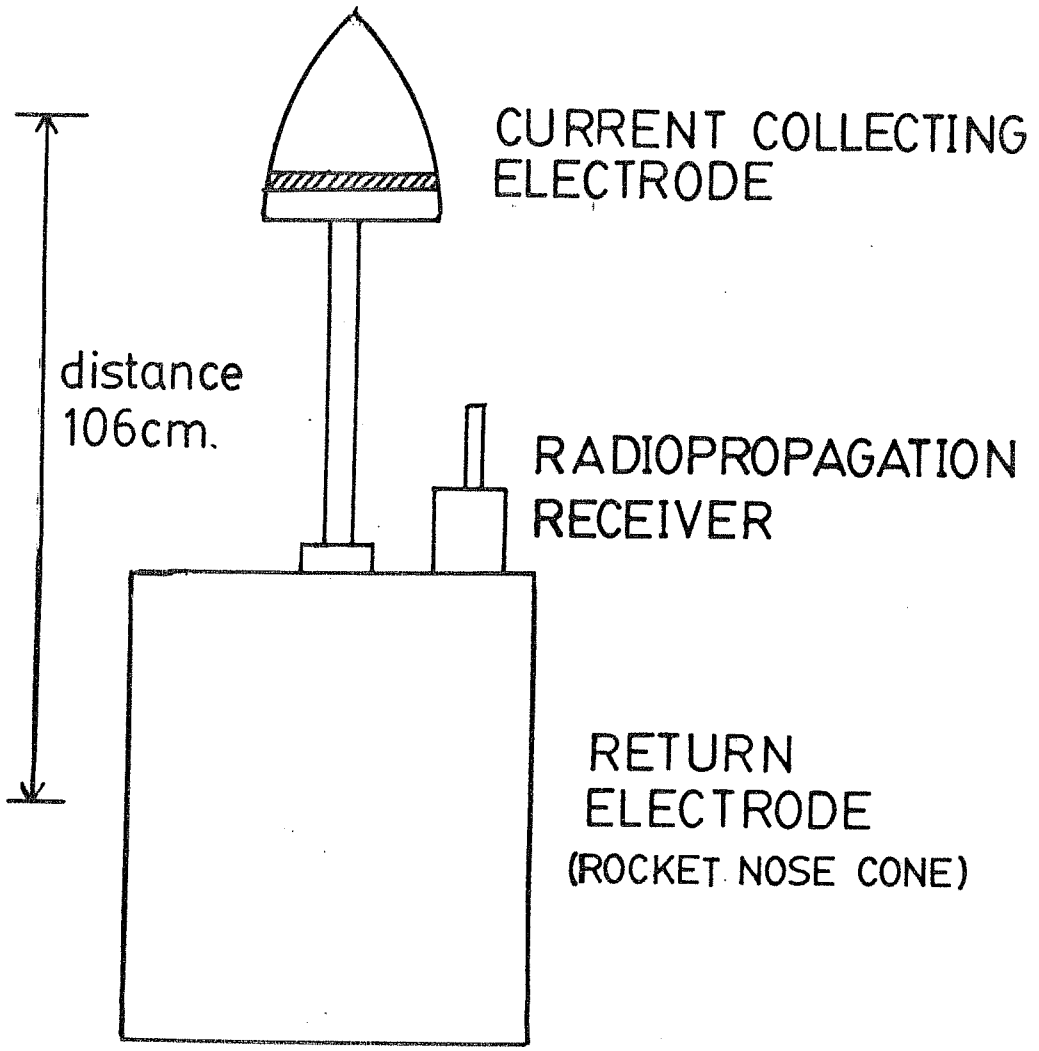

FIG 2.11 LANGMUIR PROBE WITH RETURN ELECTRODE

1971]. This method is considered quite relliable for the measurement of absolute electron density. Both the probes gave measurements between 70 km and 90 km. The electron densities obtained from radio propagation technique have been calculated by Somayajulu et al.[1982]. Langmuir probe current measured during these flights are depicted in fig 4.12. The ratio of Langmuir probe current to electron density has been given in Table 2.2. The values have been plotted with altitude and are given in figure 2.12. The ratio is nearly $\simeq 3 \times 10^{-10}$ amp.cc over the altitude region 70 to 82 km during one of the flights and 77 to 85 km during the other. The peaks which appear at higher altitudes will be seperately discussed in section 2.6.3 and 5.9.

In collision dominated regions, Ip/ne will be given by the following equation:

$$Ip = \frac{ne^2}{m_e \nu} A_p \qquad ..(2.40)$$

The collision frequency decreases exponentially with altitude so that in collision dominated regime characterised by equation 2.40, the probe current ought to increase more or less exponentially with altitude. On the other hand, the collisionless model, which is characterised by equations 2.38 and 2.39 does not predict such a change in the $\frac{Ip}{Ne}$ ratio with altitude, except for the square root of temperature dependance. Thus based on the temperature variation between the altitudes 75 to 90 km, the ratio of $\frac{Ip}{Ne}$ should be within a factor of 1.25 if the collisionless

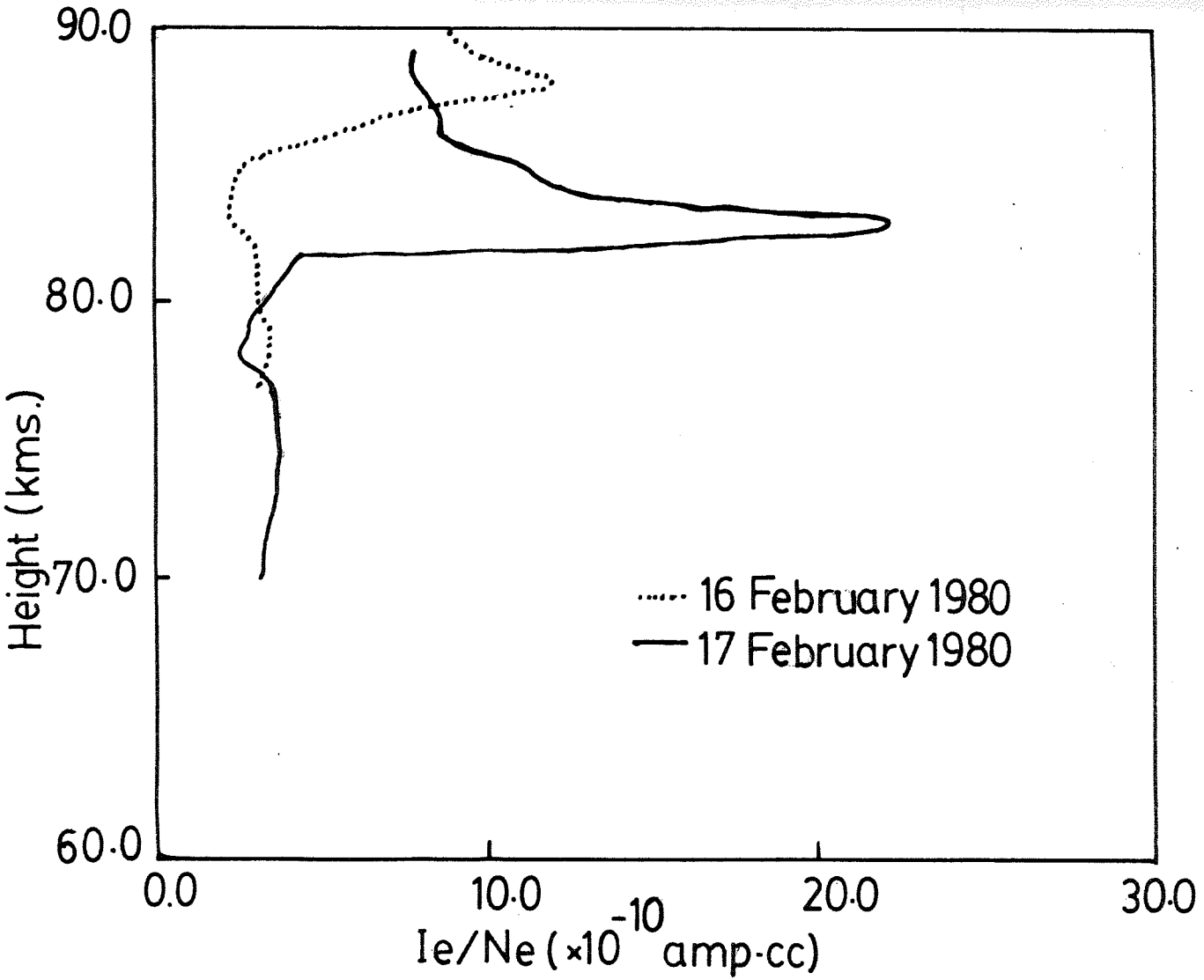

Fig 2.12 Ratio of LP current and electron density

TABLE 2.2

Ratio of LP Probe Current to electron number density

Altitude (km)	Ip/Ne(16 Feb)	Ip/Ne(17 Feb)
70	--	2.99
72	--	3.25
74	--	3.45
76	--	3.42
78	3.19	2.41
80	2.82	3.02
82	2.79	14.44
84	2.07	12.47
86	5.00	8.54
88	11.83	7.63
90	8.57	8.39

model is to be valid. The experimentally obtained ratios for the two rocket flights conducted on 16th and 17th February 1980 are depicted in figure 2.12. The ratio, as one can see, is constant within a factor of 1.75 over most of the altitude region where data is available. The error bar is about 20%. The anomalous peaks which appear in the diagram will be discussed in the next subsection. The ratio $\frac{Ip}{Ne}$ is $\simeq$ 3 X 10^{-10} ampere cc down to about 73 km. We can assume Te as $\simeq$ 200°K and solve equations 2.38 and 2.39 to get the effective probe area A = 3.67 sq.cm.

2.6.3 Floating potential of rocket body

Figure 2.12 shows the ratio of Langmuir probe current to electron density in the D region. The ratio shows an anamolous peak at 83 km altitude in one of the flights and at 88 km in the other. In this subsection, a possible mechanism for the occurance of such a peak in the Ip/ne ratio is considered.

The electron density is related to the probe current via equations 2.38 and 2.39. These equations do not contain any parameter which can have such sharp peak at this altitude. The following situation can however explain this peak in LP current.

Large potential gradients are known to exist in the mesosphere. These voltages can be as high as several volts per meter[Maynard et al., 1984]. This voltage peak can affect current collection by the Langmuir probe in the following

way:

The complete Langmuir Probe instrument involves two electrodes which interact with the ambient medium. One is the Langmuir Probe which is biased and collects current as a result of its bias potential, and the other is the return electrode. The area of the return electrode is about 100 times that of the probe. Fig 2.11 is a diagram illustrating the Langmuir probe system which was installed onboard the rockets. The two probes are seperated in the axial direction. If there is an electric field E along this direction, then the current collected by the probe is given by

$$I_{tot} = I_o + I_{EF} \qquad ..(2.41)$$

where $I_o = ko\left(1 + \frac{eV}{kT}\right)$ and $I_{EF} \simeq ko\left(\frac{e\bar{E}.\bar{d}}{kT}\right)$

Knowing the ratio of probe current by electron density under normal circumstances, one can use this to estimate the electric field in the rocket axis direction. This is given by

$$\bar{E}.\bar{d} = (I_{tot} - I_o)\frac{kT}{k_o e} \qquad ..(2.42)$$

Thus if an electric field exists in the medium, it will change the probe current of the Langmuir probe. The electric field required to generate the given peaks in fig 2.12 are about 12 volts in the case of 16th Feb. data (peak at 87 km altitude) and 24 volts in the case of 17th Feb. data (peak at

83 km. altitude).

A further discussion regarding this anomalous peak in probe current is given in chapter 5 in section 5.9.

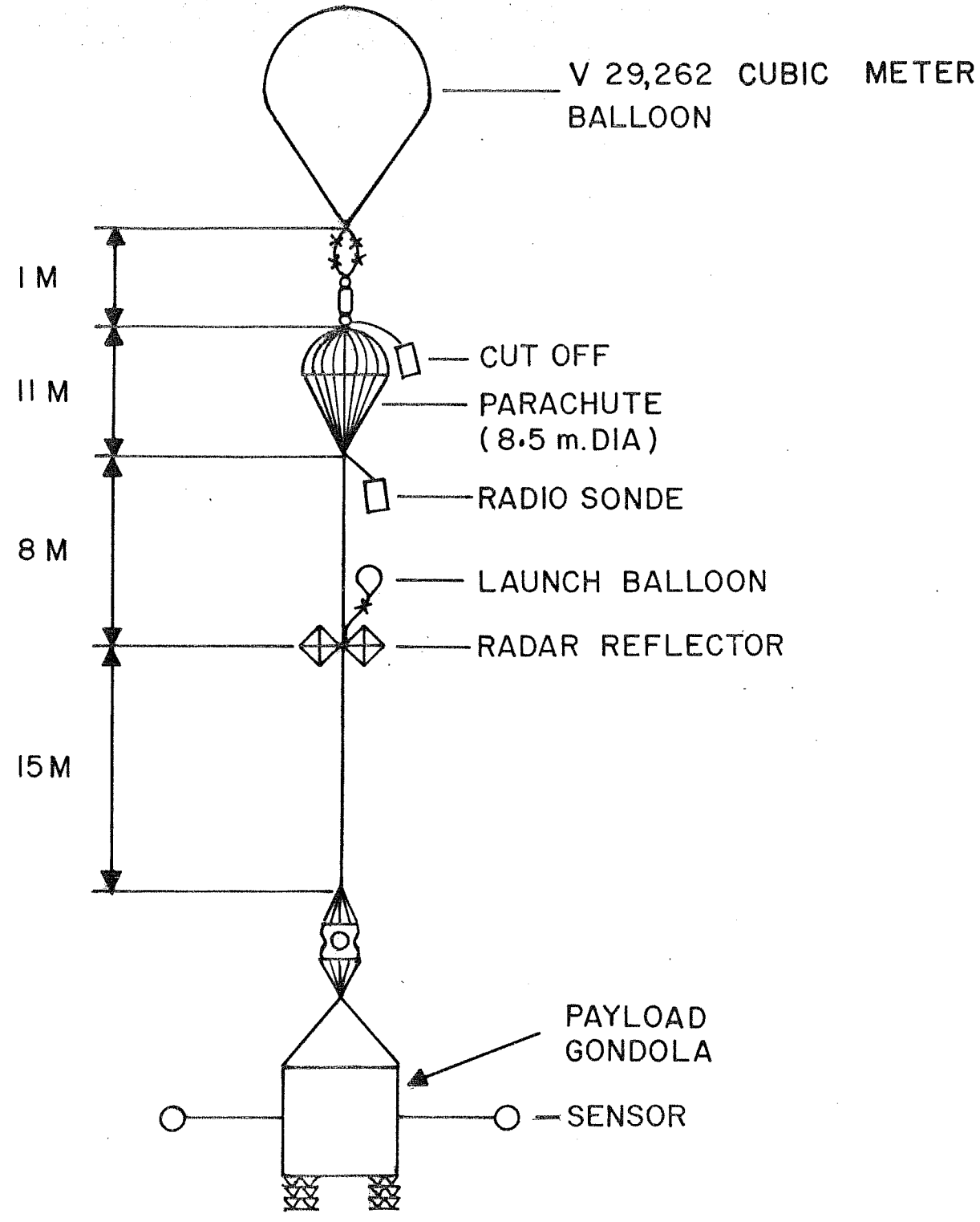

FIG 3.1 THE BALLOON PAYLOAD TRAIN

CHAPTER III

INSTRUMENTATION AND DATA ANALYSIS

3.1 Introduction

In this chapter, a detailed description of the balloon-borne instruments used for measuring the electrical conductivity and the electric field in the stratosphere is given. These instruments have been used by the author to measure atmospheric electrical parameters in the stratosphere. The electric field at the balloon altitude was measured using double probe technique. The conductivity was obtained by measuring the time constant of decay of probe voltages to the ambient values.

The instrument for conductivity measurement consists of a spherical metallic sensor acting as a capacitor which is charged and allowed to discharge through the atmosphere. The potential of the spherical sensor is continuously monitored

and its value is telemetered to the ground.

For measuring the electric field, a variation of the double probe technique has been employed. In this technique, three spatially separated identical sensors have been used in floating potential mode. The potential difference between them was measured. This gives the electric field component parallel to the axis along the sensors.

A detailed description of these instruments and the methodology which was employed for balloon borne experiment is given in this chapter.

The balloon-borne measurements were conducted from the Balloon launching Facility at Hyderabad. The Balloon Facility provides the infrastructure for launching stratospheric balloons, and gives telemetry and telecommand facility[Redkar, 1977, Annual Report: BF, 1986].

3.2 Mechanical Design

3.2.1 The Balloon payload train

A drawing of the Balloon payload train is given in Fig 3.1 (This is not a scaled diagram). The main instrument is suspended from the balloon, along with other supporting instruments in a structure which is known as the gondola. The gondola and other necessary units are suspended from the balloon. This configuration is known as the payload train.

The balloon is a large size inverted onion shaped

polythene film stratospheric balloon. Its volume is around 50000 cubic meters. Immediately below the balloon, there is a failsafe device which cuts off the rest of the payload train in the event of an accidental balloon burst. Together with the failsafe device there is a mechanism which can effect a cutoff through a telecommand from the ground station and a timer controlled cutoff device. A system of redundancy is maintained for greater relliability.

A parachute is used to bring down the payload train once the experiment is over, and the balloon cutoff is effected. This parachute, as can be seen in Fig 3.1 is situated just below the cutoff device. Further down along the payload train, is a radiosonde device, which consists of a pressure monitor, an FM encoder and a transmitter.

The radiosonde gives the balloon altitude in terms of the measured ambient air pressure. With help of a ground based direction finding radio receiver, one can determine the elevation and the azimuth of the balloon.

A radar reflector is situated below the radiosonde. This consists of a large aluminium sheet, twisted to form a shape which facilitates the reflection of incoming radar beacon from any direction. This is helpful for locating and tracking the balloon.

The main instrument gondola is situated below all these packages. This gondola contains the instrument for the main experiments. It also contains several other instruments. These include a PCM encoder (PCM stands for Pulse Code Modulation), the telemetry transmitter, the main battery pack,

and other housekeeping devices. We have used a fluxgate magnetometer for monitoring the rotation of the gondola. In one of the flights, we have used an inclinometer to study the tilting motions of the gondola.

In one of the flights(IMAP-C2, Table 4.1), an Apex valve was used. This is a valve situated at the apex of the balloon. It can be opened and closed by giving telecommand. By opening the valve part of the Hydrogen gas from inside the balloon can be let out and the gross lift of the balloon can be reduced. Apex valve operation is done in order to control the descent-rate of the balloon. Apex valve is also used when it is desired to conduct experiments at several different float altitudes.

The total distance of seperation between the balloon and the gondola is nearly 45 meters.

3.2.2 Mechanical configuration of Gondola

Fig3.2A, 3.2B and 3.2C show the configurations for the sensors in the flights IMAP-4, IMAP-9 and IMAP-7 respectively. The configuration of IMAP-7 was repeated in the flight IMAP-C2. The two flights IMAP-4 and IMAP-9 were combined flights having one payload for conductivity measurement and another payload for aerosol measurement. IMAP-7 payload was designed for conductivity and vertical electric field measurement.

We used a hollow metallic sphere as the conductivity sensor. It had a diameter of 20 cm and was made of

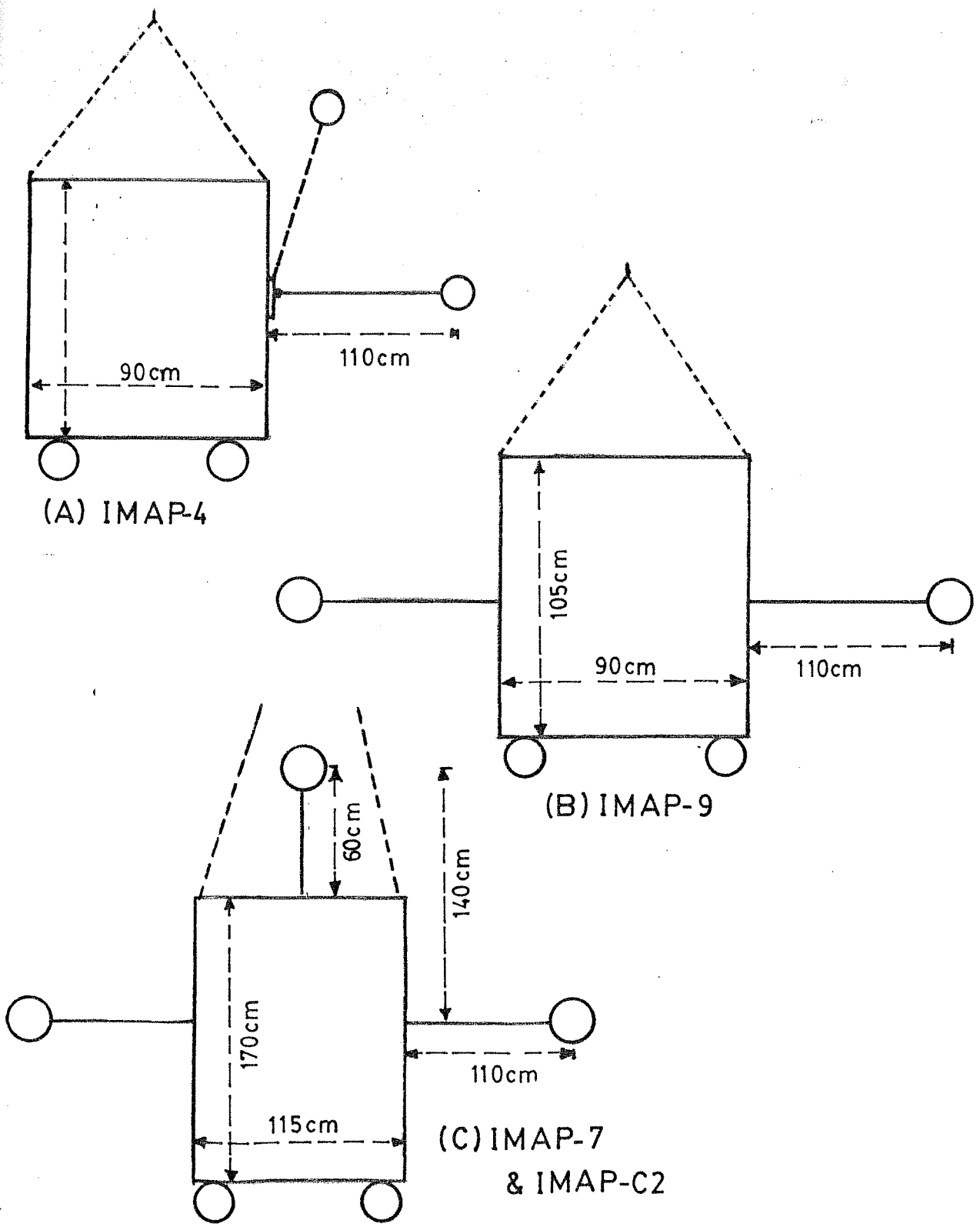

FIG 3.2 SENSOR CONFIGURATIONS DURING DIFFERENT BALLOON FLIGHTS

copper(see Fig 3.7).The sensor was at the end of a 1m.long boom which was hydraulically deployed from the gondola after the balloon launch.Deployment was necessary in order to avoid damage to the sensor during the balloon launch.The boom was about 1m. long.This length was chosen because if short booms are used,the gondola is too near to the sensor, and there is a stray capacitance effect due to its proximity. There are also contaminating effects due to gondola degassing. On the other hand,if the boom is kept very long, it creates problem during the launching of the balloon. A compromise between the two has to be done in choosing the optimum length of the boom.For a 1m long boom, the stray capacitance due to the presence of the gondola is less than 0.5 pf.

Ballast is used for controlling the balloon ascent rate. Whenever the ascent rate becomes too low,it can be boosted by dropping ballast and thus reducing the weight of the gondola. This is necessary especially at tropopause level where the temperature falls down to as low as -85^{o}c.If the balloon does not pass through this region quickly enough, the polythene film of which the balloon is made gets brittle due to the low ambient temperature.This results in a balloon burst. The amount of ballast carried by the balloon is about ten percent of the gross weight.About 50 kg ballast was kept in the gondola.Minute iron granules was used for the ballast.Ballast is dropped using a telecommand from the ground control station.

All the instruments were assembled within a sturdy

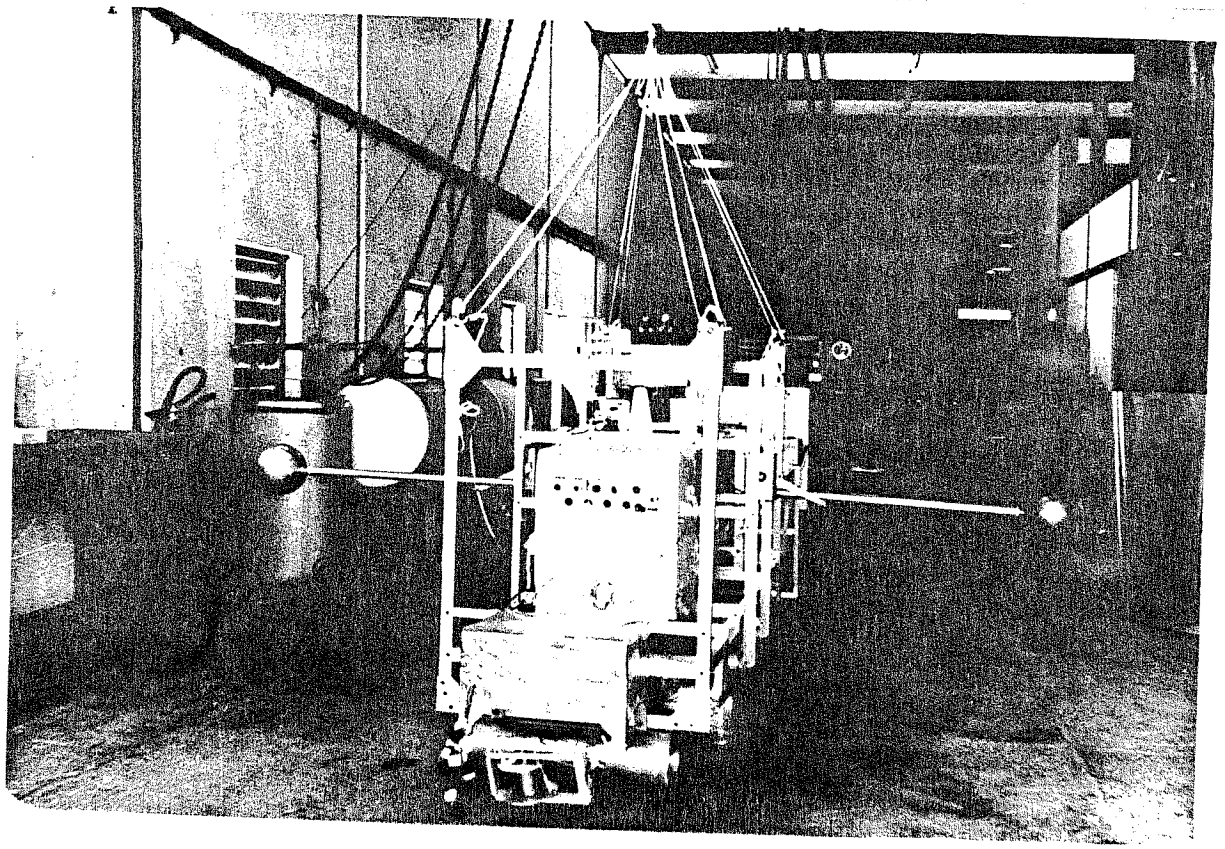

FIG 3.3 PHOTOGRAPH OF GONDOLA

aluminium frame(see photograph in Fig 3.3).This frame was fitted with crash pads at its bottom.The crash pads absorb the impact shock when the payload gondola lands on the ground after cutoff, and help in reducing damage to the instruments.

3.2.3 Thermal packaging of the gondola

Because of the extreme low temperatures encountered in the upper troposphere and the stratosphere during the balloon ascent and float periods, the gondola has to be thermally insulated from the surrounding environment.The thermal packaging of the payload gondola was done using 1 inch thick thermocole sheets.These sheets were covered on one side by a layer of aluminised mylar film.This film does not allow infrared radiation to pass through it, thus minimising radiational loss of heat from the gondola[Lichfield and Carlson, 1967]. After covering the gondola with thermocole and mylar,the gondola was wrapped in polythene film. By thermally packaging the gondola in this way, it was possible to keep the temperatures inside the gondola above $-10^{o}c$ at all time.An aluminium sheet coated with aquadag was put above this over part of the gondola surface. This served the purpose of return current electrode.

3.3 Payload Electronics

The conductivity/electric field payload consisted of an aluminium box of dimension 10.5 X 13 X 18 cm which contained the electronic circuitary for the experiment(See fig. 3.12). The preamplifier section was housed in a smaller box. This was an air-tight box whose inside was made moisture proof with help of silica gel.The full circuit was assembled on three printed cards which were stacked inside the payload box. Suitable connectors were used to connect this payload box to the magnetometer and inclinometer units. The power supply to the payload box and the outputs to the telemetry unit were taken through a common fifteen pin connector to their respective counterparts.

3.3.1 Block diagrams of the payloads

Fig 3.4 shows a schematic diagram of the conductivity instrument. This instrument contains various functional blocks which include the preamplifier,the charging pulse generator and the regulated power supply unit.

The output data is encoded using a PCM (pulse code modulation) encoder and transmitted using a FM (Frequency modulated) telemetry transmitter.

Fig 3.5 shows the schematic diagram of the conductivity and electric field payload. This instrument includes in addition to the abovementioned units,two more preamplifiers,

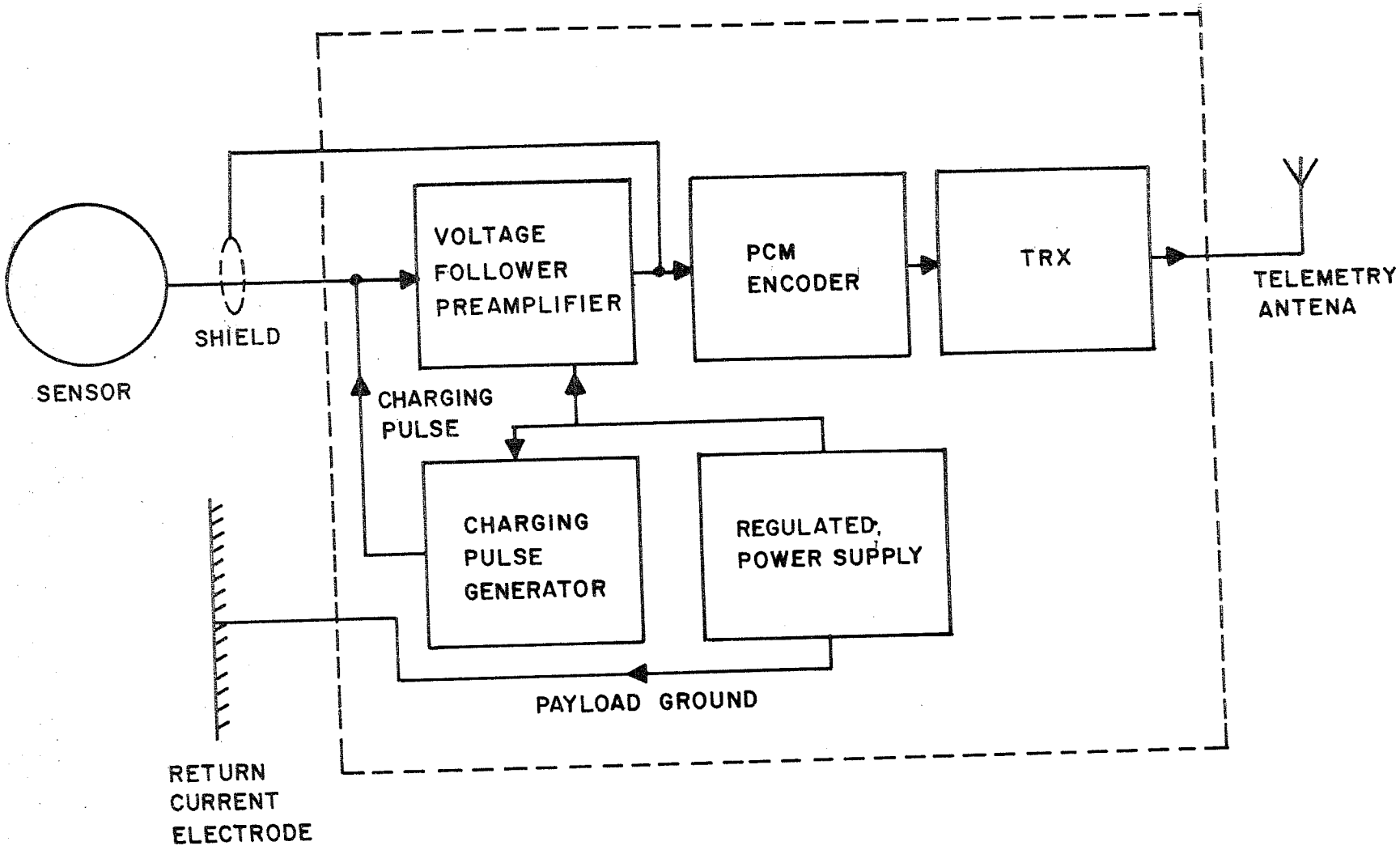

FIG 3.4 SCHEMATIC DIAGRAM OF CONDUCTIVITY PAYLOAD

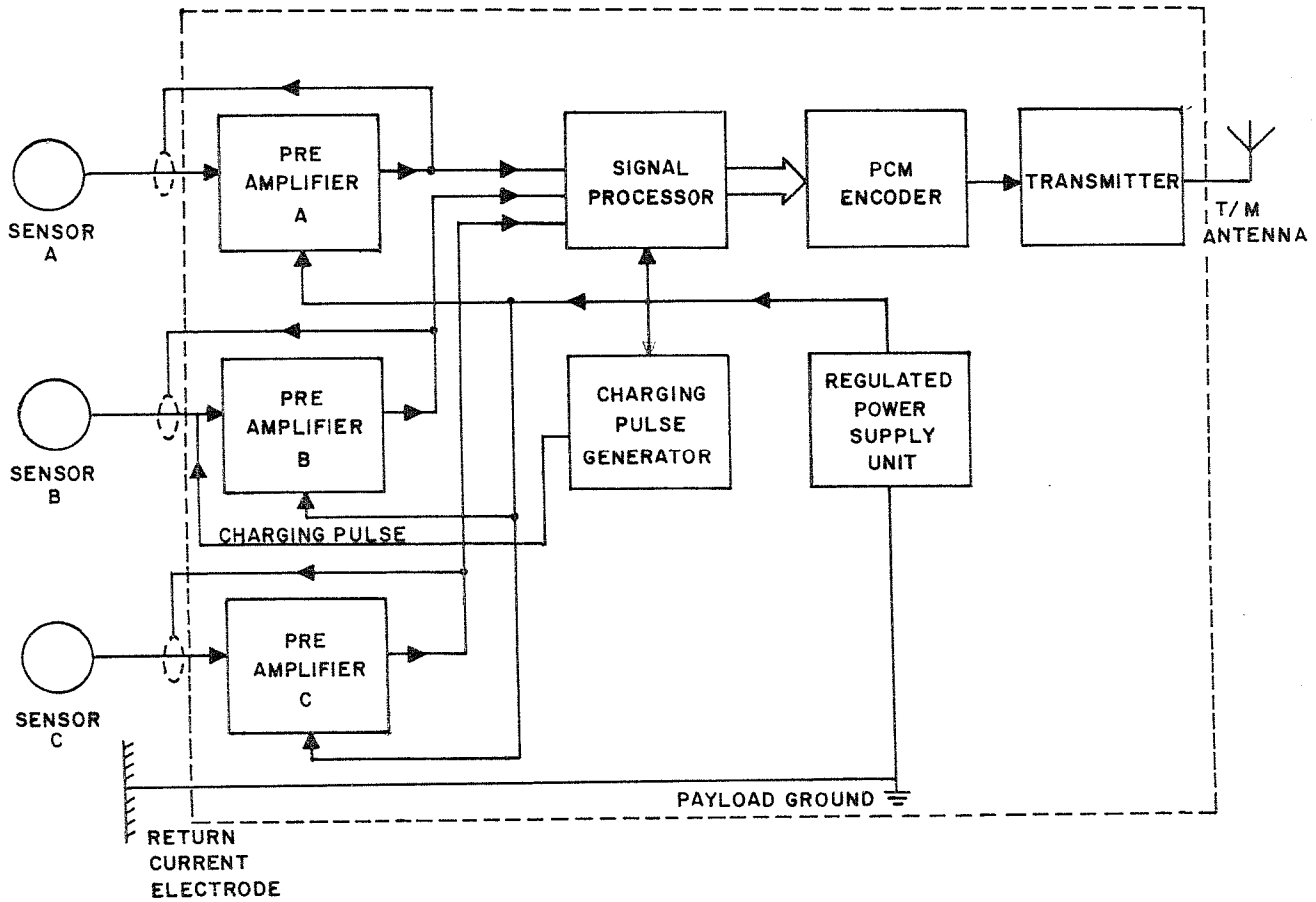

FIG 3.5 SCHEMATIC DIAGRAM OF THE ELECTRIC FIELD AND CONDUCTIVITY PAYLOAD

and an additional signal processing unit.These are used in order to get the electric field data.

3.3.2 Conductivity Sensor

A hollow metallic sphere was used as the conductivity sensor. It had a diameter of 20 cm and its sheet thickness was 0.5 mm. The weight of one sphere was 650 grams.The sensor is depicted in the photograph Fig 3.7.

The sensor was uniformly coated with aquadag.Due to its amorphous nature aquadag coating provides a surface which has a uniform work function [Mozer and Serlin, 1969, Feuerbacher and Fitton, 1972]. In order to apply a uniform coating of aquadag,the spin spraying technique was employed. This technique has been found to provide good surface uniformity. The sensor was rotated while spraying it with aquadag(an alcohol based suspension was used for this purpose). The spinning process was continued until the coating was dry. The sensor was slightly warmed by blowing hot air over it, and then stored after wrapping it in a clean conducting polythene wrapper.This precaution is taken to avoid static charge accumulation on the sensor during storage.

3.3.3 Cable and boom

The sensor has to be connected to the preamplifier using a coaxial cable which has a low capacitance and very

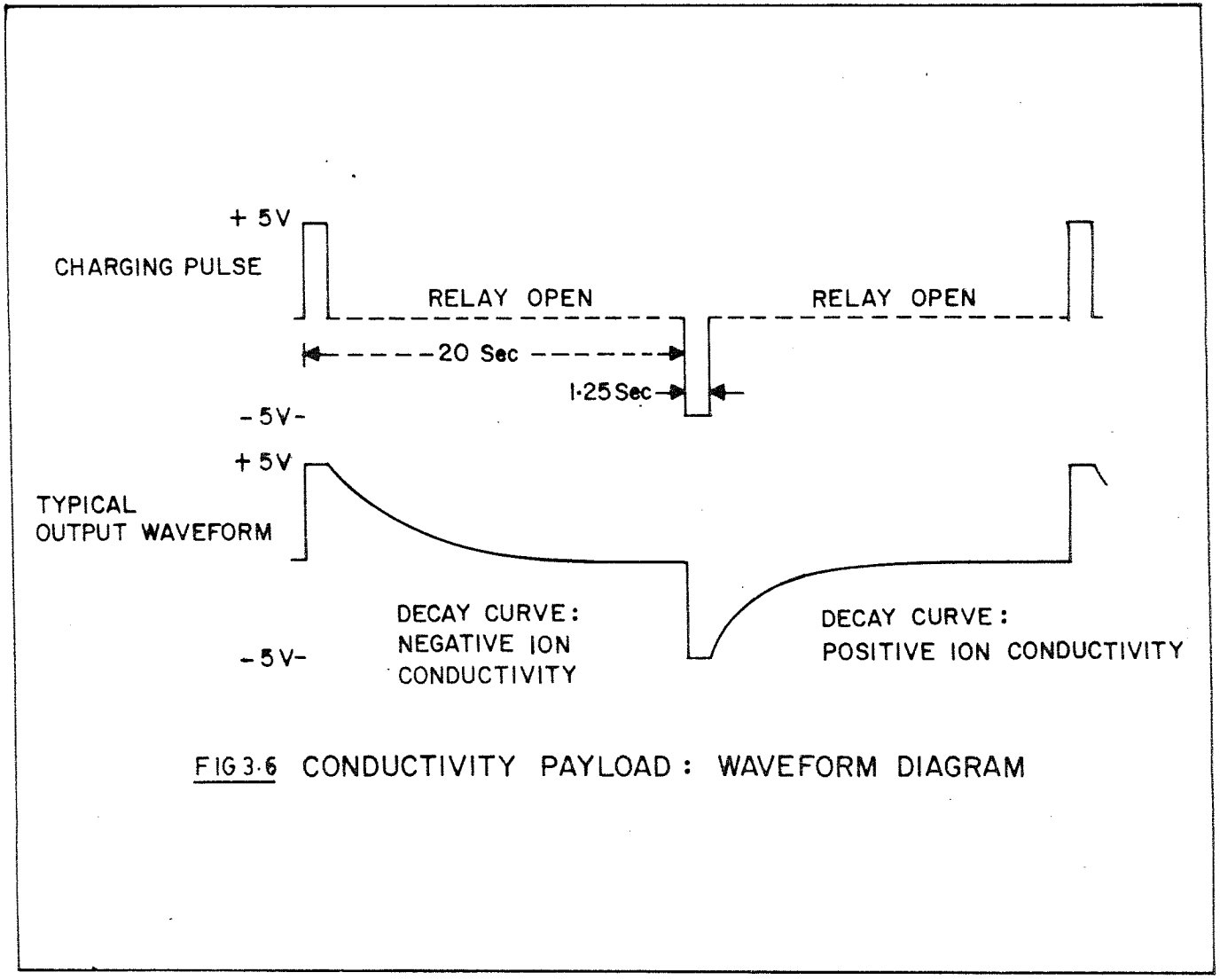

FIG 3·6 CONDUCTIVITY PAYLOAD : WAVEFORM DIAGRAM

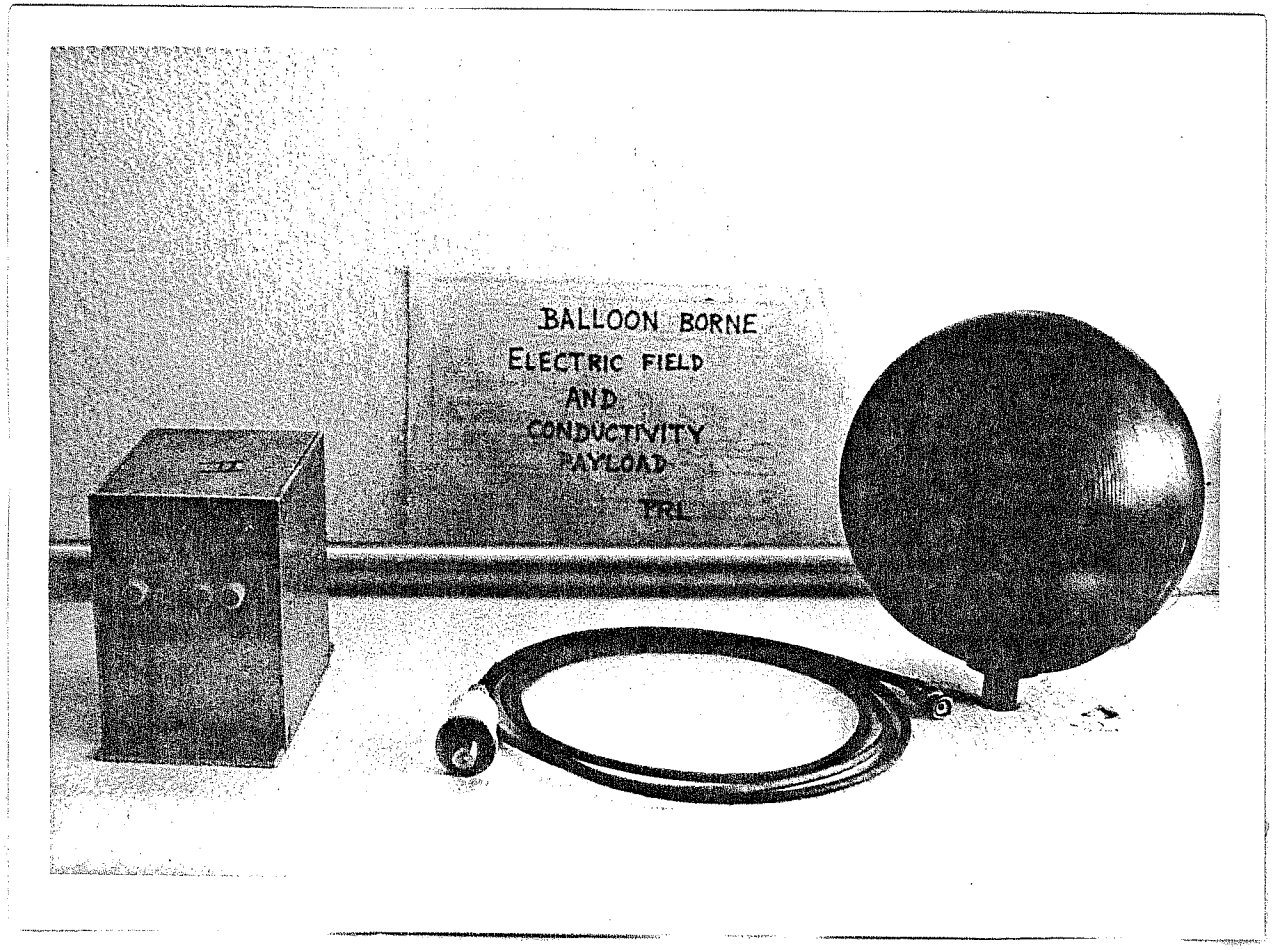

FIG 3.7 PHOTOGRAPH OF CONDUCTIVITY & E.F. PAYLOAD

high insulation resistance. The photograph in Fig 3.7 shows the sensor connections. The sensor is screwed on to a coupling. The other end of the coupling has a BNC connector. This BNC connector has to be connected to a shielded cable going to the preamplifier. The coupling resides at the end of the boom.

A typical coaxial cable has a capacitance of the order of 50pf per meter. It would be virtually impossible to make measurements where this cable is used to connect the sensor whose capacitance is of the order of 10pf. This problem is solved by driving the shield of the cable with the preamplifier output [Slamanig , 1981]. Thus the shield is at the same potential as the central (core) wire. If we are able to closely maintain this equality between the core potential and the shield potential then the effective capacitance of the cable is drastically reduced. This method reduces the effective capacitance by a factor G^{-1} where G is the open loop gain of the input preamplifier. The value of the open loop gain of the preamplifier in the present case was of the order of 10000. In the laboratory measurements which we did in order to test the cable, we obtained an effective capacitance of 3.5 m long cable as much less than 0.5 pf. The shield of the coaxial cable was connected to the output of the voltage follower so as to reduce the effective capacitance of the cable.

The boom is kept folded during the balloon launch and is hydraulically deployed soon after launch (at around 1 km. altitude). This is done so that the sensor may not get

damaged during the launching.

3.3.4 Preamplifier

The coaxial cable coming from the sensor is connected to a preamplifier which consists of a high input impedance voltage follower. The preamplifier measures the potential of the sensor with respect to the payload ground.

The circuit diagram of the preamplifier is given in Fig 3.8. It uses the IC OPA 104 which is a high impedance FET input operational amplifier designed especially for such measurements. The input bias current of the preamplifier IC is about 150 femptoampere which makes it suitable for measuring resistivities of the order of 10^{12} ohms which is typical value for stratospheric measurements.

The preamplifier module was housed inside a sealed moisture free box in order to ensure that the preamplifier input impedance does not get derated due to unwanted current leakage across the circuit elements. The performance of the preamplifier gets highly derated during damp weather if it is not protected from moisture. Silica gel was kept inside the preamplifier box to keep it moisture free.

3.3.5 The Charging Pulse Generator

During the conductivity measurement the sensor gets alternate voltage pulses of +5 V and -5 V with respect to the payload ground potential every 20 seconds. This is done

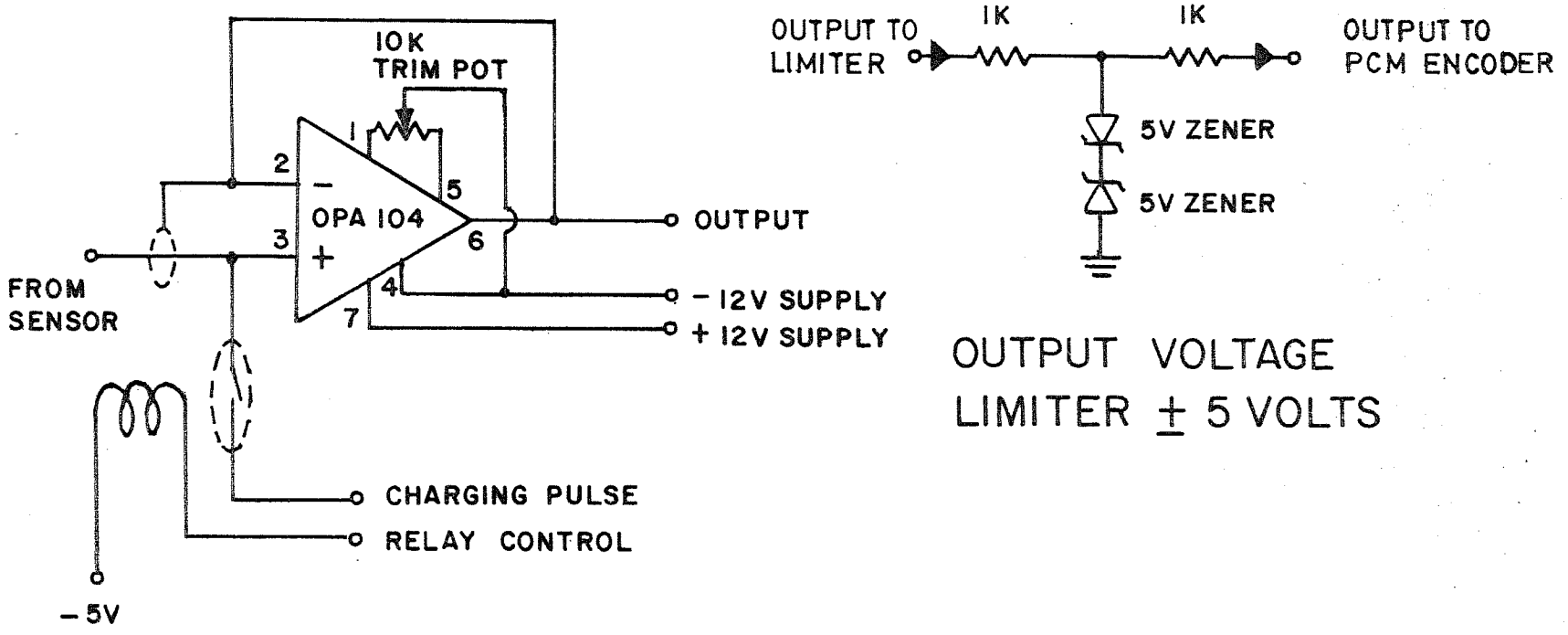

FIG 3.8: CIRCUIT DIAGRAM OF THE VOLTAGE FOLLOWER PREAMPLIFIER IN THE CONDUCTIVITY PAYLOAD

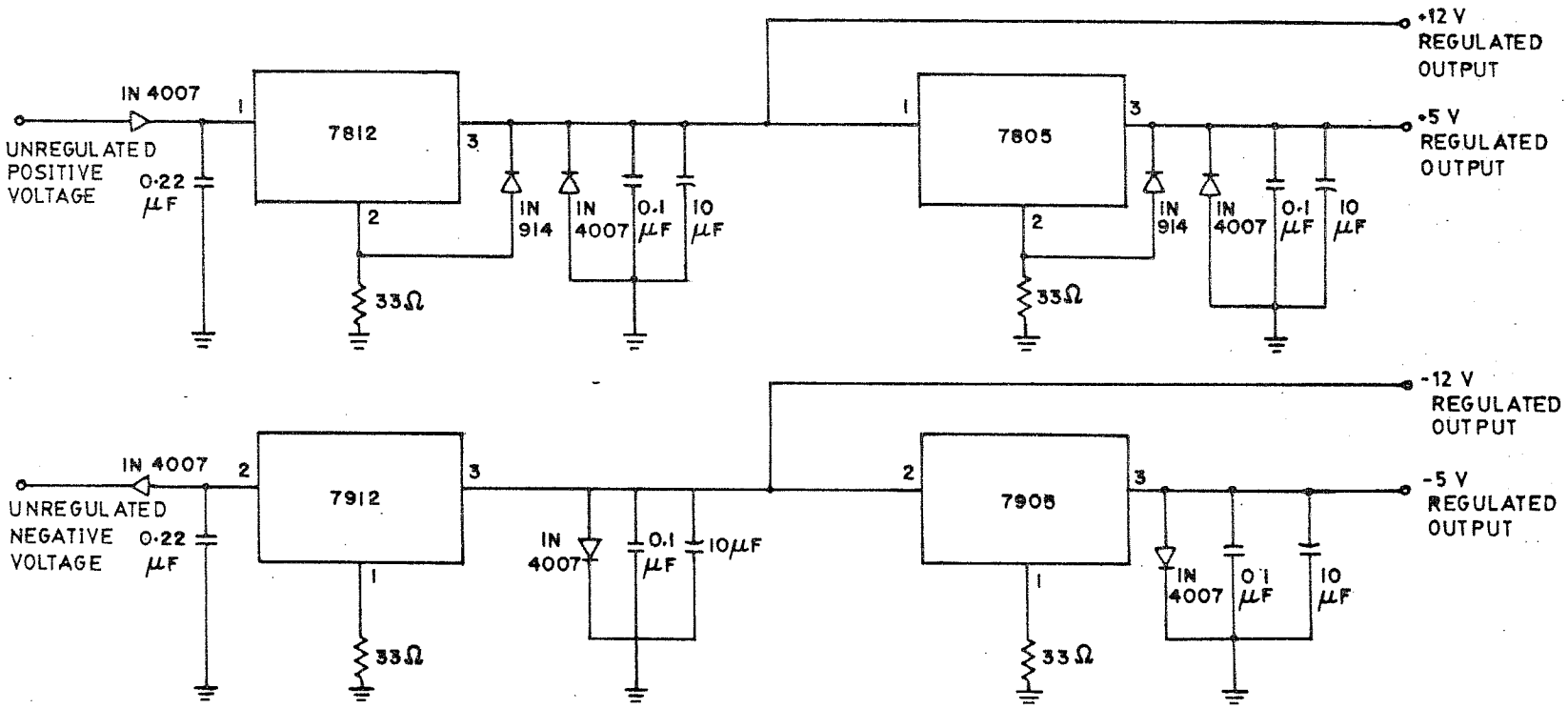

FIG 3·9 CIRCUIT DIAGRAM OF THE REGULATED POWER SUPPLY UNIT

with help of the charging pulse generator. The pulse is given through a relay which connects the sensor to the pulse source and after a predecided duration disconnects the source for the rest of the half-cycle. The charging waveform has been depicted in Fig 3.6. The duration of charging is 1.25 seconds while the sensor is kept disconnected from the pulse source for the rest of the half-cycle.

The circuit diagram of the module which provides this pulse is shown in Fig 3.10. It consists of a squarewave oscillator whose output is fed to a twelve stage divide by two counter (IC 4040). The output Q12 of this IC is used for charging the sensor. A reed relay allows the sensor to get the voltage for the duration of just one sixteenth of a cycle. Outputs Q8 to Q11 are fed to a NOR gate constructed from diodes and an inverting buffer. This inverting buffer drives the reed relay coil.

To avoid the problem of leakage in the reed relay we have put a shield over the body of the relay. This shield is driven at the same voltage as the sensor by the preamplifier output. The shield being a low impedance point at the same potential as the sensor, prevents any leakage of current across the relay reed.

3.3.6 Power Supply Unit

The conductivity payload requires regulated power supply of $\pm$12v and $\pm$5v. In order to get these voltages from the raw

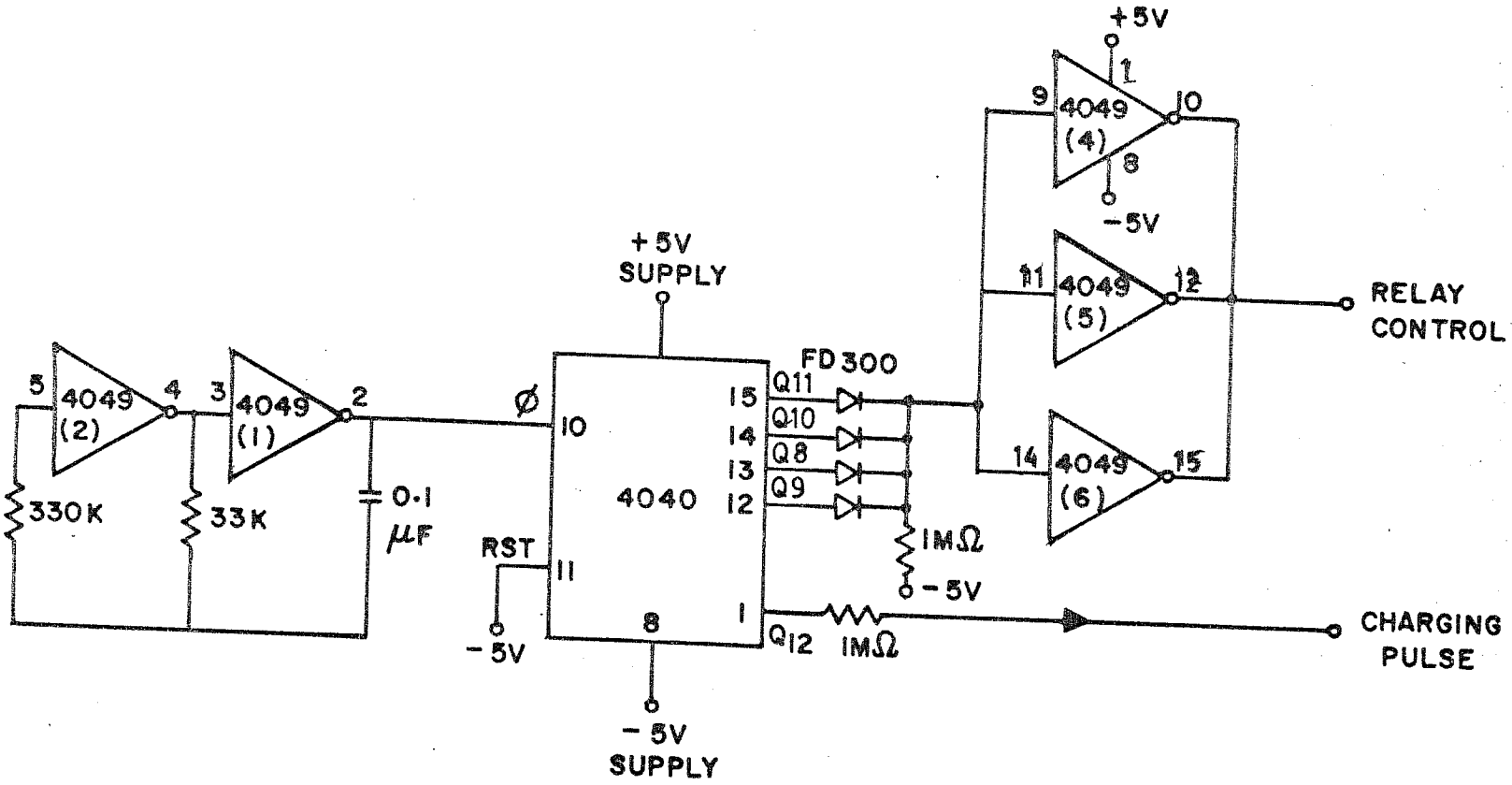

FIG 3.10 CIRCUIT DIAGRAM OF THE CHARGING PULSE GENERATOR

voltages (which vary between ±22 to ±18 volts depending on the flight battery condition), a regulated power supply unit was used. This PSU(power supply unit) employs voltage regulator IC's of 78XX series for positive voltage regulation and 79XX series for negative voltage regulation. The circuit diagram of this module is depicted in Fig 3.9. The 0.22 mfd capacitors in the input side are required for stability of the operation of the IC. Protection against voltage surge during switching is provided by the reversed diodes on the output side. Latching of the negative supply during dual supply operation is avoided by putting a protection diode between the common and the output points of the positive supply as shown in Fig 3.9.

The voltage regulator provided the power supply for the conductivity payload, the fluxgate magnetometer and the inclinometer sensors. The power requirement of the conductivity payload is around ±80ma. The total power requirement does not exceed ±150 ma.

3.4 Method of Measurement

3.4.1 Method of Conductivity Measurement

In order to make conductivity measurement, the sensor was alternately charged to suitable positive and negative voltages and was allowed to discharge through the ambient medium. Charging was done by giving the sensor a voltage pulse through a reed relay. The relay switch was then made

open so that the sensor voltage would decay to the ambient potential. The variation of the voltage with time was monitored continuously and was telemetered to the ground via a PCM/FM telemetry link. Conductivity is obtained from these voltage/time curves.

During every cycle of measurement, the sensor was charged alternately to +5v and -5v with respect to the payload ground potential. In this way, we could obtain both the negative ion conductivity and the positive ion conductivity. The procedure is similar to that used by Holzworth et al.[1984].

3.4.2 Method of Electric Field Measurement

A variation of double probe method was used for electric field measurement. Three probes were used(see Fig 3.2C) for the measurement of electric field. The probe B was also used for conductivity measurement. The two measurements cannot be done simultaneously because for the conductivity measurement, the transient part of the voltage-time curve is required while for the electric field measurement the steady portion of the curve is required. The part of the curve just before the onset of the charging pulse was used for electric field measurement. The potential difference($Va-\frac{Vb+Vc}{2}$) was directly obtained using the electronic circuit depicted in Fig 3.11. The output was telemetered and recorded on the strip chart recorder. This was used for deriving electric field values.

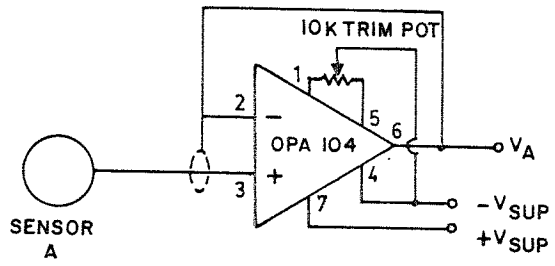

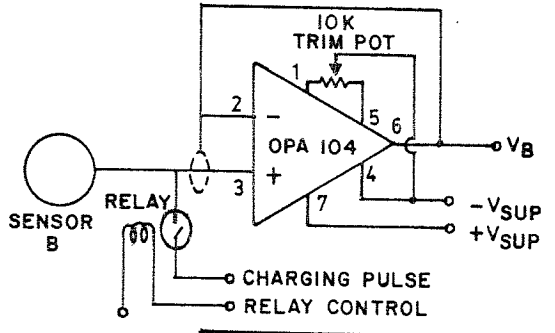

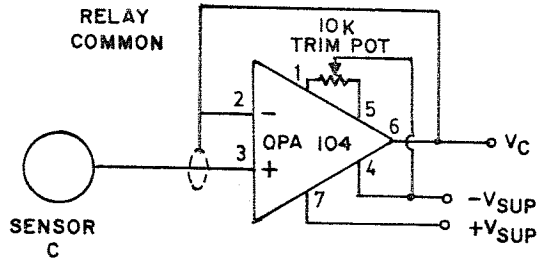

PRE AMPLIFIERS

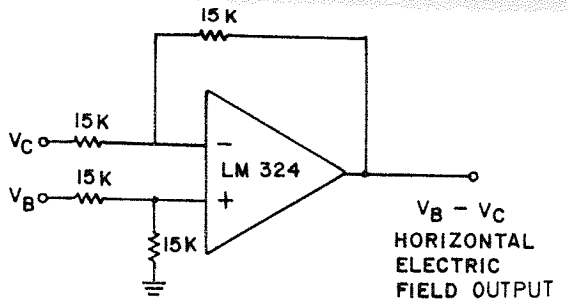

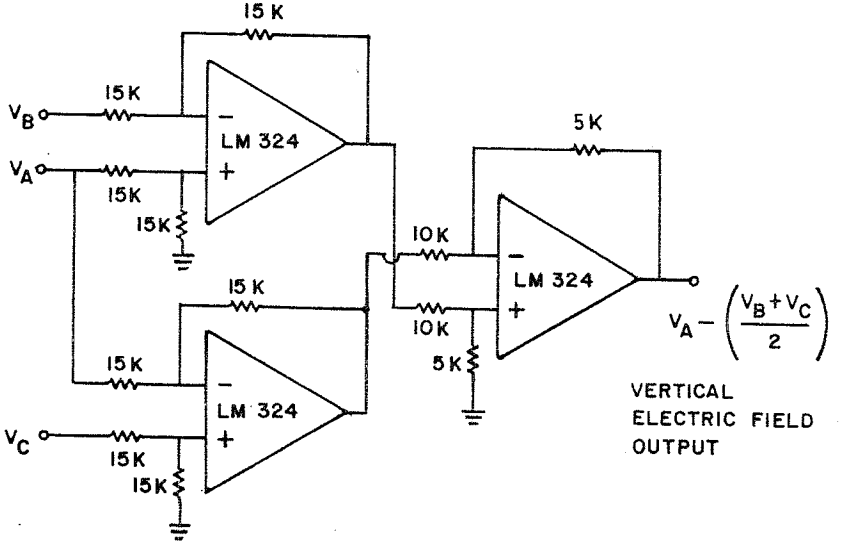

CIRCUIT DIAGRAM OF SIGNAL PROCESSOR UNIT

FIG 3.11

3.5 Support Instrumentation

In addition to the conductivity and the electric field payload, the gondola carried several other units which were necessary for the experiment. These included the main battery pack, magnetic aspect sensor, the PCM encoder, the telemetry transmitter, telecommand unit and the radiosonde. This section gives a brief description of the support instrumentation.

3.5.1 Battery pack

Power supply to the various instruments in the gondola is provided by a common battery pack. The battery pack for our instruments used Lithium cells(Eterna cells). These cells have a working voltage of 3 volts and have a very large current providing capacity. The cells are connected in a series-parallel fashion according to the requirements of various instruments that are in the gondola. The voltages are not fixed. They decrease by roughly 20 percent towards the end of their useful life. If steady voltages are required, a voltage regulator has to be used.

3.5.2 Magnetic aspect sensor

Magnetic aspect sensor is used for determining the

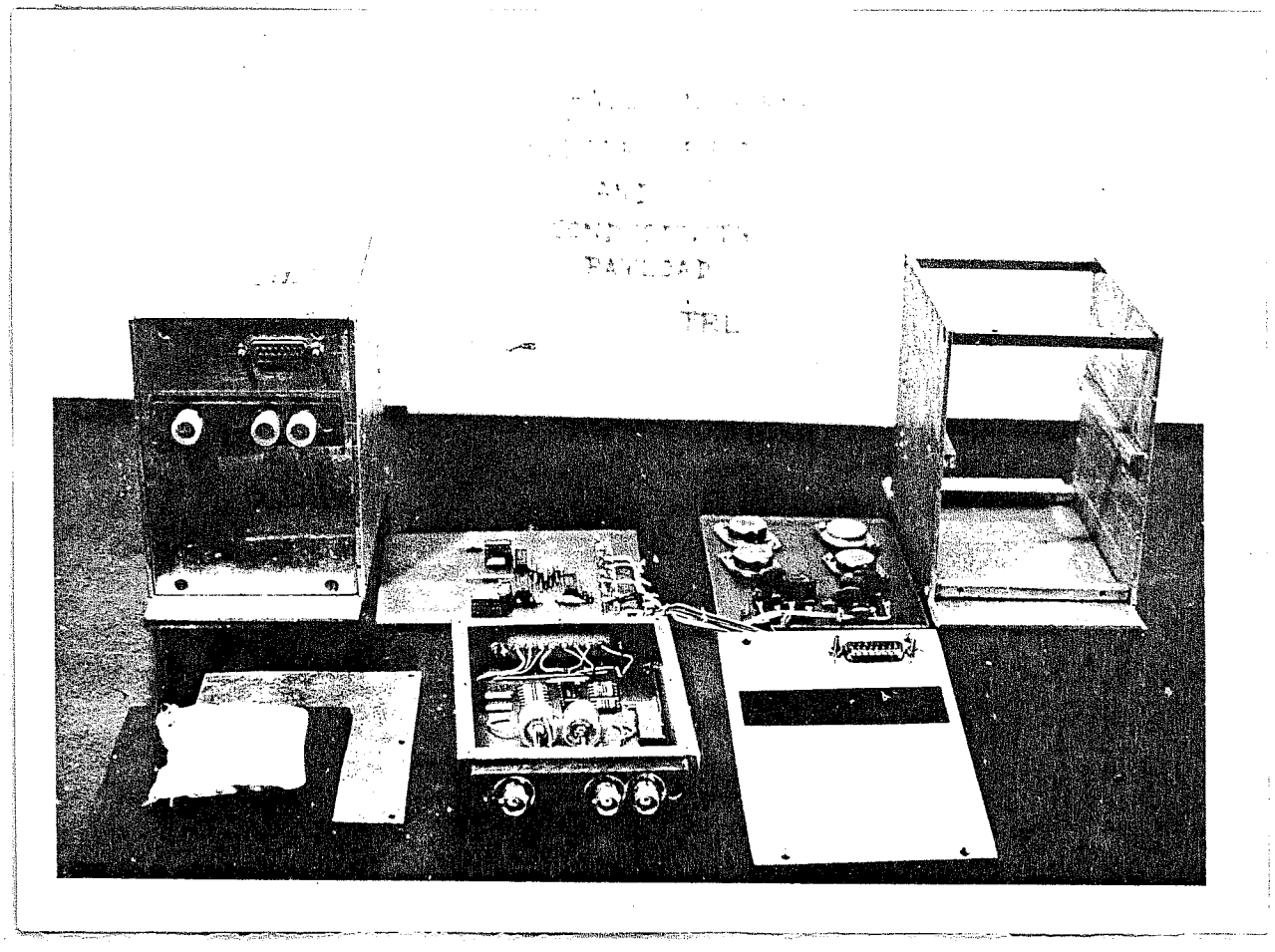

FIG 3.12 PAYLOAD ELECTRONICS

orientation of the gondola at any given time. It consists of two fluxgate magnetometers oriented perpendicular to each other. A fluxgate magnetometer measures the component of the earth's magnetic field parallel to the axis. It gives a voltage output which is proportional to the cosine of the angle between the axis of the magnetometer and the magnetic north direction. The output voltage is scaled in such a way that it is nearly 5 volts when the magnetometer points north and 0 volt when the magnetometer points south. The magnetic aspect sensors used in our experiments were provided by TERLS and were qualified for use onboard rockets. Since requirements for balloon are much less stringent, this could be used onboard the balloon borne gondola without any problem.

3.5.3 Data transmission

The output data from the conductivity/Electric field & conductivity instrument was first digitised and then transmitted serially using a radio link. A PCM encoder was used for digitising the data and later converting it into a coded serial output. The encoded data was then transmitted using a FM/VHF transmitter.

3.5.4 PCM Encoder

The PCM (Pulse code modulation) encoder is used for converting several analog and/or digital data channels into

a single serial digital data channel in order that it may be transmitted conveniently and relliably. All the channels to be telemetered are input to the PCM encoder. The conversion to a single stream of serial data is accomplished in several steps.

A multiplexer is used which samples all the incoming data channels in a cyclic fashion. The sampling frequency for a given channel is the frequency at which the data for that channel is sampled. This frequency determines the time resolution of the data. The sampling frequency for our experiment was nearabout 12 per second. Any variation in the data faster than 6hz will not be observed through this telemetry system according to the Nyquist criterion[Gruenberg, 1967].

The sampled analog data was converted into digital form using a twelve bit Analog to digital converter(A/D convertor). The A/D converter which was used converted a given voltage signal into a twelve bit number(a number which lies between 0 and 4095) proportional to the voltage output at the given channel($\frac{Vo - Vmin}{Vmax-Vmin}$ X 4096).

The data was then put into a serial form according to a predecided format(see Appendix I at the end of this chapter). The output from the PCM encoder is in the form of a serial string of "0"s and "1"s called a bit string, output at a rate of 10 kilobits per second. The bit string was converted into a NRZ format(see Appendix I) before feeding it to the transmitter.

3.5.5 Telemetry Transmitter

An onboard VHF transmitter, operating at a frequency of 137 Mhz was used for telemetering the data. The output power of the transmitter was 1.5 watts. The PCM encoder output was in the form of a bit string in NRZ format. The serial data was first used to modulate a carrier frequency of 137 Mhz. The modulated carrier was then stepped up and transmitted via a radio link to the ground receiving station.

3.5.6 Telecommand system

A telecommand system was used for sending various commands to the balloon borne system from the ground control station. It used a PDM/AM/AM system of transmission.

The ground segment of the telecommand system consists of a command encoder and a transmitter. The onboard segment consisted of a receiver, a command decoder and a command control unit. The transmitter operated at a carrier frequency of 148.25 mhz and its output power was ≃35 watts. The transmitter was modulated at a subcarrier frequency of 6.25 khz which was amplitude modulated by the command signal. The onboard unit receives the telecommand signal and decodes it. The command control unit then activates or deactivates the respective relay switches in response. A confirmation is sent through the telemetry channels to the ground station. Details of the telecommand system is given

in Appendix II at the end of this chapter.

3.5.7 Radiosonde

A radiosonde gives the balloon height and ascent rate information. The basic information is derived using a pressure transducer kept inside the gondola. This transducer monitors the ambient atmospheric pressure at the balloon altitude. This information is transmitted by the radiosonde using a 375 Mhz FM transmitter. The output power of this transmitter is 2 watts.

At the receiver end, a beat frequency oscillator is used to retrieve the signal. The altitude information is obtained with help of a calibration chart. The accuracy in height is $\pm$ tens of meters at 15 km altitude and $\pm$1 km at 35 km alititude.

The radiosonde receiver has a direction finding antenna which can give the balloon azimuth and elevation information within $\pm 3^{o}$. This tracking system supplements the main radar tracking system described in section 3.9.4.

3.6 Instrument testing and standardisation

The basic aims for instrument testing are threefold. (1) To test proper functioning of the instrument, its repeatability and reliability. (2) To test the compatibility of the payload with the rest of the system and (3) To test the payload operation under the

environmental conditions expected during the flight, i.e. to qualify the payload for the flight.

3.6.1 Test for payload operation

Testing the input impedance of the preamplifier: The purpose of this test is to find out whether the input impedance of the preamplifier is high enough for the measurements to be accurate. The input impedance was considered "high enough" if the preamplifier did not show appreciable change(5 percent) in voltage at the end of 1 minute. This corresponds to an input impedance $\simeq 1.1 \times 10^{14}$ ohms.

A 10 pf polysterine capacitor was connected to the input point of the preamplifier, which was charged to +5 volts and left to discharge. Since no external resistor was connected to the circuit, the discharge path was through the input end of the preamplifier. In such a case the voltage decay time will correspond to the bias current of the preamplifier and the value of the capacitor.

A careful null adjustment and clean and moisture free handling of the preamplifier section is required in order to achieve this level of input impedance. Null adjustment of the preamplifier IC is required for its optimum performance. This was done by connecting the preamplifier input to ground via a 1 teraohm resistor(10^{12} ohms) and then adjusting the potentiometer between pins 1 and 5 of the OPA 104 operational amplifier until an output of 0 volts is obtained. This operation has to be performed in a dry

atmosphere. The preamplifier circuit has to be shielded from the 50 hz Powerline AC pickup during the operation.

Testing for stray capacitance: The purpose of this test is to make sure that the total stray capacitance introduced by the preamplifier box is within the experimental tolerance (within 5 percent).

A 100 gigaohm resistor was connected in parallel with a 10 pf capacitor to the input of the preamplifier in the payload in order to measure the stray capacitance at the preamplifier end. The other end of the resistor capacitor pair was grounded. The time constant of the voltage decay curve was measuerd and it was verified whether the expected value of 1 sec is obtained or not within tolerance of 5 percent.

Testing the cable: The actual capacitance of the cable is 50 pf. per meter. For a typical cable which is 2 meter long, the capacitance is much higher than the sensor capacitance. By using an active feedback process, the effective capacitance is brought down to a value well below the capacitance of the sensor. To test whether a given cable satisfied this condition or not, a 1m. long cable was connected with a grounded 100 gigaohm resistor in parallel with a 10 pf. capacitor at one end and the preamplifier input point at the other end, and the voltage decay curve was observed. An identical configuration was used with the length of the cable as 3.5 m. No difference between the two decay curves could be made out. This implies that the

effective capacitance of 2.5 m of cable(the difference) is very small (<0.5 pf).

Testing the sensor: In actual measurement the sensor is a metallic sphere having a radius 10 cm. Theoretically, the capacitance comes out to be 10 pf. The actual measurement of the sensor capacitance is difficult because of the presence of a large amount of 50 hz. powerline AC which is picked up by the sensitive preamplifier under normal circumstances. We have tested the system by putting the sensor within a faraday cage. Under laboratory conditions, actual simulation was difficult mainly because ground level air conductivity is too small(~ 10^{-14} Siemens per meter) to be measured by our instrument.

Electric field and conductivity payload: The linearity of the output channels was also tested. The output voltages of the electric field channels represent the differences between the different combinations of the input voltages. So when a particular set of voltages is applied at the input points, one expects a particular output voltage. This test was done for each of the channels for the different possible combinations of the input voltages.

3.6.2 Payload compatibility tests

Payload compatibility tests include the following tests. (1) Test for the power consumption of the payload, (2) Testing the output impedances of each of the output channels, and (3) testing whether the output voltage

limiters are properly working or not.

Telemetry channel output impedance test: The input impedance for the analog channels of the PCM encoder is 100 kiloohms. The output impedances of the telemetry channels of the payloads are 2 kiloohms. The payload was tested to see that it would not get loaded by the encoder inputs by measuring the output voltage, first as it was and then with a 100 kiloohms resistor connected between the output point and the ground line. If a difference larger than 2 percent of the output voltage is observed, it implies that the channel is getting loaded, and it has to be seen to as to why this is happening.

Voltage limiter operation: To test whether the voltage limiters are working properly or not, input voltages were applied which would give output voltages exceeding the specified voltage range. The output voltages were measured to see if they exceed the prescribed limits or not.

3.6.3 Environmental tests

Low temperature test: The purpose of low temperature test is to check whether the payload would continue to function in case the gondola temperature goes down to subzero values in the tropopause region or at the float altitude. The gondola is thermally packaged and our experiences show that the temperature seldom falls below zero degrees celcius. A tolerance of 10^{o} celcius is kept. In the low temperature test, the payload is kept at a temperature of -10^{o}c for 2

hours and at around -18^{o}c for two hours. A low temperature chamber situated at the Balloon facility was used for conducting this test.

In the low temperature test, the payload was kept switched ON in the low temperature chamber. The payload operation was continuously monitored (1) while the temperature went down, (2) during the time the temperature was kept at steady value, and (3) while the temperature was again brought back to the room temperature.

3.6.4 Mechanical and electrical Integration

After these tests are over, the mechanical and electrical integration of the gondola is done.

The gondola frame is made of angled aluminium. Inside the frame there is a provision for keeping the instruments in a multitiered rack. The placement of different instruments is decided keeping in mind the requirements and compatibilities of all the instruments. The instruments are finally mounted on the racks firmly with clamps and screws.

A wiring harness is prepared for interconnecting the different units within as well as outside the gondola (in the payload train). All the interconnections are checked and the payload is tested for proper functioning using an external power supply (regulated power supply units which use the 220 VAC line for their power source). If there are any operational snags, they are removed at this point. The fully integrated gondola is then tested using the flight

battery for a short while.

3.6.5 Long Duration test at room temperature

The long duration test is conducted after the electrical integration is over. The complete system is operated on external power supply under flight ready condition for a duration which is approximately twice the expected flight duration This test ensures that the the payload can continuously operate for the duration of the flight without any problem.

3.7 The launch Procedure

The launching of the balloon is a complex procedure which requires the coordinated effort of more than fourty persons. Success of the launch depends on a number of factors[Gokhale et al., 1966]. A description of the launch procedure is given below.Fig 3.14 depicts the sequence of the balloon launch.

3.7.1 Decision to launch

Just before the take-off,a final test is conducted to check whether all the different payload units are properly functioning or not.This test is called Launch pad test.

The decision to launch is taken only after the gondola is in flight-ready condition. Stratospheric balloons are

very large. A successful launch is dependent on many factors. The surface wind condition is an important parameter. If it is high then difficulty will be encountered during the gas filling operation. The balloon may flutter and flap so much because of the wind that it can burst. Therefore balloons are not launched during high surface wind conditions. A limiting wind speed of 5 knots(which is a little more than 5 miles per hour) has been decided as the upper limit for balloon launching.

The second parameter which is considered in the decision is the maximum wind shear during ascent. This is the rate of change of wind velocity per unit increase of altitude. Wind shear is considered in terms of the balloon ascent rate. The maximum allowed limit of wind shear is 35 m/s per minute of balloon ascent. The balloon ascent rate is nearly 2 to 3 meters per second. If the wind shear is high the horizintal shearing forces of the wind on the balloon may cause it to burst.

The third parameter also related to the wind is the wind condition at the balloon float altitude. A specific area has been prescribed by the civil aviations department and the balloon is not supposed to drift out of this area. This is called the balloon flight corridor and is shown in Fig 3.15. The wind at the float altitude should be such as to allow the experiment to be performed while the balloon is still within the boundary of the flight corridor.

In order to find out about the wind shear and the upper wind conditions, a special rubber balloon known as the totex

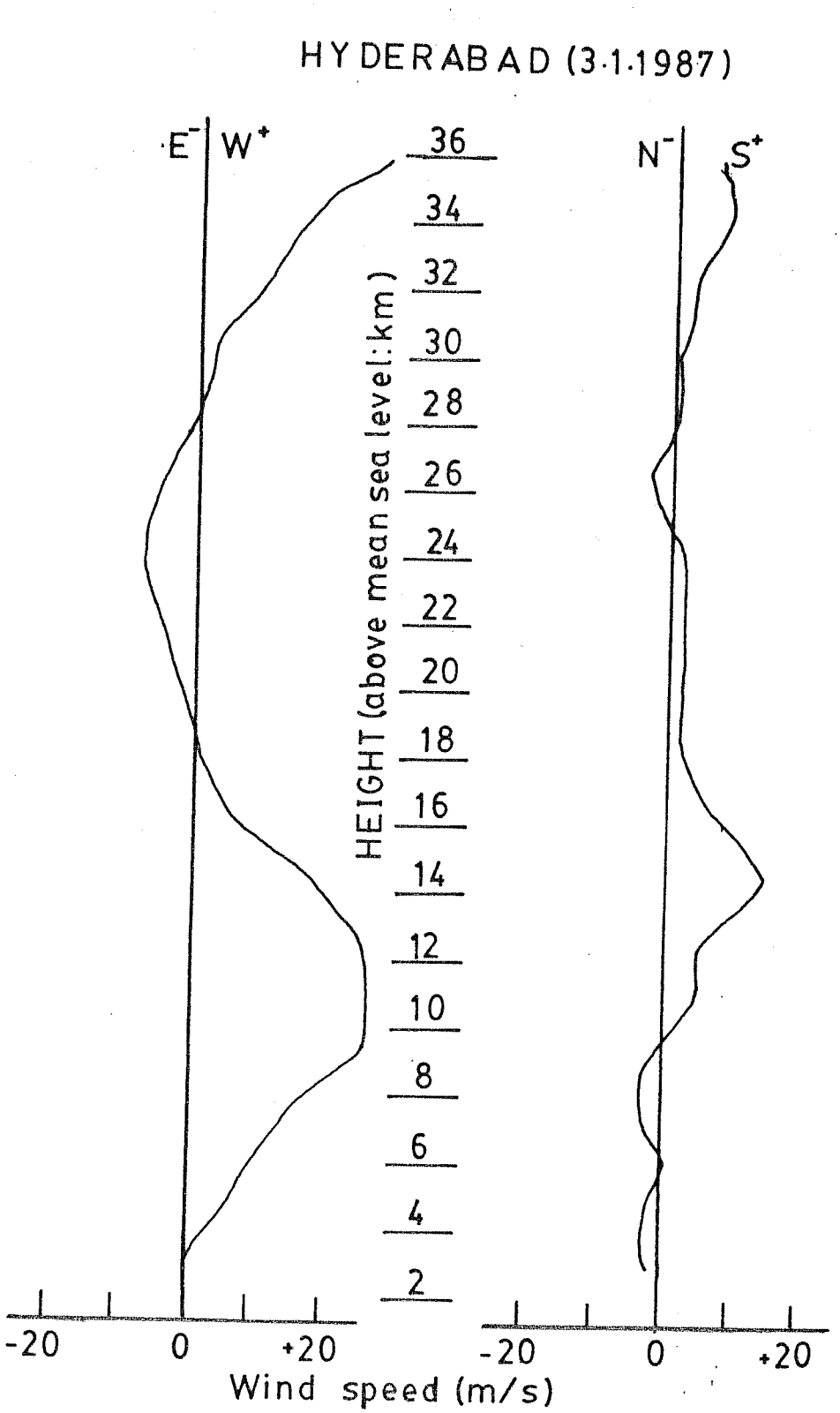

FIG 3·13 TYPICAL WIND PROFILE

rubber balloon is launched. It carries a radar reflector and it is tracked by Radar in order to get the necessary wind informations. Wind conditions at different altitudes are deduced from the trajectory of the balloon. Fig 3.13 shows a typical wind profile obtained from a totex balloon flight.

Apart from the winds, the cloud coverage over the launching ground are also considered. The cloud coverage should be less than two octa(two eighths of the sky). This condition is necessary because the balloon accumulates a large amount of electrical charge if it passes through a cloud. If it happens so, this may result in a balloon burst and the instrument may also get damaged.

The abovementioned factors are the major factors which can affect the balloon performance during the flight. They have to be taken into consideration before launching the balloon.

3.7.2 The Launch

Once the decision has been taken to launch the balloon, the payload gondola is suspended from the launch truck in the front side and moved to the centre of the launching ground around three hours before the launch time. The various units like the hydrogen cylinders, the filling buffer, and other accessories are also brought to the launching ground. Then, depending on the surface wind direction, the balloon and the loadline are laid on the ground. All the instruments that go with the balloon are

BALLOON EXPERIMENT

AEROSOL AND CONDUCTIVITY MEASUREMENTS

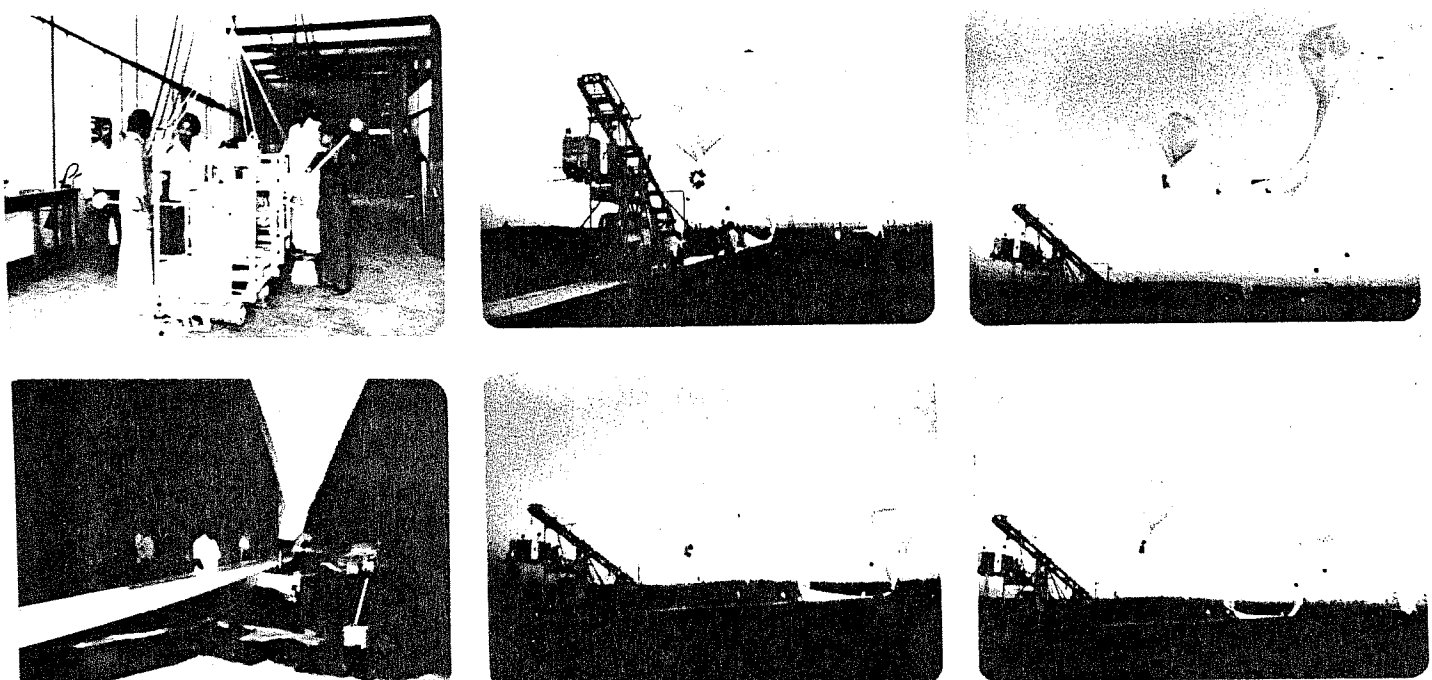

FIG 3.14 THE BALLOON LAUNCHING SEQUENCE

then properly interconnected and hooked onto the loadline at their proper places. The prelaunch test is then conducted and the experimenters as well as the control instrumentation groups iindividually certify that their instruments are working all right. Then only the balloon filling operation is started. The balloon is filled to roughly one tenth of its full volume capacity. This is done so as to allow for the expansion of the gas when the balloon reaches higher altitudes. Once the filling operation is over, the balloon launching is done. The launching sequence for the IMAP 4 flight is shown in Fig 3.14.

3.7.3 Tracking and recovery

The balloon is continuously tracked after the launch A system of redundancy is maintained in the tracking process and three methods are employed for tracking: Using radar, theodolite and radiosonde.

Tracking by radar: A 32 cm X band Selenia radar stationed at the Begampet airport, Hyderabad was used for tracking the balloon. This radar has a tracking range of around 300 km and can give the balloon's position with an accuracy of ± 1 km.

The operation of the radiosonde has been discussed earlier in section 3.5.7. Tracking by radiosonde is not very accurate and gives only an approximate value for the distance. The advantage is that radiosonde tracking is continuously done while radar tracking facility is only

available when it is free. If the radar loses track of the balloon, it can be redirected to the target(balloon) with the information provided by the radiosonde. Theodolite can be used for balloon tracking during daytime only.

The Indian Civil Aviation Department has granted a certain area over which the balloon can overfly. The balloon is not permitted to drift beyond this flight corridor. This corridor has been depicted in Fig. 3.15. The balloon is cutoff using telecommand before it drifts out of this air corridor.

After the cutoff command is given the payload train drops down with help of a parachute. Tracking is continuously done during this operation by the radar. This way, the location of fall is known within a radius of five km. Later on, a team is sent for recovering the payloads. The payloads can be reused after recovery if it has not got damaged by the fall.

3.8 Data recording and Analysis

At the ground station, a Microdyne 1100 AR VHF telemetry receiver was used for receiving the telemetry signals[Damle et al., 1981]. The received signals were fed to a Dpad II unit which is a microprocessor controlled PCM decoder and display unit. The incoming data was also recorded on analog tape on an AMPEX PR 2230 tape recorder and on digital tape on PERTEC T8840-9-45 tape recorder.

The dpad II decoded the incoming PCM data into

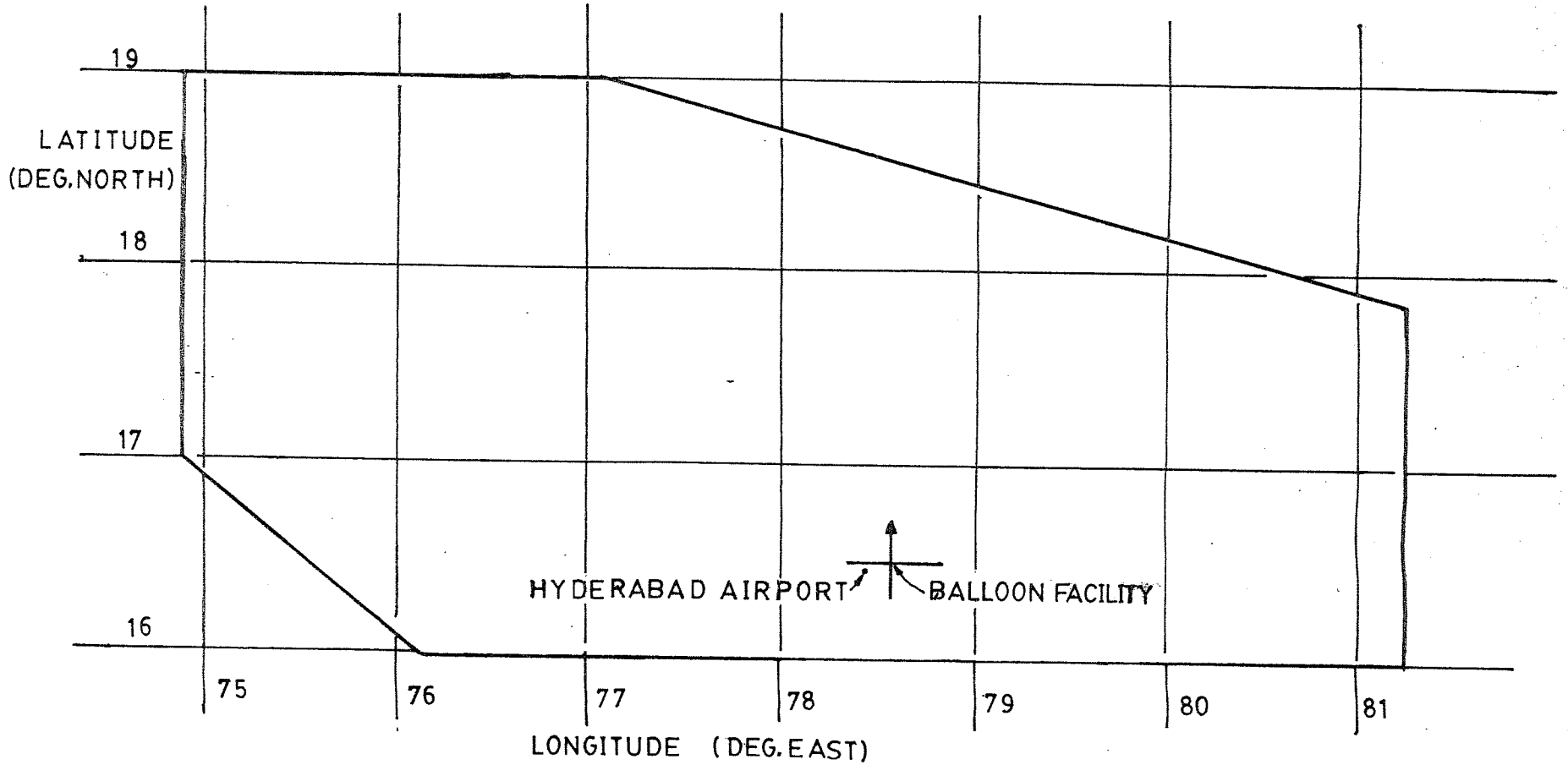

FIG 3.15 AIR CORRIDOR FOR BALLOON FLIGHTS

individual channels. A Watanabe strip chart recorder was used for the on-line recording of the telemetry data. The chart recorder can do simultaneous recording of four channels of data. Raw data from our experiment was recorded on this chart recorder at a speed of 250 mm/min. Data recording was also done on digital tapes on the PERTEC tape recorder.

3.8.1 Analysis of conductivity data

In order to determine conductivity from the raw data, it is required to measure the decay time constant of the probe. The voltage decay curves are obtained in the form of strip-chart records as shown in Fig 3.16. Some of the curves exhibit large fluctuations and time constant measurement is not possible for these curves. Hence these curves cannot be used for measuring conductivity. (Examples of such curves are shown in Fig 3.17). Only good exponential decay curves are used for conductivity determination. The present section briefly describes the method of data analysis.

The relaxation time constant is defined as the time taken for the sensor potential to decay from any given value to 1/e of that value. For exponentially decaying curves, the value of time constant will be same, no matter what portion of the curve one chooses for making this estimation. Thus one will obtain the same time constant value whether one makes measurement over the portion of the curve starting from 5 volts or from 1.5 volts (or from any

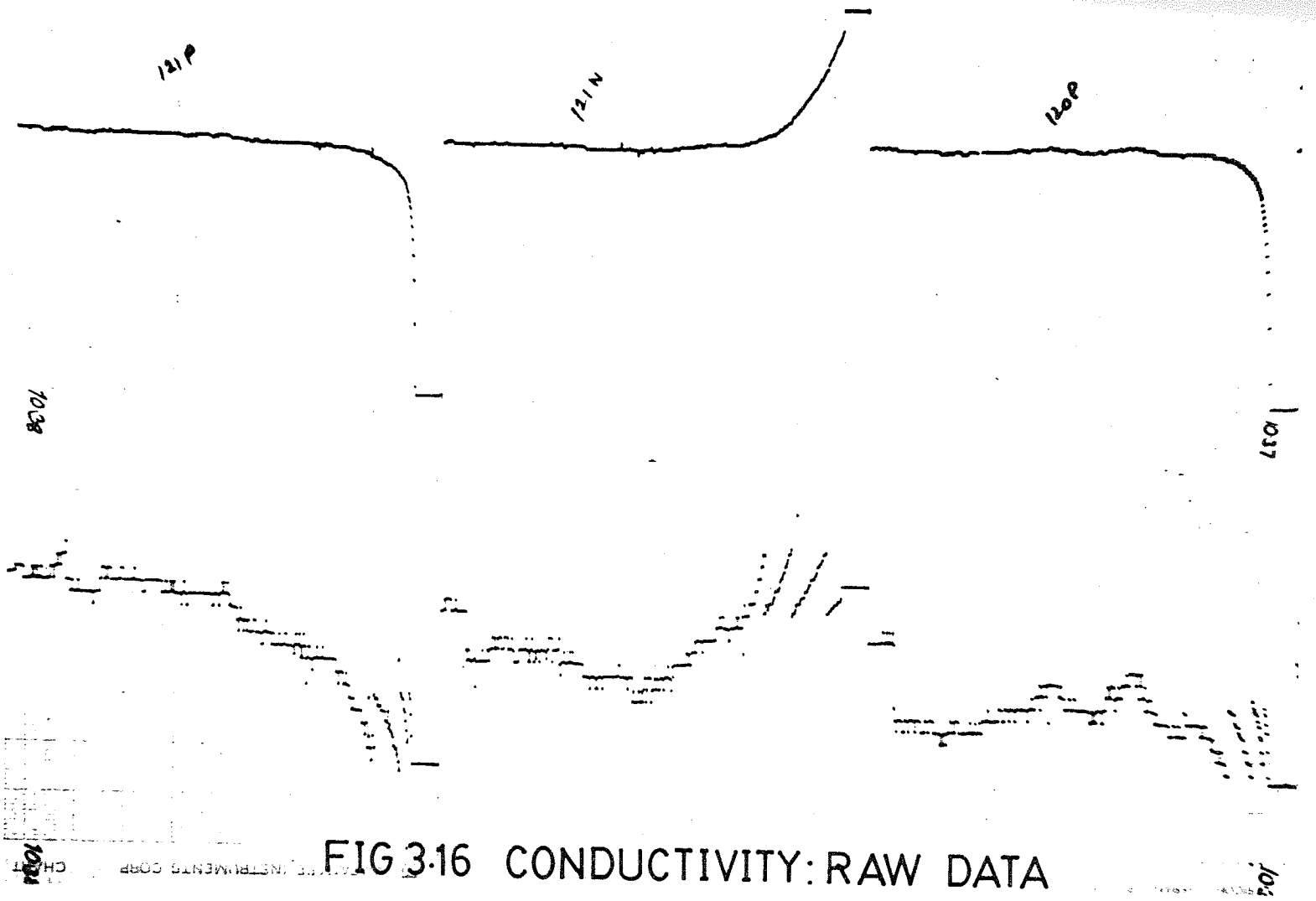

FIG 3.16 CONDUCTIVITY: RAW DATA

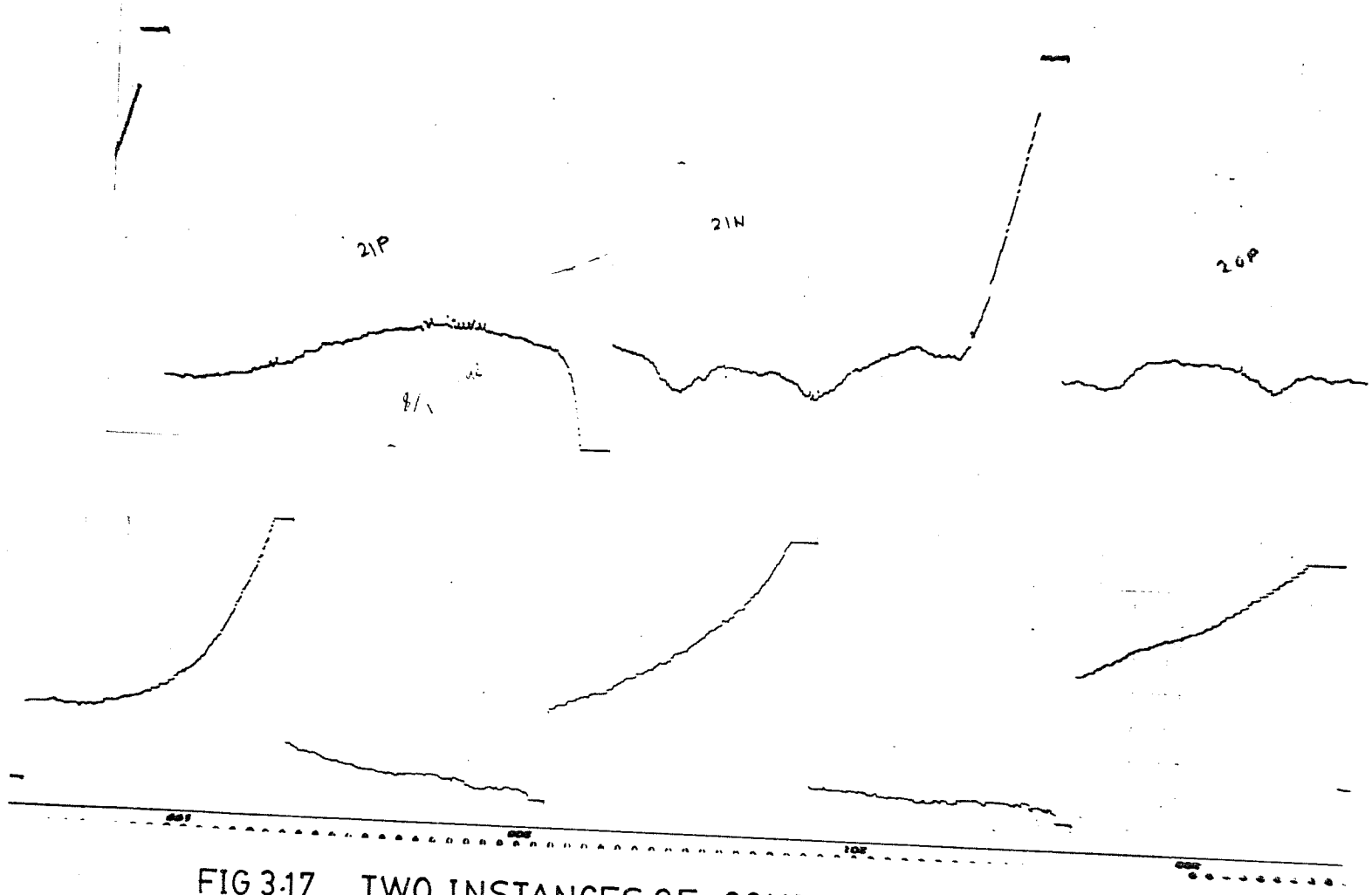

FIG 3.17 TWO INSTANCES OF CONTAMINATED RAW DATA

other value). This is no longer true if the curve is not exponential. For analysis of the present data two suitable voltage levels were chosen with a ratio of 1:e (e = 2.7183) between them and the amount of time taken for the probe potential to change from one value to the other was measured. Similar measurement was repeated over a different portion of the same decay curve in order to cross-check the results.

Throughout the experiment, a chart speed of 250mm/min was used for recording the data. Thus for the analysis, a scaling factor of 4.16 mm for 1 sec was used. The time constant was obtained by evaluating the time elapsed between the occurances of the given two voltages. Conductivity was obtained using the relation $\sigma=\frac{\epsilon_0}{\tau}$. The permittivity of air has been taken as 8.85×10^{-12} Farad per meter. Time constant values are in seconds. This gives the conductivity in S/m.

3.8.2 Error estimation in conductivity

Owing to the inherent difficulties in the measuring process, measurement of the atmospheric electrical parameters is always accompanied by a number of uncertainties. In the present section, an attempt has been made to estimate typical and maximum errors in our conductivity measurements due to different sources.

Some of the sources of error for conductivity measurement have been described in Chapter 2. The error due

to finite input impedance of the preamplifier was shown in section 2.3.5 to be negligible compared to other sources. In section 2.3.3 the error due to a finite gondola size was discussed. This effect can cause an overestimation of conductivity by about 5 percent. The maximum error possible is about 10 percent. The error due to photoemission from the probe is not known. But it was shown in section 2.3.4 using theoretical considerations that errors in conductivity measurement which can occur due to photoemission from the probe during daytime, can alter the shape of the decay curve. The magnitude of shape distortion in the decay curve gives an indication of the magnitude of the error due to photoemission. In the decay curves that we obtained, a shape distortion was observed. But it was not large and one cannot make out whether it is due to a finite gondola size or due to photoelectric emission from the probe. The total error due to shape distortion was estimated to be within 10 percent.

Due to the presence of small fluctuations in the gondola floating potential, an uncertainty can occur in the measurement of the time constant. As mentioned above, those curves having large fluctuations have not been analysed for conductivity. For other curves, an error bar can be assigned in the measured values of conductivity. This is done in the following way.

Fluctuations can cause an uncertainty in the asymptotic voltage levels of the decay curves upto a maximum of 0.4 volts. As a result of this an error upto ± 7.5 percent can

occur in evaluating the time constant. Thus the total error bar including shape errors due to finite gondola size and photoemission is $\pm$ 12.5 percent. In worst cases, the error can go upto 17.5 percent.

Note that errors in voltage calibration of the telemetry channels does not lead to error in conductivity measurement because time constant determination for exponential curves is independent of voltage scaling.

3.8.3 Electric Field data analysis

The two flights IMAP-7 and IMAP-C2 carried payloads for electric field measurement. The sensor configuration is depicted in Fig 3.2c. If V_A, V_B and V_C are the ambient potentials measured by the probes A, B and C respectively, the vertical electric field is given by:

$$Ev = \frac{1}{d} \left(V_A - \frac{V_B + V_C}{2} \right) \qquad ..(3.1)$$

where d is the effective distance of seperation between the two probes. The value of d was estimated using the method described in Chapter 2 section 2.5.2. It came out to be 1 m $\pm$ 0.15m.

During the experiment, probes A and C were kept floating in the ambient medium. Probe B was charged periodically for the conductivity measurement. So it was not possible to use the probe B during the periods of charging and discharging.

Electric field measurements were done after the probe B had attained the ambient potential. The time constant of discharge was less than 5 seconds. So a half-cycle time of 20 seconds was adequate for the probe to attain steady voltages. Electric field measurement can be done only after such a potential has been attained. Measurement of electric field was done just before giving the charging pulse. The voltage at the electric field channel was measured and was divided by the effective probe distance to give the electric field.

3.8.4 Error estimation for electric field measurement

As discussed earlier in chapter 2, error in electric field measurement can occur due to several factors. These are, mainly, (1) Error in the effective distance between the probes, (2) Error due to instrumental sources, and, (3) Error in measuring the voltage during data analysis.

The effective distance was calculated to be 1 m $\pm$ .15m. The rounding error in voltage measurement is $\pm \frac{1}{2}$ division which is equal to $\pm$0.0575 volts. Typical readings are around 0.4 volts. Hence this amounts to $\pm$ 12 percent error.

A detailed discussion of the various sources of error in electric field which are of an instrumental nature are given in chapter 2 section 2.5.1. These sources are, (1) difference in work functions of the probe surfaces, (2) error due to finite input impedance of the instrument, and, (3) error introduced due to the gondola charging mechanism.

As discussed earlier, the first two of these are not serious. The third source, i.e. error due to gondola motion is more serious because its nature is not yet understood. The large fluctuations observed in the electric field measured during IMAP-7 flight as shown in Fig 4.10 can be attributed to such a source. Since these fluctuations are statistical in nature, a 2 minute running average was taken to smooth out these fluctuations. Such a smoothing also takes care of rounding error during data analysis. A ten percent error will remain inspite of such a smoothing. Thus a total error bar of $\pm$ 20 percent can be assigned to the measured electric field values.

APPENDIX I

DETAILS OF TELEMETRY SYSTEM

The telemetry system used during the balloon flights from Hyderabad were of PCM/FM (Pulse Code Modulation/Frequency modulation) type.The telemetry encoder was provided by the Control Instrumentation group of TIFR. The details of the telemetry encoder are as follows:

Bit rate	: 10 Kilobits per second
Output code	: Biphase (L)
Output Level	: 0 to 5 volts
Bits per word	: 8 bits (7 data + 1 parity)
Parity	: Odd

Analog Channels :

There are 8 (multiplexed) analog channels of input range 0 to 6 volts;The output is straight binary.

There are 8 (multiplexed) analog channels of input range -4.25 to +4.25 volts; The output is complementary binary.

Resolution	: 12 bits (7 bits for quick look).
Digital data	: 16 seven bit data words.
Analog data	: Total 16 analog channels.
Frame counter	: 7 bits (0 ti 127)
Data alignment	: MSB first

Frame Structure

Sync	:W0,W1
Frame Counter	:W2
ADC (0 - 6V)	:W3,W4
ADC(-4.25-4.25V)	:W5,W6
Digital Channels	:W7-W22
Timer	:W23-W25

Transmitter Power: 1.6 Watts
T/M Transmitter Frequency: 137 Mhz.

APPENDIX II

Details of Telecommand System

Total Number of Commands	33
Carrier Frequency	145.25 Mhz
Transmitter Power	35 Watts
Polarisation	Vertical
Modulation	PDM/AM/AM
Carrier Modulation	75 %
Subcarrier Frequency	6.25 Khz
Subcarrier modulation	100 %
Bit Rate	87 Bits per second
Word Length	8 Bits (Sync, 6 code bits, blank)
Command Frame Structure	2 address words followed by Command words.
Address Code	111111 (Six "1"s)

CHAPTER IV

RESULTS

The author was involved in conducting six balloon flights. These balloon flights were conducted during the period of 1983-87 under the Indian Middle Atmosphere program (IMAP) for measuring conductivity and electric field in the stratosphere. Out of these six flights, good data was obtained from four flights. The other two flights did not give data because of balloon burst at tropopause altitudes. Two of the four balloons that gave data were launched in the morning hours while the third and the fourth ones were launched at night. Table 4.1 gives the list of the balloon flights conducted.

In the present chapter, the results obtained during these balloon flights are discussed. Apart from these measurements, the results of three rocket-borne measurements of mesospheric ion conductivity and electron density are also discussed. Two of these rocket flights had been conducted during 16 February 1980 and 17 February 1980

TABLE 4.1

Flight	Date	Payload	Launch time	Remarks
IMAP-2	20-10-1983	Conductivity and Aerosol	morning	Tropopause Burst
IMAP-4	18.4.1984	Conductivity and Aerosol	morning	Successful
IMAP-3G	27.11.1984	Conductivity and E-Field	night	Tropopause Burst
IMAP-9	22.10.1985	Conductivity and Aerosol	morning	Successful
IMAP-7	29.12.1985	Conductivity and E-Field	night	Successful
IMAP-C2	8.4.1987	Conductivity and E-Field	night	Successful

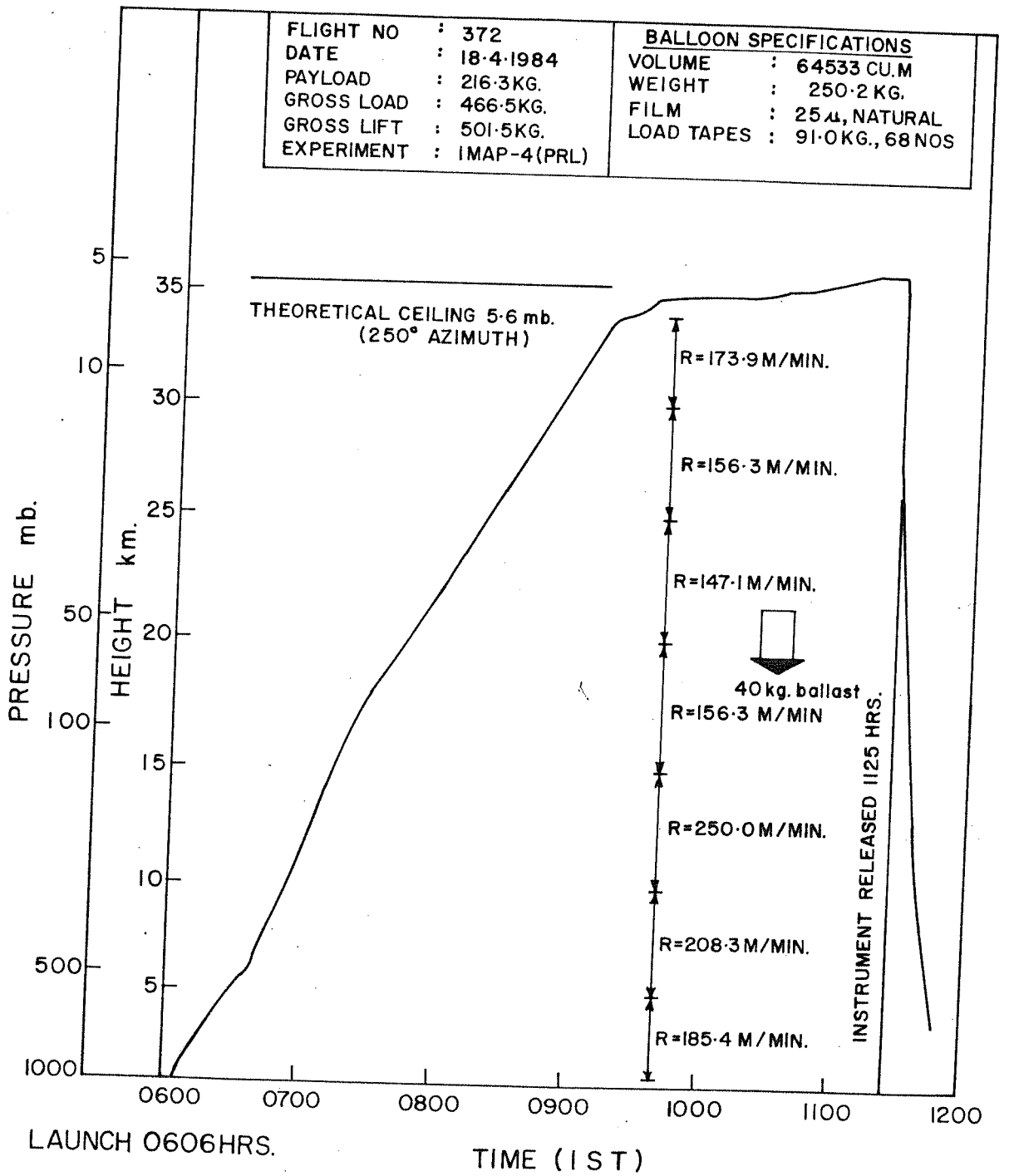

FIG 4.1 BALLOON ASCENT PROFILE- IMAP- 4

while the third one had been conducted on 12th August 1972. The latter gave ion conductivity values for mesosphere.

4.1 Results of Conductivity Measurements

The main results of conductivity measurement obtained during the four successful balloon flights are given in this section.

4.1.1 Results from IMAP-4 Balloon flight

The IMAP-4 balloon was launched on 18th April 1984 at 6.10 a.m. I.S.T. (Indian Standard Time. The local time at Hyderabad is 15 minutes ahead of I.S.T). The balloon carried a payload for measuring conductivity. Along with it there was a fluxgate magnetometer for monitoring the payload gondola rotation.

Fig 4.2 shows the positive and negative ion conductivities measured during this balloon flight at the ceiling altitude of 35 km. The positive ion conductivity varied between 7 X 10^{-12} s/m and 2.2 X 10^{-11} s/m. The negative ion conductivity varied between 2 X 10^{-12} s/m and 6 X 10^{-12} s/m during this flight. The following features were observed in the data.

1. The measured positive ion conductivity was observed to be three to five times higher than the negative ion conductivity.

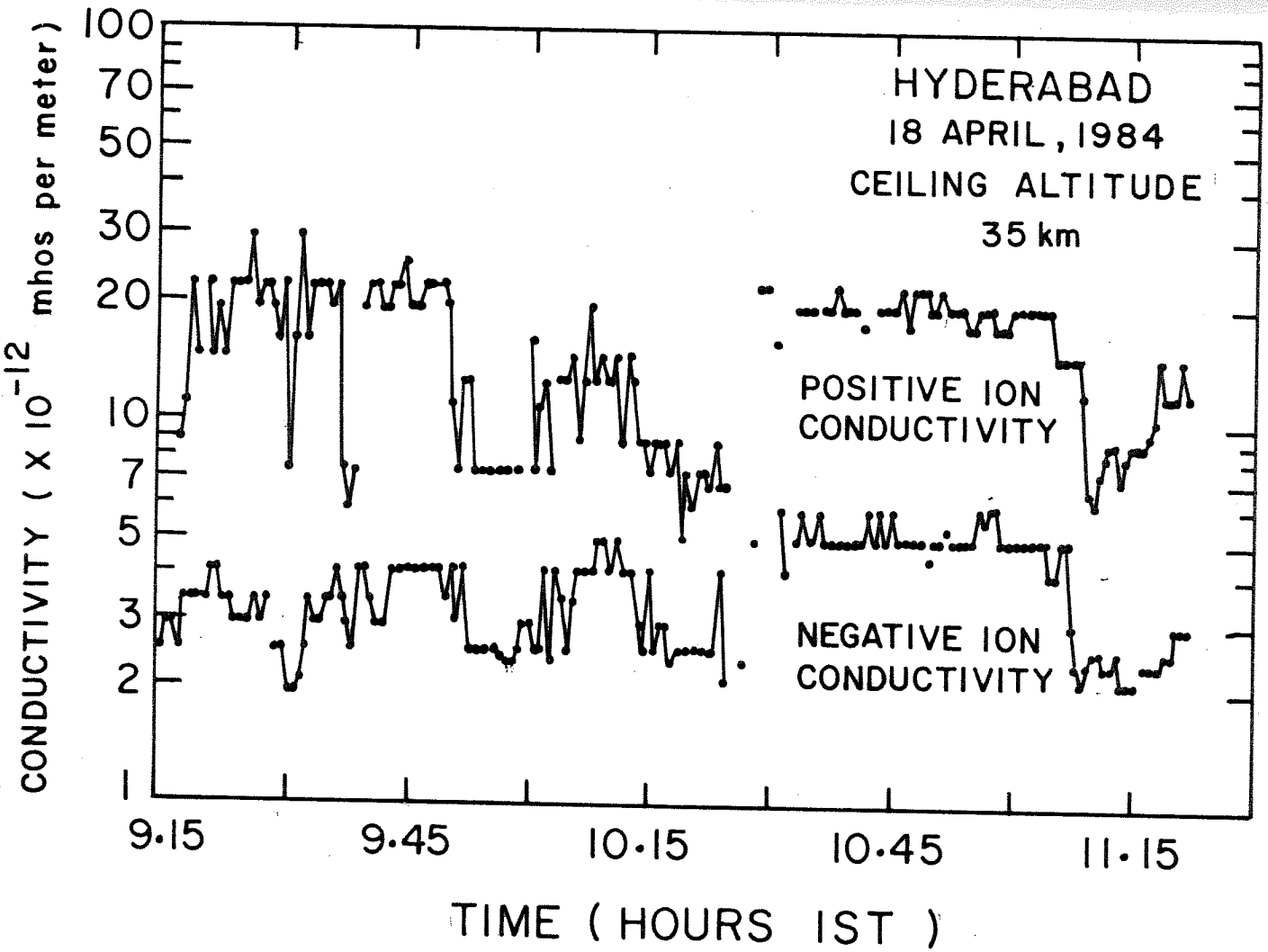

FIG-4.2 CONDUCTIVITY MEASUREMENTS: IMAP-4

2. The two conductivities themselves show a large variation in their magnitude. The variation is approximately by a factor of three between the maximum and minimum values.

3. The variations are in phase. Thus, when the positive ion conductivity is high or low, the negative ion conductivity is also high or low respectively.

The solar zenith angle changed from 43^{o} to 10^{o} between 9.15 a.m. and 12.00 noon. The total conductivity varies between 1.0×10^{-11} s/m and 2.8×10^{-11} s/m at the ceiling altitude of 35 km. However the variations do not show any trend and they are not correlated with the solar zenith angles.

The balloon flight trajectory was monitored using a Radar. It was also monitored optically using a theodolite. Thus the balloon's position was known within an accuracy of five km. An on-board rosemount device gave the balloon altitude. Fig 4.1 shows the balloon ascent profile. As can be seen in the diagram, the balloon reached the ceiling altitude of thirtyfive km at around 9.10 a.m. and this altitude was maintained within ± 1 km throughout the rest of the flight.

4.1.2 Results from IMAP-9 Balloon flight

The IMAP-9 Balloon was launched on 22nd October 1985. This balloon carried a payload identical with the one carried by IMAP-4. It consisted of an instrument for measuring conductivity together with a magnetic aspect sensor. The balloon was launched at 6.00 a.m. and it reached the ceiling altitude of 32 km at around 9.00 a.m. I.S.T. The balloon ascent profile is shown in Fig 4.3. The balloon maintained its altitude within ± 1 km for the remaining time until its cutoff. The balloon was cut off at 11.45 hrs.

Fig 4.4 shows the conductivity measured at the ceiling altitude during the IMAP-9 Flight. The positive ion conductivity during this flight was measured to be 1.2×10^{-11} s/m at the ceiling altitude. The negative ion conductivity was about 2.8×10^{-12} s/m. The following features were observed in the data.

1. The positive ion conductivity was around four and half times larger than the negative ion conductivity.

2. The variation in the absolute magnitudes of the two conductivities was very small unlike the situation during the IMAP-4 flight.

3. There appears to be little evidence of increase in conductivity with solar zenith angle variation. The solar zenith angle at 9.30 a.m. was 40^{o} while at 11.45

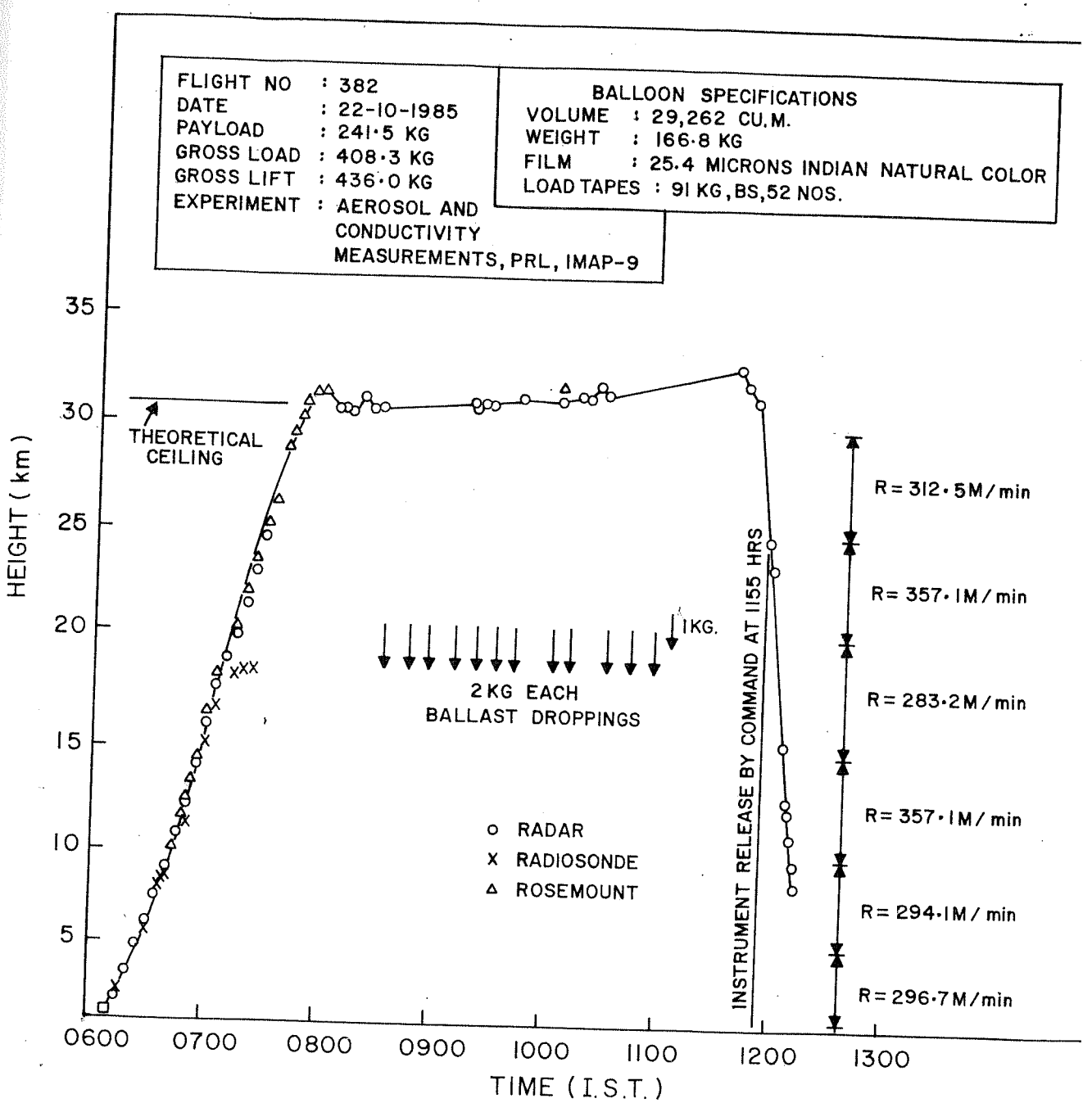

FIG 4.3 BALLOON ASCENT PROFILE- IMAP-9

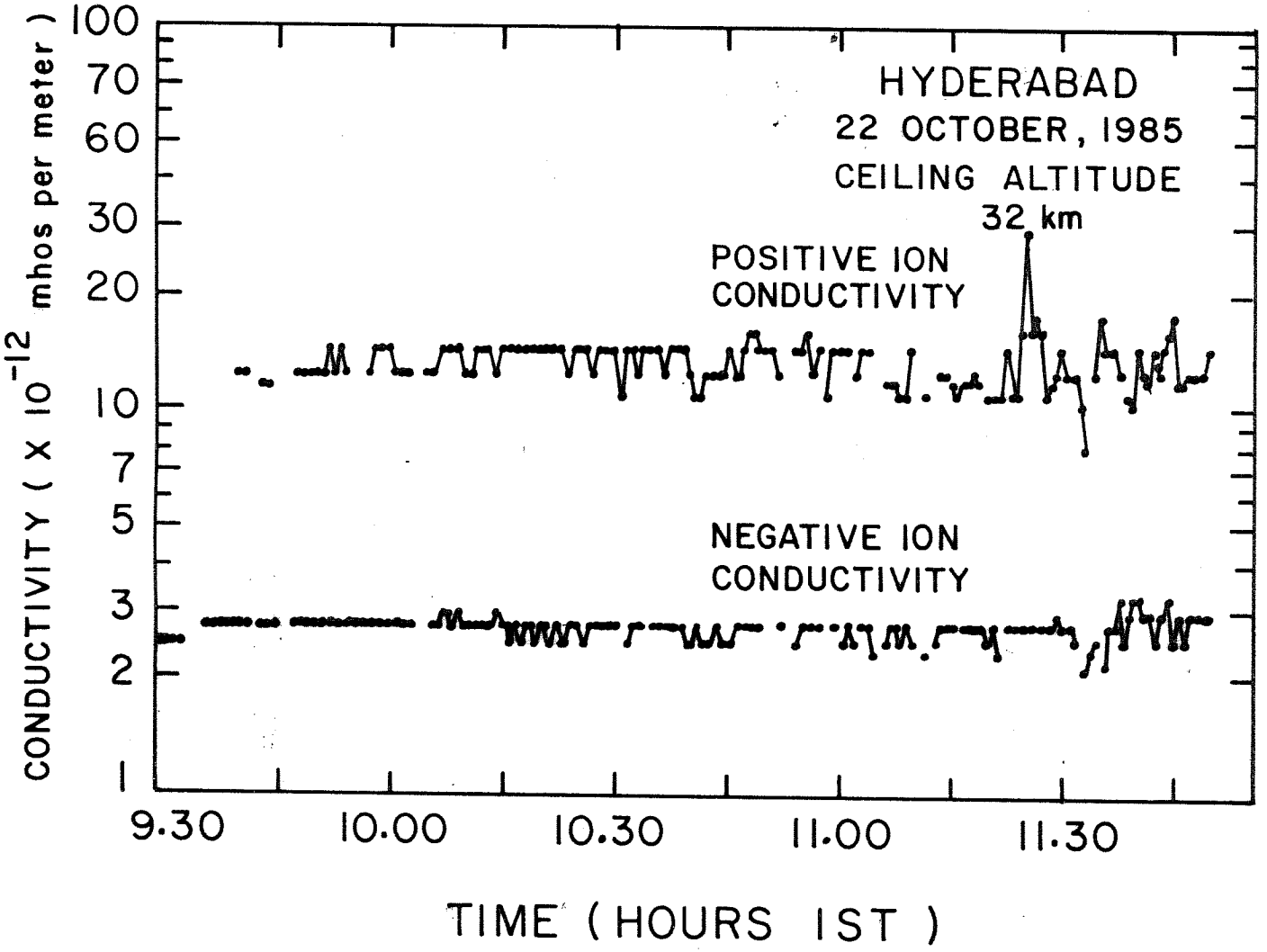

Fig 4.4 Conductivity measurements: IMAP-9

a.m.(cutoff time) was 27^{o}.

4.1.3 Results from IMAP-7 Balloon Flight

The IMAP-7 Balloon was launched on 29 December 1985. The date of launching was one and half months after a major volcanic eruptiin in Nevado Del Rouiz, Colombia (Lat 5^{o}N, Long 75^{o}W). The volcanic dust takes normally about 20 days to go around the globe[Rampino and Self, 1984]. This balloon flight took place at a time when volcanic dust and gases were believed to be present in the stratosphere over India. The launch time was 1.00 a.m. I.S.T. This balloon carried a payload for measuring the vertical electric field and conductivity. It also carried an aspect sensor.

The balloon ascent profile is shown in Fig 4.5. As the launching was done at night time, optical tracking of the balloon was not possible. The IMD Radar stationed at Begampet, Hyderabad tracked the balloon. The balloon reached a ceiling altitude of 34 km at 3.00 a.m.

The conductivity measurements done during this flight are shown in Fig 4.6. The conductivity values which were obtained during this flight are around 3 X 10^{-12}s/m for positive ion conductivity, and 2.2 X 10^{-12}s/m for negative ion conductivity. These values are lower than those which were obtained during the two previous flights. The following features were observed.

1. The positive ion conductivity obtained during this

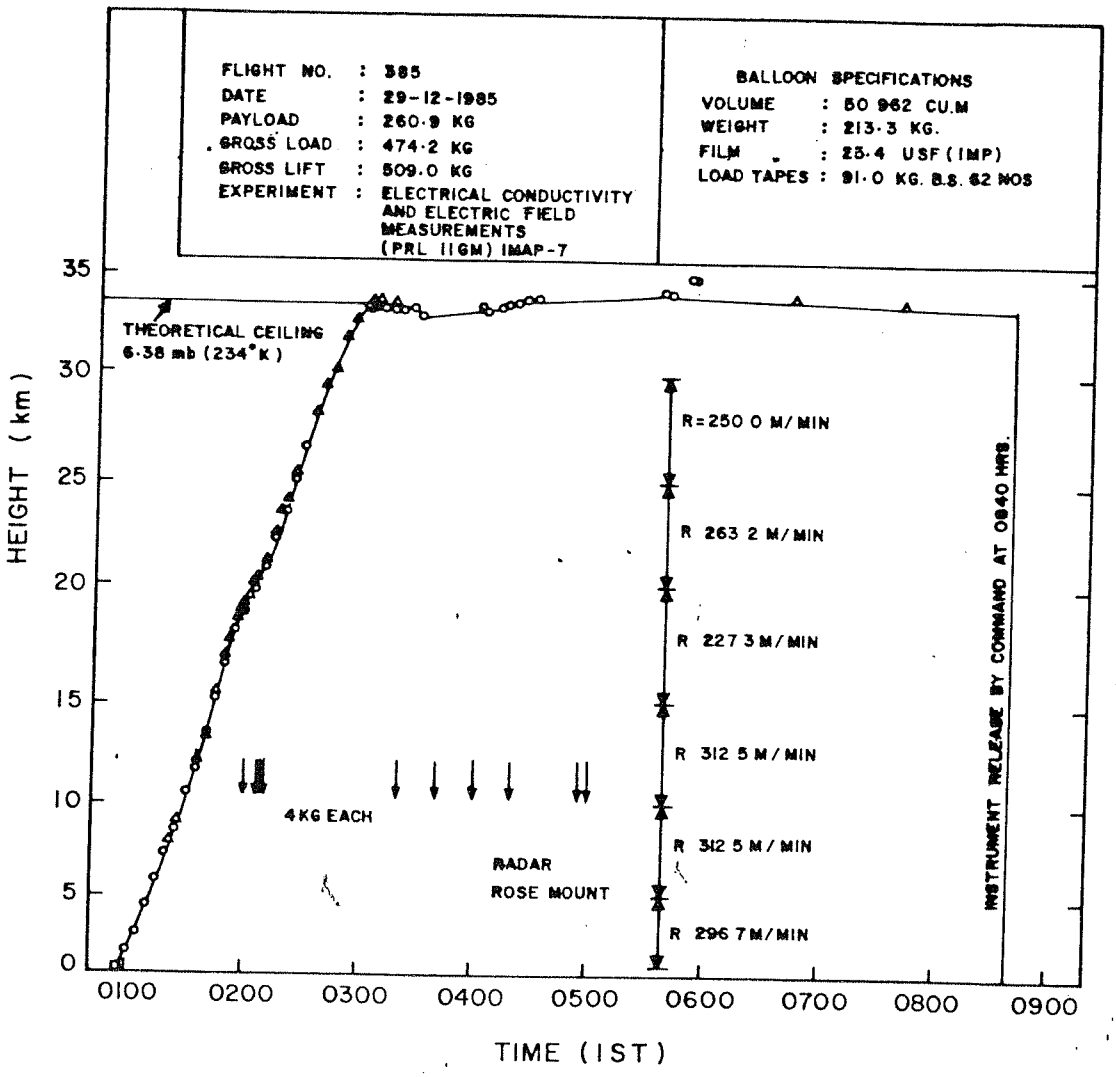

FIG 4.5 BALLOON ASCENT PROFILE - IMAP-7

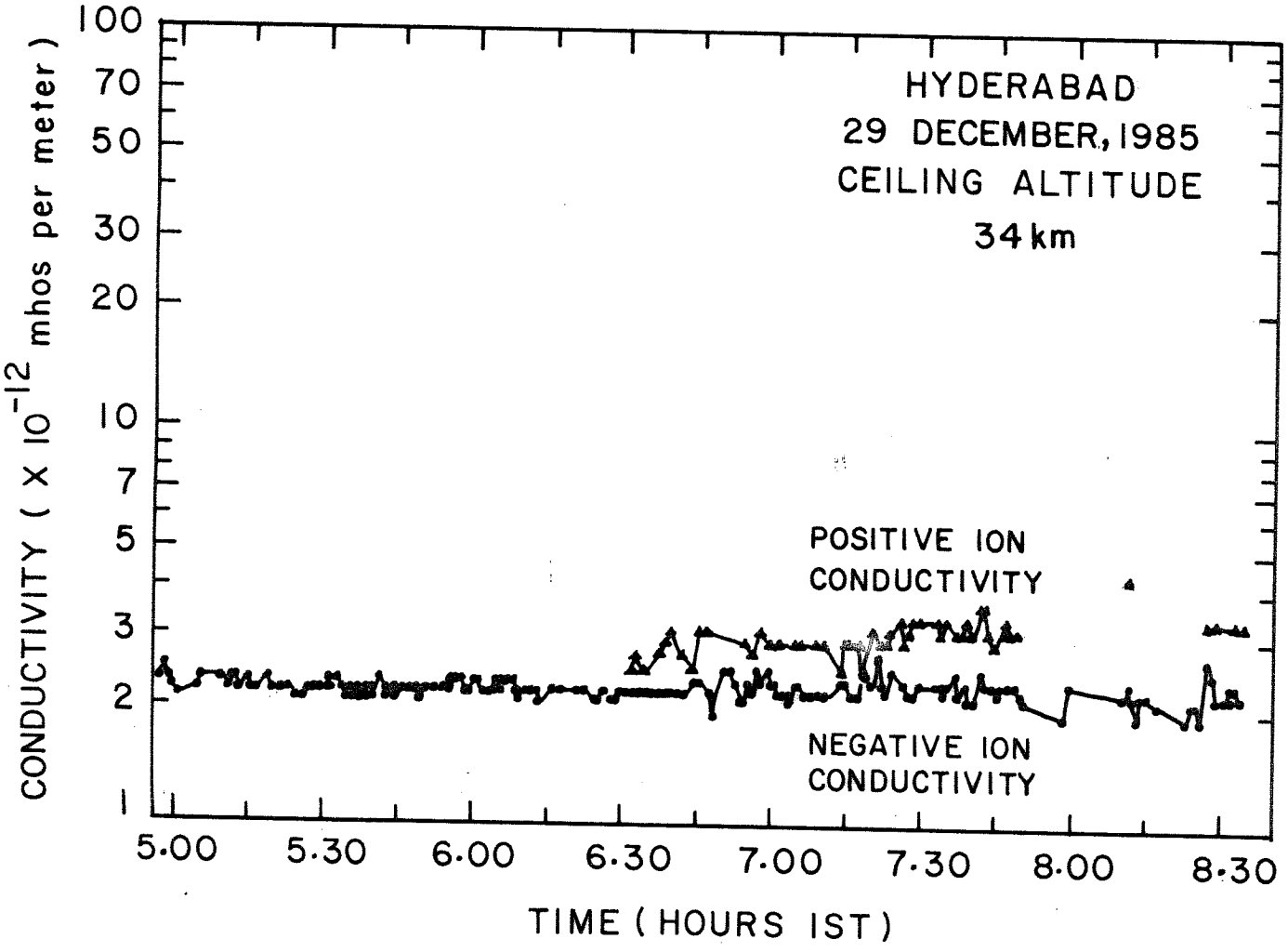

Fig 4.6 Conductivity measurements: IMAP-7

flight is higher than ther negative ion conductivity. However the ratio between the two conductivities is only of the order of 1.3 this time.

2. The ratio of the two ionic conductivities show a very gradual increase after sunrise. The sunrise at the balloon float altitude took place at 6.23 a.m. I.S.T. The solar zenith angle at cutoff time (8.40 a.m.) was 62^{o}. The positive ion conductivity increased from 2.6 X 10^{-12} s/m to 3.1 X 10^{-12} s/m during this period of time.

3. The conductivity values do not show a very large amplitude variation as the IMAP-4 measurements had shown.

4.1.4 Results of IMAP-C2 Balloon Flight

The IMAP-C2 Balloon was launched on 8th April 1987 at 1.00 a.m. I.S.T. This flight was conducted about two and half months after the eruption of the Pacaya volcano in Gautemala(Lat 15^{o}N, Long 90^{o}E). An Apex valve(Described in section 3.2.1) was used on this balloon.This method is used in order to get measurements at more than one altitudes.

The balloon flew over disturbed weather area.This was indicated by the fact that the electric field channel showed a reversal in the electric field direction as compared to the fair weather situation.The electric field

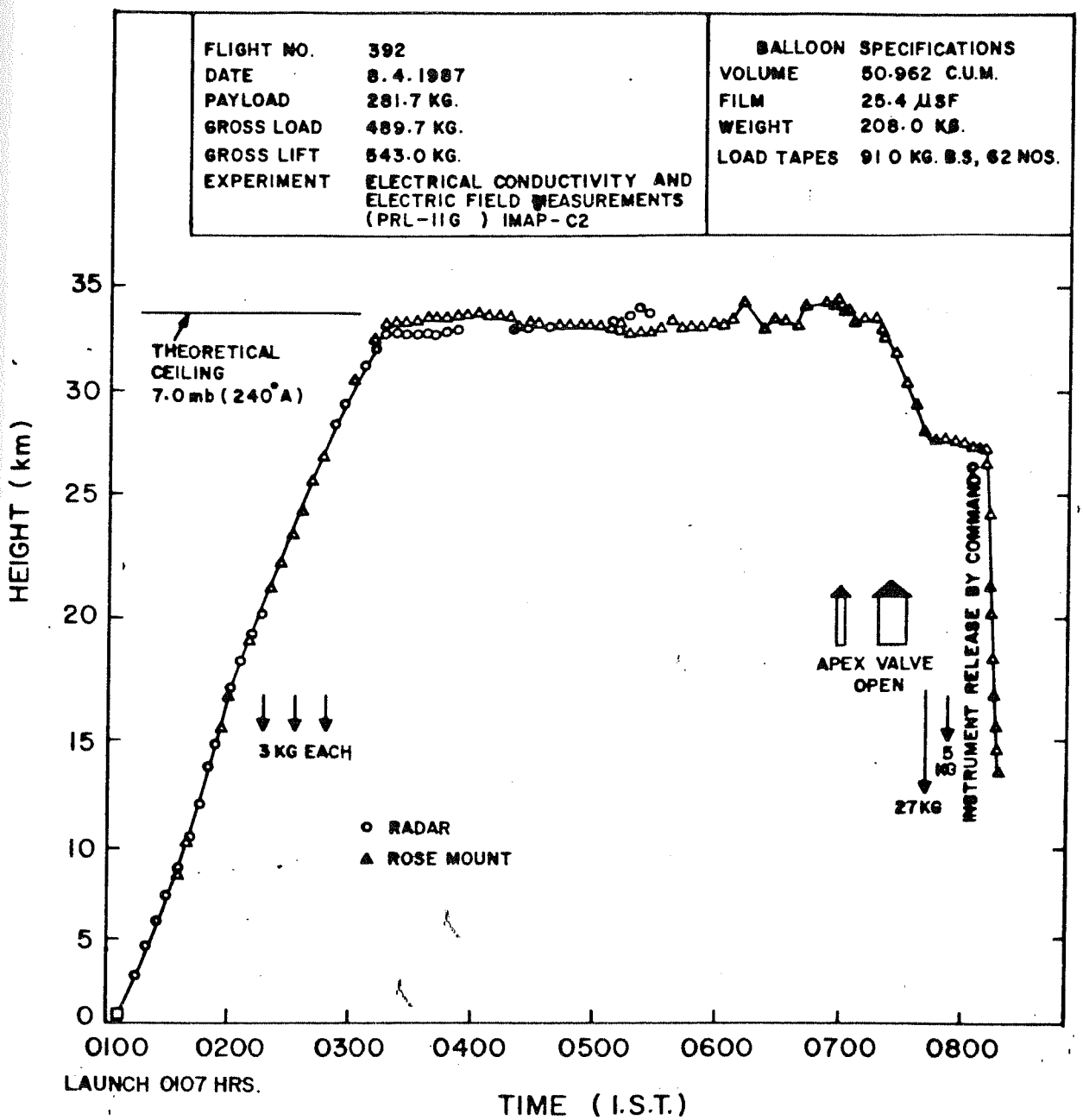

FIG 4.7 BALLOON ASCENT PROFILE: IMAP-C2

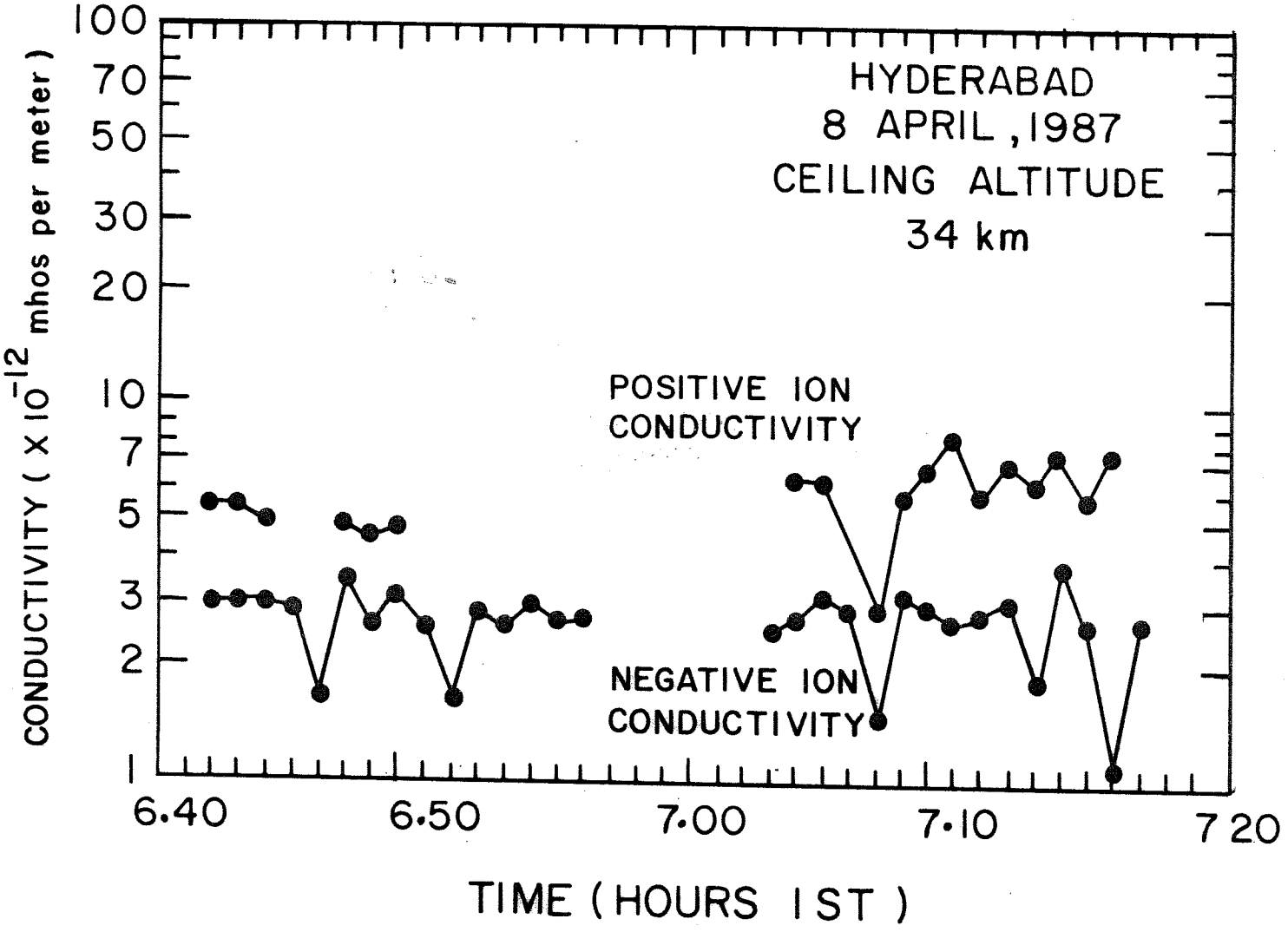

Fig 4.8 Conductivity measurements: IMAP-C2

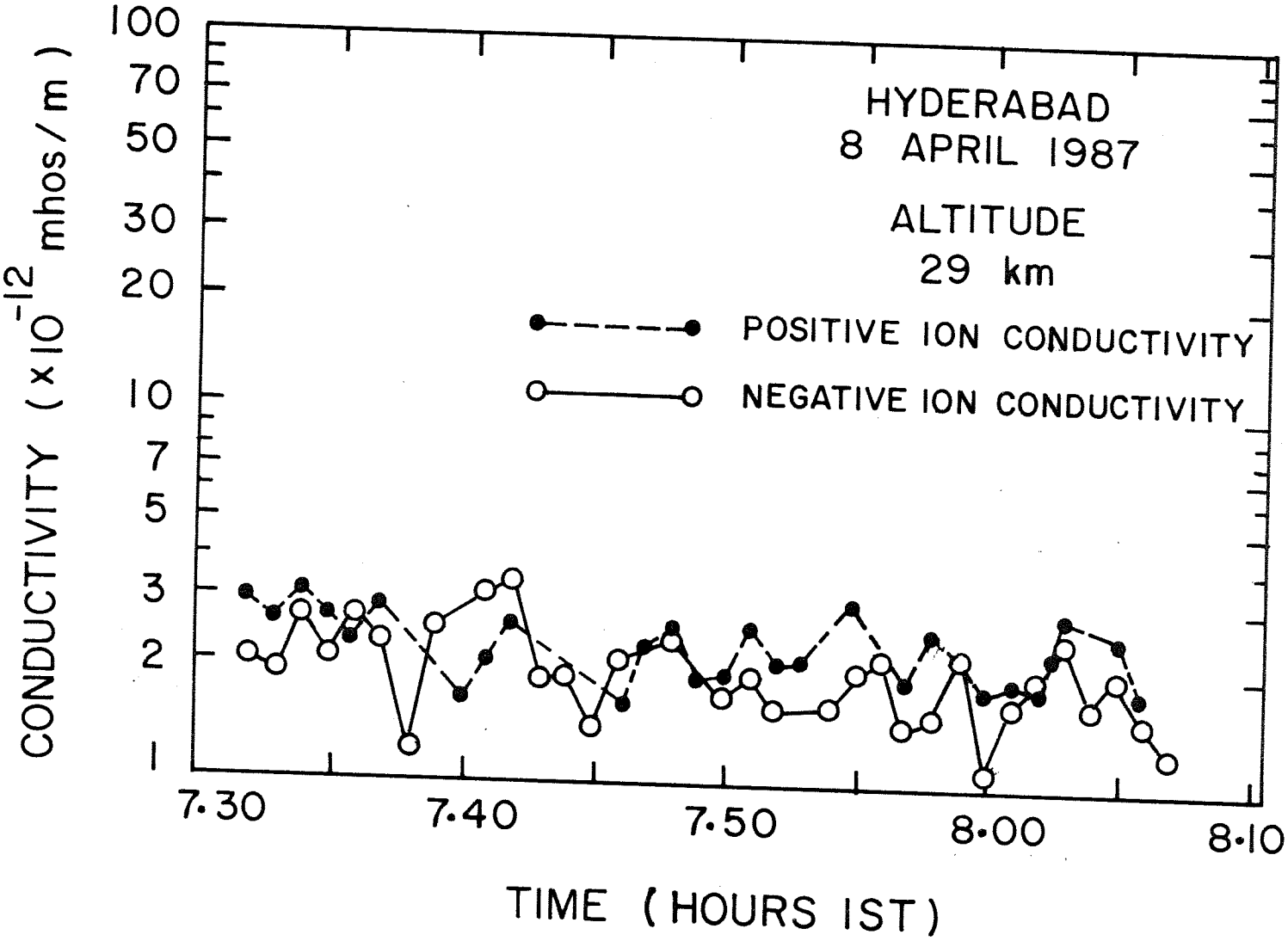

Fig 4.9 Conductivity measurements: IMAP-C2

channel remained saturated almost throughout the duration of measurement.

Conductivity values were obtained at two altitudes. Because of an unexpected high wind condition during the balloon flight, the observations had to be restricted to very short duration(from 6.45 a.m. to 8.10 a.m.). The conductivity results are shown in Fig 4.8 and Fig 4.9. The positive conductivity at 34 km altitude was around 6×10^{-12} s/m and at 29 km altitude was 2.1×10^{-12} s/m. The negative conductivities at these two altitudes were 3×10^{-12} s/m and 1.8×10^{-12} s/m respectively. The following features are observed in the data.

1. The ratio of the two polar conductivities $\sigma_+/\sigma_- \simeq 2.35$ at 34 km. This ratio is $\simeq$ 1.25 at 29 km altitude.

2. At several places the conductivity values are smaller than the average values by almost a factor of three.

3. The positive ion conductivity at 34 km altitude showed a tendency to increase. It increased from about 5×10^{-12} s/m at 6.40 a.m. to 6.5×10^{-12} s/m at 7.15 a.m.

4.2 Results of Electric Field Measurement

The two balloons IMAP-7 and IMAP-C2 carried payloads for measuring electric field. Only the results of IMAP-7 flight are given here. During the IMAP-C2 flight, the electric field was observed to be in the upward direction

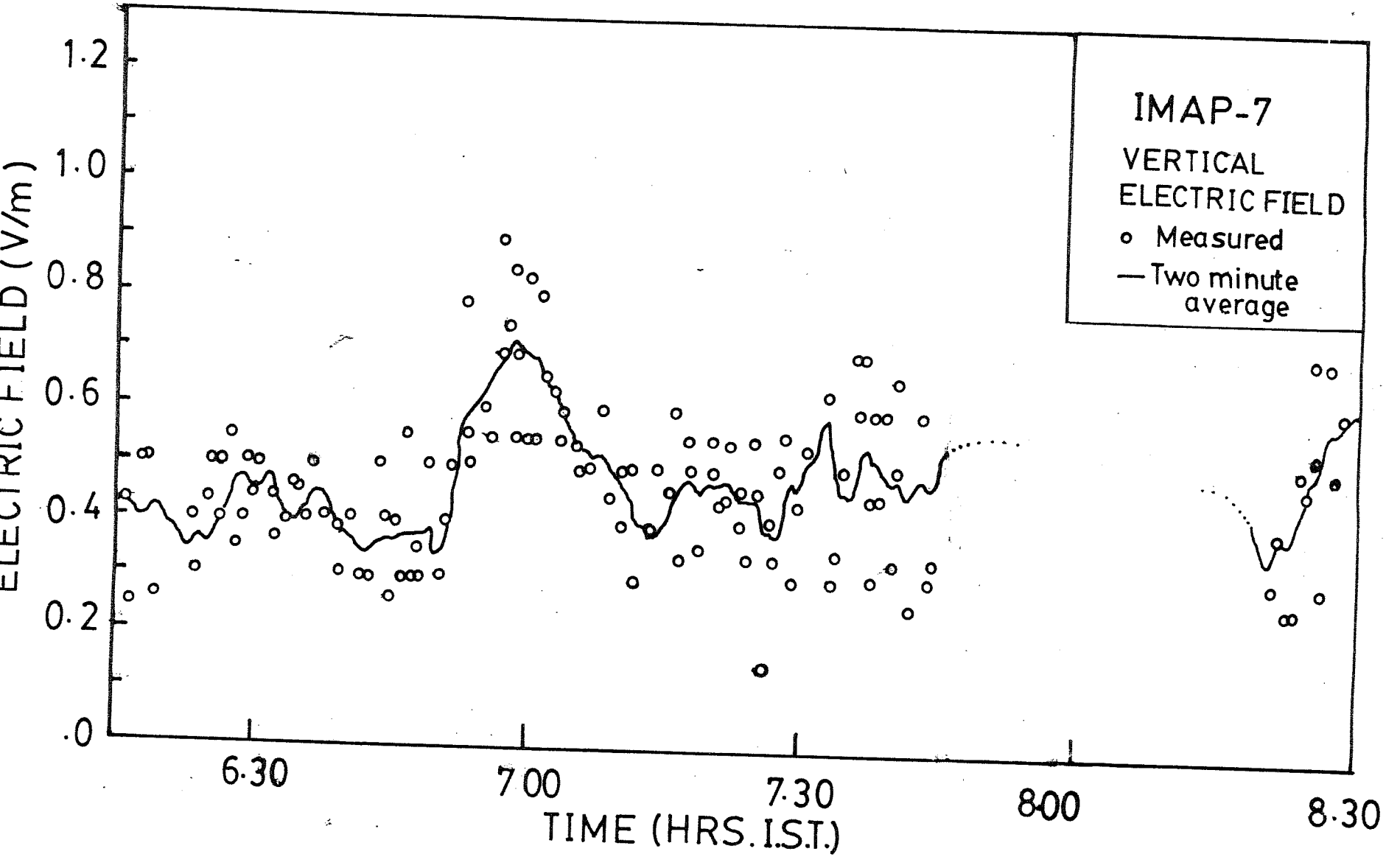

FIG 4.10 VERTICAL ELECTRIC FIELD: IMAP-7

(which is opposite to the normal fair weather direction) and throughout the flight, its magnitude was more than 10 volts per meter(which is the maximum electric field which the instrument could measure).

Fig 4.10 shows the values of electric field obtained during the IMAP-7 flight between 6.15 a.m. and 8.20 a.m. The electric field data before 6.15 a.m. is not shown here because it was contaminated by the charging of the payload gondola. The vertical electric field was measured to be of the order of 0.4 to 0.5 volts per meter.The electric field values showed a variation with time. The electric field varied between around 0.6 to 0.7 volts per meter at 7.00 a.m. and around 0.4 to 0.5 volts per meter at 8.20 a.m.

4.3 Mesospheric Rocket-Borne Ion and Electron Conductivity Data

The results of rocket-borne measurement of ion and electron conductivities in the mesosphere are presented in this section. The Langmuir probe technique was employed for these measurements. The first of these measurements was carried out on 12th August 1972. The D region measurements of electron and ion conductivities from this rocket flight are presented here. The second and third measurements were done on 16 and 17 February 1980 respectively.These measurements were carried out using Centaur rockets which carried Langmuir probe and radio propagation receiver for electron density measurement. The results of this flight were used

for the calibration of the Langmuir probe sensor in the D region. These results are presented in section 4.3.2.

4.3.1 Electron and Ion Conductivity measurement results

A Centaur rocket flight (Flight no. CO 5.14) was conducted from Thumba (Lat 8.5°N, Long 77°E) on 12 August 1972 which carried a Langmuir probe. This probe was operated at both positive and negative bias voltages. The rocket was launched in the morning hours at 7.45 hrs. I.S.T. It reached an altitude of 145 km. Electron and ion currents were measured during the flight. The altitude profiles of these currents are shown in Fig 4.11. These current profiles were used for calculating electron and ion conductivities at the mesospheric altitudes according to the method given in section 2.6. Fig 5.5 (Chapter 5) shows the ion conductivity which was calculated on the basis of the LP data. It was observed that the conductivity increases almost exponentially with altitude between 60 and 90 kms. Its value at 60 km is 6.5 X 10^{-10} s/m and at 90 km is 1.0 X 10^{-7} s/m. The scale height is approximately 6.5 km.

4.3.2 Results of February 1980 measurements

A campaign of three Centaur rocket flights was conducted during the total solar eclipse on 16 February 1980. These rockets carried Langmuir probes (PRL) and radio propagation receivers (NPL, New Delhi). The Langmuir probes gave data on

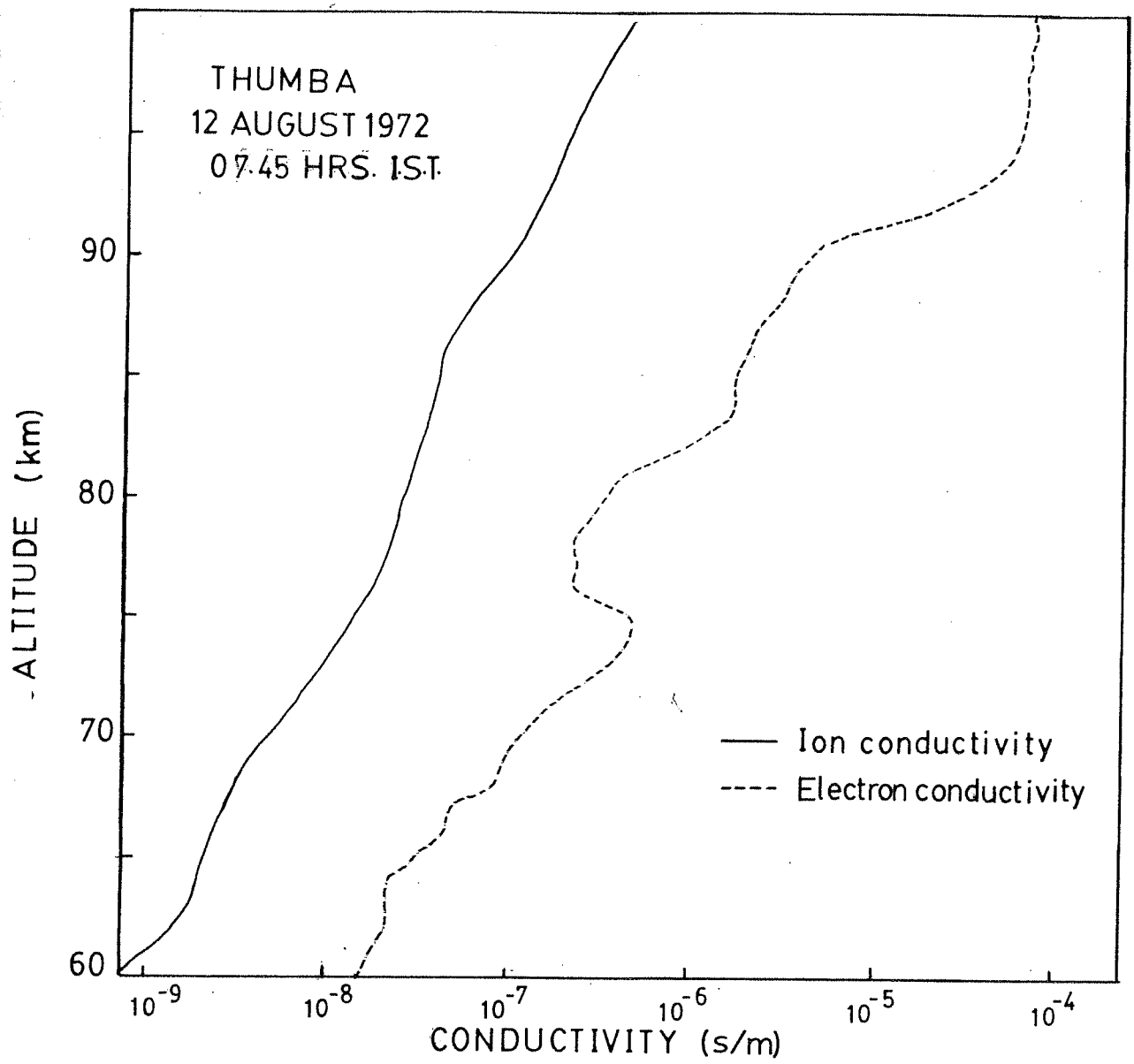

FIG 4.11 POSITIVE ION & ELECTRON CONDUCTIVITY IN MESOSPHERE

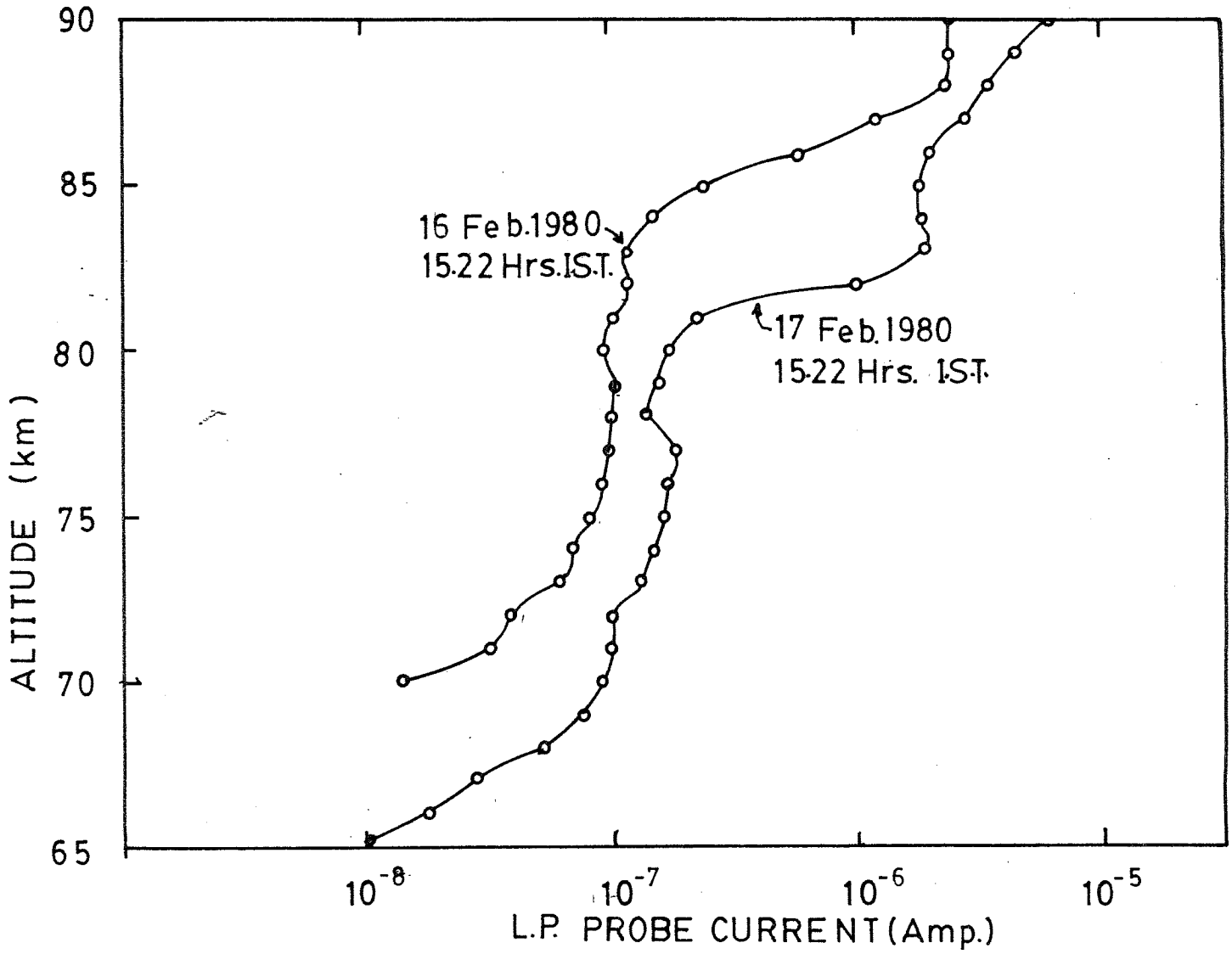
90
85
80
75
70
65
ALTITUDE (km)
16 Feb.1980
15.22 Hrs.I.S.T.
17 Feb.1980
15.22 Hrs. I.S.T.
10^{-8}
10^{-7}
10^{-6}
10^{-5}
L.P. PROBE CURRENT (Amp.)

FIG 4.12

all the three flights while the propagation receiver worked during two of the three flights. The two flights in which both the instruments worked will only be discussed here. These two rockets were launched on 16 February 1980 and 17 February 1980. The launching time for both the flights was 15.22 hrs. I.S.T. The 16 February flight was conducted during the solar eclipse at a time when there was 70 percent obscuration. The technique and the results of measurement of the latter experiment has been described by Somayajulu et al.[1982]. The Langmuir probe results have been given by Gupta and Narayan[1984]. The data was used by the author for the calibration of Langmuir probe as explained in section 2.6.2.

CHAPTER V

DISCUSSIONS

The present chapter contains discussions on various topics of the middle atmospheric electrodynamics. The chapter is divided into several sections, each dealing with a different aspect of the problem. In section 5.1, a comparison has been made between our conductivity measurements and other measurements which have been done using relaxation technique. In section 5.2, an estimate of the ratio of polar conductivities has been done which is based on the experimentally observed ion compositions in the stratosphere. This has been compared with the ratios which we have obtained during our measurements. In section 5.3 various ionisation related parameters have been calculated with help of our results. During two of our balloon flights conducted in the month of April, large fluctuations were observed in the measured conductivity. These are discussed in section 5.4. Section 5.5 deals with some of our observations related to decrease in

conductivity after volcanic eruptions. Sestion 5.6 contains a discussion on the electric field measurements done during IMAP-7 flight. In Section 5.7, our balloon-borne measurements have been presented together with rocket-borne measurements of ion conductivity in order to get an overall view of conductivity in the middle atmosphere. Section 5.8 deals with certain observations of variation of floating potential of rocket body in the mesosphere and its possible interpretations.

5.1 Conductivity measurements: a comparative study

In the present section, a comparative study has been made between our measurements and those done by other groups at various locations. Firstly, a comparison with those results will be done which have been obtained using the relaxation technique. Most of the measurements have been of a single altitude-long duration type. Thus it was found appropreate to reduce all conductivity values to a common altitude. The values presented in Table 5.1 are measurements done by various groups which have been reduced to the corresponding value at 30 km using equation 2.35(page 57). This has been done for the sake of convenience in comparison. The scale height has been taken as 7.7 km (This scale height value appears to be appropreate in the two cases of Mozer and Serlin[1969], and Ogawa in Rosen et al.[1982] where a height profile was available: Fig 5.1).

Figure 5.1 summarises various conductivity measurements

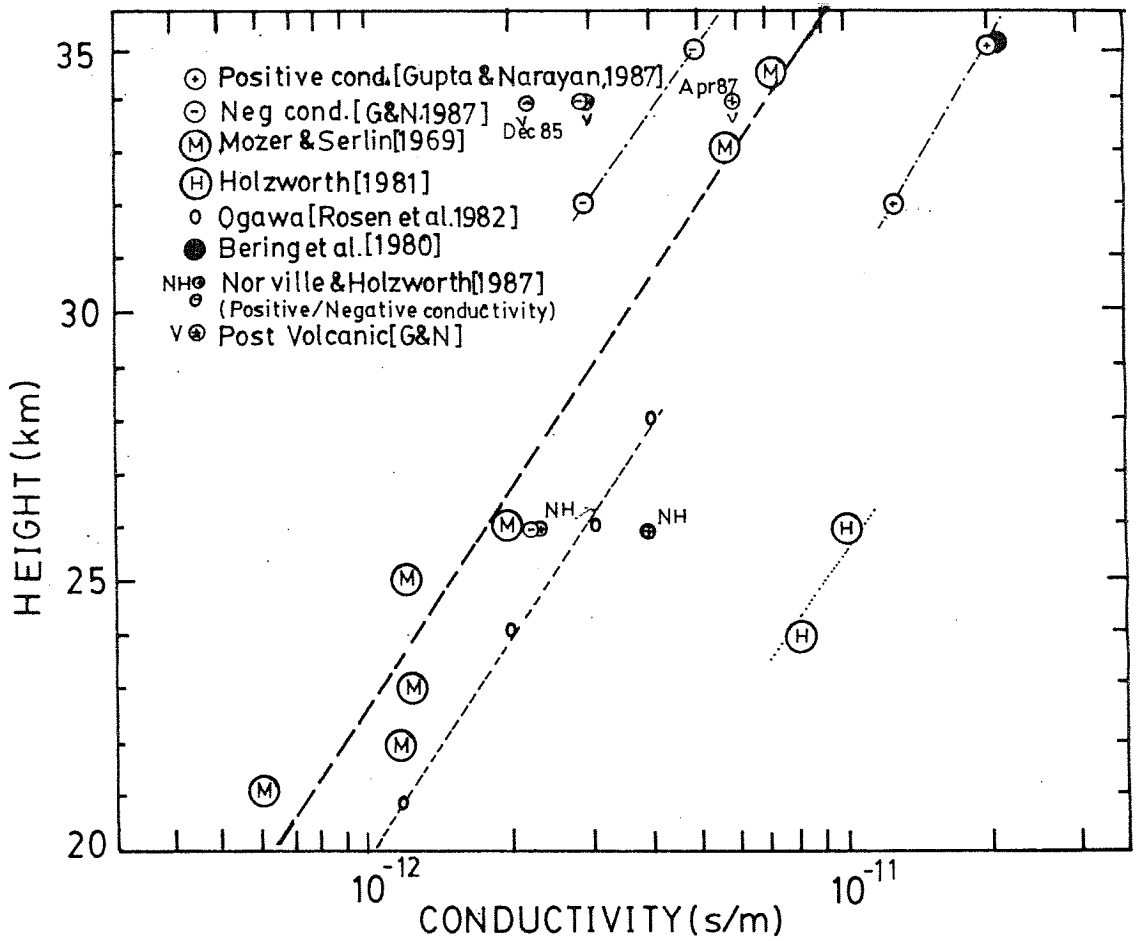

FIG 5.1 CONDUCTIVITY MEASUREMENTS: A COMPARATIVE STUDY

Table 5.1

List of various measurements of conductivity using Relaxation Technique
(The values are reduced to 30 km altitiude level)

Quantity measured	Value ($\times 10^{-12}$ s/m)	Remarks
Total Cond.	3.3	Mozer and Serlin[1969] (Several altitudes)
Total Cond.	10.9	Bering et al.[1980] (35 km alt.)
Total Cond.	16.8	Holzworth [1981] (26 km alt.)
Pos. Cond.	6.0	Ogawa [Rosen et al.1982] (Several altitudes)
Total Cond.	8.6	Holzworth et al.[1984] (26 km alt.)
Pos. Cond. Neg. Cond.	4.4 4.2	Norville & Holzworth [1987] :(26 km alt.) measured: Mar 1983
Pos. Cond. Neg. Cond.	8.7 4.2	Norville & Holzworth [1987] :(26 km alt.) measured: Feb 1984
Pos. Cond. Neg. Cond.	9.25 2.15	Gupta & Narayan [1987] :(32 km alt.) measured: Oct 1985
Pos. Cond. Neg. Cond.	1.78 1.3	Gupta & Narayan [1987] :(34 km alt.) measured: Dec 1985

which have been done using relaxation technique. Measurements done by Mozer and Serlin[1969], Bering et al.[1980], Holzworth et al.[1981, 1984], Norville and Holzworth [1987], and Ogawa [Rosen et al., 1982] have been compared with our measurements[Gupta and Narayan, 1987]. If one compares the various conductivity values reduced to 30 km(Table 5.1), one finds a large difference in value among the different measurements. For example, the measurements done by Holzworth[1981] reduce to a value 1.9 times larger than ours. At the same time our IMAP-4 and IMAP-7 values are about 2 times larger than Ogawa's values and 3.5 times larger than Mozer and Serlins' values. Bering et al's values at 35 km are almost same as our values. The various measurements span a range of about one order in magnitude.

There are two main reasons for variation in conductivity. One is the variation in ion composition between different altitudes. The other reason is variation in ion production rate with latitude. This is due to the latitude effect in the cosmic ray flux. The ion production rate towards the pole at a given altitude is larger than that at the equator[Heaps, 1978]. Norville and Holzworth[1987] have observed a variation of conductivity with latitude and their measurements fit a latitude dependence of $\sigma = (A+B\sin^4\lambda)^{1/2}$ as suggested by Heaps. A and B are constants and λ is the geomagnetic latitude. Such a dependence can account for the variation in conductivity between high and low latitudes which is present in different measurements shown in table 5.1. Holzworth's high

latitude measurements[1981] appear to be the largest out of these. Bering et al's measurements[1980] are also quite high. Both are high latitude measurements ($\lambda > 70^{o}$). It is not clear why Mozer's measurements conducted at Fort Churchill is so low. The measurements by Ogawa are done from the mid-latitude station of Laramie and have a value lower than the high latitude values. Out of the measurements done by us, the negative ion conductivity measurements are in agreement with the abovementioned dependence on latitude. At the same time, a factor of 4 high value of $\sigma+$ as compared to $\sigma-$ does not fit into this picture.

Most of the measurements presented here as well as other measurements of polar conductivity[e.g. Paltridge, 1965] show a $\sigma+/\sigma-$ ratio of $\simeq$ 1. Almost all of them have been done below an altitude of 30 km. Our measurements at 35 km altitude show a significantly large $\sigma+/\sigma-$ ratio of about 4. Norville and Holzworth[1987] have also reported measurements(done in Feb. 1984 at 26 km altitude) in which the $\sigma+/\sigma-$ ratio is $\simeq$2 which is significantly different from 1. Norville and Holzworth have also mentioned observing day-night variation in positive ion conductivity which they have attributed to instrumental sources. But the author has reasons to believe that such variations may not be fully instrumental. A detailed discussion of various instrumental sources of error has been done in chapter 2 of this thesis, including a discussion of photoelectric effect (Section 2.3.4, p47). If photoemission is present and is appreciably large, then no measurements of conductivity will

be possible at all. The photoelectric currents have to be in a range of about 10 percent to 60 percent of the maximum probe current(corresponding to the charging pulse voltage) to make the distortion in the exponential curve not very large so that the curve can still be interpreted to give an erroneous conductivity value. Beyond that the distortion will be obvious, and can easily be detected because the best fitting exponential curves will have different time constants at different portions of the curve. In such cases the data cannot be interpreted to give conductivity values.

Continuous measurements of conductivity between sunrise time and noon would have been useful in understanding the nature of sunrise effect better. Measurements of conductivity over a period between the sunrise time and noon as well as measurements done while keeping the sensor in shade are needed to positively resolve these doubts about presence of sources of error. There are plans for conducting such measurements in future.

In Fig 5.2, we have shown our mesospheric conductivity values obtained from Thumba rocket data and have compared them with Maynard et al.'s [1984] values. These latter measurements were made from high latitude station Andoya, Norway(69.3^{o}N, 16^{o}E). The diagram shows positive ion conductivity values measured between 60 km and 90 km altitude, by the use of rocket-borne Langmuir probes and the positive conductivity values obtained during various balloon flights in the stratosphere.

The three measurements of Maynard et al. are night-time

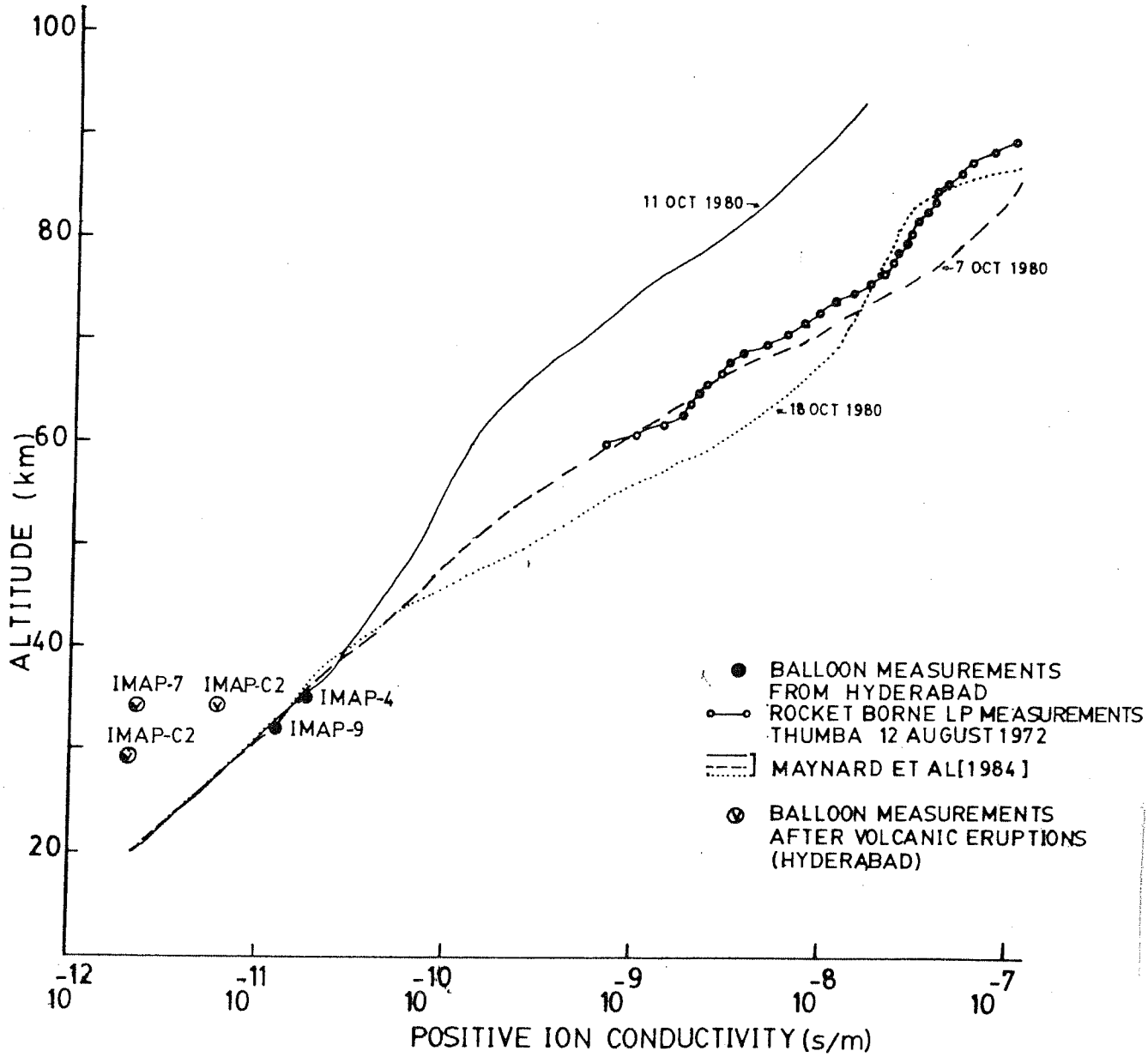

FIG 5.2 POSITIVE CONDUCTIVITY IN MIDDLE ATMOSPHERE

measurements and they show a factor of 10 variation at 60 km altitude. Out of these the measurements of 7th and 18th October correspond to magnetically disturbed days while the 11th October measurement corresponds to a magnetically quiet day. The magnitude of X ray and electron energy deposition for the magnetically disturbed days were measured by Goldberg et al. [1984]. Since low latitudes should not show auroral effects, so a less amount of variation due to fluctuations in magnetic conditions are expected. The main mesospheric sources of ionisation at low latitudes are solar Lyman α radiation, and meteoric showers as discussed in chapter 1(section 1.3.1). Thus although variations in conductivity can occur at these latitudes, the range of variation should be smaller. The only mesospheric measurement done by us at low latitudes is shown in Fig 4.11. It was done during morning hours (7.45 Hrs. I.S.T.) when the solar zenith angle was $\sim 60^{o}$. Considering an error of about 20 percent, these measurements appear to be about same in magnitude as high latitude values.

5.2 Mobility and Ion composition

Ionic mobility is a function of the masses of constituent ions in the atmosphere. The positive and negative ion mobilities are related to the masses and relative abundances of corresponding ions via equation 1.7.

$$\mu\pm = \frac{e}{N\pm} \sum_{\pm} \frac{ni}{mi\,\nu i}$$

With the advent of balloon-borne cryogenic mass spectrometers, it has now become possible to measure the relative abundances of the ionic species present in the air. Thus it has become possible to calculate the mobility of positive and negative ions in the stratosphere.

Using the ion composition measured by Arijs et al.[1983] and Schlager and Arnold[1987] and theoretical profiles of Arijs and Brasseur[1986], the positive and negative mobilities were calculated for various altitudes on the basis of equation 1.7. Apart from the relative abundance and mass of the constituent ions, this equation also requires a knowledge of the collision frequency. The collision frequency ν is a function of the mass and scattering cross section of the colliding particles[Rief, 1965, p470].

$$\nu = n\tilde{\sigma}\bar{v} \qquad ..(5.1)$$

where n is the number density of air molecules, $\tilde{\sigma}$ is the scattering cross section and $\bar{v}$ is the average relative velocity between the two molecules.

For most of the cluster ions present in the stratosphere the scattering cross section information is not available. Therefore a calculation of mobility using equation 1.7 directly is not possible. Meyerott et al.[1980] have discussed laboratory measurements of mobility by Huertas et al.[1974] and others, as a function of ionic mass and suggested that they can be used to obtain the knowledge

of ionic masses if moility measurements are available(or vice versa). These studies have their own limitations and cannot be taken as final. A rough calculation of the relative values of collision cross sections was done for several molecular mass values. The calculated values of average molecular diameters are shown in Table 5.2. If we assume the mobilities as given in the paper[Meyerott et al., 1980], then the average molecular diameters do not seem to increase with increasing molecular masses. This obviously cannot be true. On the basis of this discrepency, the author feels that in actuality, variation of mobility with mass ought to be much more than what these measured values show.

The author has done a theoretical estimation of mobility for different masses (based on the assumptions given below) and calculated the expected ratio of the two mobilities at different altitudes. The method used is given below and the results are given in Fig 5.3.

One can use a modified version of equation 5.1 to do this calculation. For heterogeneous molecules the collision rate is given by the following expression[Cadle and Kiang, 1977]:

$$z = \frac{NaNb}{8} (\tilde{\sigma}_a + \tilde{\sigma}_b)^2 \left[8\pi RT\left(\frac{Ma+Mb}{Ma.Mb}\right)\right]^{1/2} \quad ..(5.2)$$

where z is the heterogeneous collision rate, Na and Nb are the number densities of species A and B, $\tilde{\sigma}_a$ and $\tilde{\sigma}_b$ are their (average) molecular diameters, and Ma and Mb are their respective masses.

The collision fequency for species (B) is just $\frac{z}{Nb}$. Since

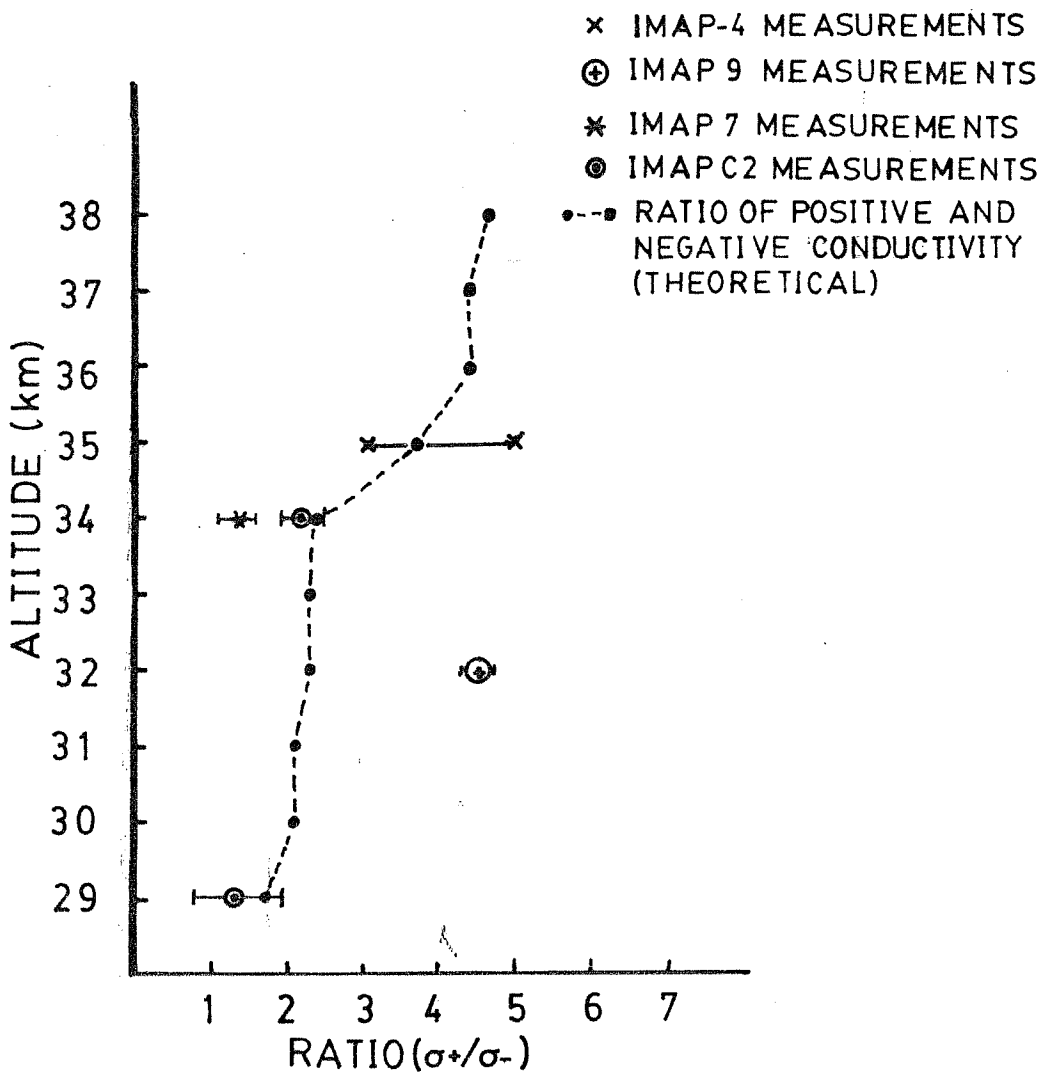

FIG 5.3 RATIO OF POLAR CONDUCTIVITIES

Table 5.2

Calculated (Relative) Molecular sizes from the Mobility-mass relation in Meyerott et al.[1980]

Mass	Reduced mobility	Coll.Freq. (relative) (ν: $1/(m\mu_{red})$)	Cross Section (relative) ($\tilde{\sigma}$: $\nu_{red}\sqrt{m}$)
amu	cm^2/v.sec	(arb.units)	(arb.units)
70	2.0	7.143 $X10^{-3}$	0.0319
100	1.75	5.714 $X10^{-3}$	0.0267
350	1.0	2.857 $X10^{-3}$	0.0145
1000	0.65	1.538 10^{-3}	0.00803
10000	0.14	7.4128 10^{-4}	0.00377

one does not know the scattering cross sections, they have to be assumed. The following assumptions were made regarding the scattering cross sections: Firstly, the cluster ions were assumed to be spherical in shape. (The larger an ion is, the more its shape approaches a spherical shape). Secondly the molecular volume was calculated by dividing the mass by its density. A weighted average of densities of cluster components (e.g. H_2SO_4, H_2O, etc.) was used, and the cross secions corresponding to different masses were calculaed. This method for calculating the size of molecules appears to be adequate for a first order calculation of molecular size [Lange's Handbook of Chemistry, 1973]. Using the above assumptions the collision frequency and the reduced mobility for different ionic species were calculated (Table 5.3). These were used for calculating the average reduced ionic mobilities for positive and negative species at different altitudes. The measured ion composition data of Schlager and Arnold[1987] and Arijs et al.[1983] were used. Fig 5.3 shows the calculaed ratio of polar mobilities.

According to equation 1.10, the ratio of polar conductivities is same as the ratio of the average mobilities of the positive and the negative ionic species. We have carried out balloon-borne measurements of polar conductivity in the stratosphere during four occasions. During two of these effects of volcanic aerosols were present (section 5.5), but during the other two flights (IMAP-4 AND IMAP-9), volcanic effect was not there. The ratio of polar conductivities observed during all these

Table 5.3

Collision Frequency(at NTP) and Reduced Mobility for different Stratospheric Ions

Ionic Species	Mass (amu)	Density $\times 10^3 kg/m^3$	Coll. Freq. $\times 10^9 sec^{-1}$	Mobility $\times 10^{-4} m^2/Volt\,sec$
$NO_3^-.HNO_3$	125	1.5	7.263	10.554
$HSO_4^-.HNO_3$	160	1.68	7.524	7.958
$NO_3^-.(HNO_3)_2$	125	1.5	7.263	10.554
$HSO_4^-.H_2SO_4$	195	1.8	7.837	6.269
$HSO_4^-.(HNO_3)_2$	223	1.64	8.500	5.054
$HSO_4^-.(H_2SO_4)_2$	293	1.8	9.063	3.608
$HSO_4^-.(H_2SO_4)_3$	391	1.8	10.13	2.419
$HSO_4^-.(H_2SO_4)_4$	489	1.8	11.11	1.763
$H^+.(H_2O)_3$	55	1.0	6.743	25.84
$H^+.(H_2O)_4$	73	1.0	7.375	17.79
$H^+.(H_2O)_5$	91	1.0	7.683	13.7
$H^+.X.(H_2O)$	60	0.84	7.325	21.8
$H^+.X.(H_2O)_2$	78	0.88	7.712	15.92
$H^+.X.(H_2O)_3$	96	0.9	8.125	12.28
$H^+.X_2.(H_2O)$	101	0.81	8.598	11.03
$H^+.X_2.(H_2O)_2$	119	0.84	8.715	9.238

occasions are also shown in Fig 5.3 along with the theoretically estimated values of μ_+/μ_- ratio. During the IMAP-9 flight(22 October 1985),we observed a $\sigma+/\sigma-$ ratio of roughly 4.5 at the ceiling altitude 32 km(Fig 4.4). During the IMAP-4 flight we observed large fluctuations in the conductivity data. This data will also be discussed in section 5.4. The polar conductivity values appeared to switch between a set of lower limit values and one of higher limit values. These changes were in phase with each other(Fig 4.2). The ratio of $\sigma+/\sigma-$ at these two limits were 3 and 5 respectively.

The ratio $\sigma+/\sigma-$ was found to be much less after volcanic eruptions on both the occasions. The ratio during IMAP-7 flight was around 1.3 while that during IMAP-C2 was around 2.1 at 34 km and around 1.25 at 29 km.(This aspect will be dealt with in more detail in section 5.5).

The high value of $\sigma+/\sigma-$ ratio ($\simeq$ 4.5) that we obtained during our measurements thus are consistent with the measured relative abundances of the ionic species. It was also noticed that the ratio of polar conductivities becomes smaller when volcanic aerosols are present in the stratosphere. The increase in $\sigma+/\sigma-$ ratio from ~1.25 at 29 km to ~2.1 at 34 km which was observed during IMAP-C2 flight seems to go in line with the model results (Fig 5.3) which predict an increase of σ_+/σ_- ratio by a factor of 2 between 29 km and 36 km altitude.

Measurements done elsewhere using balloon-borne Gerdien condensers and relaxation technique [Paltridge, 1965,

Holzworth, 1981] have shown a ratio 1 upto 30 km. Parachute-borne Gerdien condensers at 30-40 km altitudes have also reported $\sigma+/\sigma-$ ratio as $\simeq 1$[Maynard et al. 1984]. The reason for this discrepency in the ratio of polar conductivities is not clear.

Norville and Holzworth[1987] have reported measuring a σ_+/σ_- ratio of $\simeq 1$ during 1983 and $\simeq 2$ during 1984. These measurements were done at 26 km altitude. The reason for this difference is not yet explained. But one would expect on the basis of the μ_+/μ_- ratio shown in fig 5.3 that the ratio will further increase at altitudes around 35 km. Also, one can expect that the altitude at which the σ_+/σ_- ratio increases significantly, i.e. at which the nature of the predominant ions changes, has a latitude dependence. This might be the reason why even at 31 km, we observed a σ_+/σ_- ratio of 4.5.

Regarding the solar zenith angle dependence of conductivity as discussed by Mitchell et al.[1976] and observed by Norville and Holzworth[1987], it is difficult to say at this point what is the magnitude of such an effect in our data. We did observe a small tendency of conductivity to increase after sunrise, but it was small. We would like to have some more measurements before making any conclusive remarks.

5.3 The small ion number density and mobility

Apart from conductivity and electric field, there are

several other parameters of importance in the middle atmospheric electrodynamics. These parameters are related to each other. During our balloon flights we have measured conductivity in the stratosphere. It is of interest to see how our conductivity measurements relate to some of these other atmospheric electrical parameters.

The number density of small ions is governed by the continuity equation given below(equation 1.1). For steady state,

$$q - \alpha n_+ n_- - \beta n_{\pm} n_A = 0$$

Since $n+ \simeq n-$ we can write that

$$q - \alpha n^2 - \beta n n_A = 0 \qquad ..(5.3)$$

In the above equation, the first term q is the ion production rate. The other two terms are loss terms. The second term gives the ion loss rate due to recombination while the third term gives the rate of loss of ions through attachment to aerosols. Under normal circumstances, the loss of small ions by attachment process is much less than loss by recombination so that we can write [Gringel et al. 1978],

$$n = (q/\alpha)^{1/2} \qquad ..(5.4)$$

This relation is generally used to estimate q from the experimentally measured values of n and α [Gringel et al.

1978]. The small ion number density is usually measured with a Gerdien condenser operated in saturation mode[Paltridge, 1965, Rosen and Hofmann, 1981B].

The same equation, if one knows q and α, can give the number density also[Datta et al., 1984]. An estimate for the number density of ions for low latitudes was done in the following way:

In order to get α, we used the experimentally determined values of Smith and Adams[1982]. These appear to be the most representative out of all the values of α obtained so far.

The ion production rate corresponding to the geomagnetic latitude of Hyderabad(11.1°N) has been measured by Neher[1967]. There are also theoretical estimates. A calculation based on Velinov's method[1968] has been done by Datta et al.[1987A] which gives the ion production rate due to primary and secondary cosmic rays for altitudes between 18 km and 45 km. These values at 30 - 35 kms. altitudes are smaller than Neher's measured values. Verma and Bhatnagar[1987], Verma and Kothari[1987] have measured the albedo and the re-entrant components of CR from Hyderabad (Geomag. Lat. 11.1°N) and estimated their contribution to the ion production rate. They showed that at low latitudes, a substantial contribution to the ionisation rate comes from the albedo and the re-entrant components. The theoretically calculated values of Datta et al. and Verma et al. have been used for obtaining the overall ionisation rate.

A third estimate of ionisation rate can be done on

basis of Heaps' parametric formula. Heaps[1978] has given a semiemperical formula for the ion production rate. The ionisation rate calculated from Heaps' formula has also been used for estimating ion density. These ion density estimates have been shown in Table 5.4.

The number density obtained in this way has been used for calculating the average mobilities of the positive and negative ions. The mobility is given by

$$\mu = \sigma/ne \qquad ..(5.5)$$

We have used our $\sigma+$ and $\sigma-$ values at 32 and 35 km altitudes for calculating the mobilities. The mobilities obtained are tabulated in Table 5.4.

If one assumes that the dominant positive and negative ions are generally the same as those at midlatitudes, then out of the three formulas for ion production rate, the first one appears to be nearest to the actual situation. These calculations also point out to the possibility that the values of number density assumed so far might be underestimates. Direct measurements apart from those done by Neher[1967] are lacking.

5.4 Conductivity fluctuations observed during premonsoon period

The April-May months in the Indian zone are characterised by frequent thunderstorms and showers. This is

Table 5.4

Estimates of Ion Density and Mobility from Ion Production Rates given by different authors

Altitude(km)	25	30	32	35
Ion Production Rate				
(a) Datta et al.[1983] (due to Primary CR)	1.16	0.52		0.24
(b) Verma et al.[1987] (due to Albedo & Re-entrant CR)	4.81	2.34		1.12
(1) Sum of (a)+(b)	5.97	2.86		1.36
(2) Heaps[1968]	2.17	0.73	0.52*	0.31*
(3) Neher[1967]	1.7	0.85	0.64*	0.42*
Recomb.Coef, α X 10^{-13} $m^3 s^{-1}$ [Smith & Adams, 1982]	6.03	3.32	2.66	1.95
Ion density(= q/α X 10^9 per m^3)				
N (1)	2.8	2.6	2.4*	
N (2)	1.9	1.5	1.4	1.26
N (3)	1.7	1.6	1.55	1.47
σ_+ (X 10^{-12} s/m)			13.0	20.0
σ_- (X 10^{-12} s/m) [Gupta & Narayan, 1987]			2.8	5.0
Mobility(m^2 per v.sec)				
$\mu+$:(1)			0.03	0.052
$\mu+$:(2)			0.058	0.099
$\mu+$:(3)			0.052	0.085
$\mu-$:(1)			0.0068	0.013
$\mu-$:(2)			0.0125	0.0248
$\mu-$:(3)			0.0113	0.0212

(*) Interpolated values

the premonsoon period. Two of our balloon flights (see table 4.1) have been conducted during the months of April, and during both these flights the measured conductivity displayed large fluctuations.

The conductivity measurements done on 18 April 1984 (IMAP-4) are shown in Fig 4.2. We observed fluctuations in conductivity which was by a factor of 3 in the case of $\sigma+$ and 2 in the case of $\sigma-$. The polar conductivity values appeared to switch between a set of lower limit values ($\sigma_+ \simeq 7X10^{-12}$ s/m and $\sigma_- \simeq 2X10^{-12}$ s/m) a set of upper limit values ($\sigma_+ \simeq 2.2X10^{-11}$ s/m and $\sigma_- \simeq 6X10^{-12}$ s/m). The variations of the two polar conductivities were in phase with each other.

One can enquire whether such observations represent genuine geophysical phenomena or whether these fluctuations have instrumental origin. The only possible instrumental source of such behaviour can be photoelectric effect. But, (1) No correlations were found to exist between the sensor's orientation (whether it was in the sunshine or in the shade of the gondola) and the fluctuations, (2) The fluctuations did not appear to be correlated to changes in solar zenith angle. Thus we can deduce that photoemission is not the source of the observed fluctuations and consider that these observed fluctuations have a geophysical origin.

This kind of fluctuations in conductivity can happen either if there are some extra sources of ionisation or if some ion sinks are present in the atmosphere. Enhancement in ionisation has been associated with solar activity[Bering

et al., 1980, Holzworth, 1981] or with thunderstorm activity[Holzworth et al., 1986]. On this particular day there was no such solar event which can cause this enhancement. Also, the weather was not disturbed during the balloon flight. Thus both these sources were absent and enhancement in density can safely be ruled out.

Let us consider ion depletion. Ion depletion can occur if dust or aqueous clouds are present at the location. A value of βN (in equation 1.1) equal to $1.2X10^{-3}$ per cc per second would be required to produce a depletion of this magnitude. This corresponds to roughly 400 particles per cc assuming β to be 1.2×10^{-3}. Such a magnitude of depletion is possible if there is either aqueous clouds pesent or wind-borne desert sands are present at that altiude. The time scale of these fluctuatuins are $\simeq$15 minutes as seen in Fig 4.2. During this period of time the balloon drifts over a distance of 5 to 10 km. Thus the spatial structure is $\simeq$ 10 km.

A different type of fluctuations in conductivity was observed during the IMAP-C2 flight (8 April 1987, Fig 4.8 and 4.9). A reversal in vertical electric field had been observed during this flight which indicated a presence of some global current source below the balloon. The conductivity measurements could be carried out for a short duration of time only. Fig 4.8 depicts the conductivity measured at 34 km. There are occasional dips in the conductivity values. Fig 4.9 shows the conductivity measured at 29 km. The fluctuations are seen here quite clearly.

Unlike the two other cases, the variations in this particular case seem to be random. Such a pattern of conductivity variation has been observed above thunderstorms by Holzworth et al.[1986] and our measurements more or less support their observations. In this case, unlike IMAP-4, a possibility of increase in conductivity due to the presence of an active source of ionisation in the vicinity of the balloon or below it cannot be ruled out[Holzworth et al., 1986].

In the context of the global circuit, such measurements are important because normally, the conductivity in and around the thunderstorms is implicitly assumed to be the same as the fair weather value when global currents are estimated. This is done primarily because measurements of conductivity under these circumstances are lacking. Thus it is important to have measurements which can give an idea of the magnitude of conductivity above thunderstorms. As shown by our measurements and those by Holzworth, the conductivity above thunderstorms can be quite different from fair weather values and can have a spatial and temporal structure.

5.5 Effect of volcanic aerosols on conductivity

There have been several volcanic eruptions during this decade. The major volcanic eruptions of this decade are Mt. St. Helens(18 May 1980), El Chichon(4 April 1982), Nevado Del Ruiz(13 November 1985) and Pacaya(25 January 1987). Large

volcanos are known to throw a large amount of dust and gases in the stratosphere. Such a loading of the stratosphere by the volcanic dust causes a number of changes in the optical[Rosen, 1969, Cadle and Grams, 1975, Ashok et al., 1982] and electrical properties [Rosen, 1969, Kondo et al., 1982B] of the stratosphere. The present section describes the observations of the effect of volcanic activity on electrical conductivity in the stratosphere made at Hyderabad by the author. Fig 5.4 shows the dates of volcanic eruptions together with those on which our balloon measurements were done. The observed positive and negative conductivity values obtained during these measurements are also given.

The first measurement (IMAP-9) was carried out on 22nd October 1985 at a float altitude of 32 km. Prior to this, there had been no major volcanic eruption since El Chichon's eruption in April 1982. It takes about six months time for the aerosols of volcanic origin to settle down[Hunten, 1975]. The three and half year period elapsed before the IMAP-9 balloon flight is thus believed to be long enough for aerosols of volcanic origin to have settled down. Thus this measurement represents a condition of the stratosphere free from volcanic aerosols.

On 13 November 1985, the volcano Nevado del Ruiz erupted in Colombia (Lat. $\simeq 5^{\circ}$N, Long. 75°W). According to A.G.U. report, this was a strong eruption. The volcanic dust which is thrown out into the stratosphere covers the globe within about 20 days[Rampino and Self, 1984] and it spreads mainly

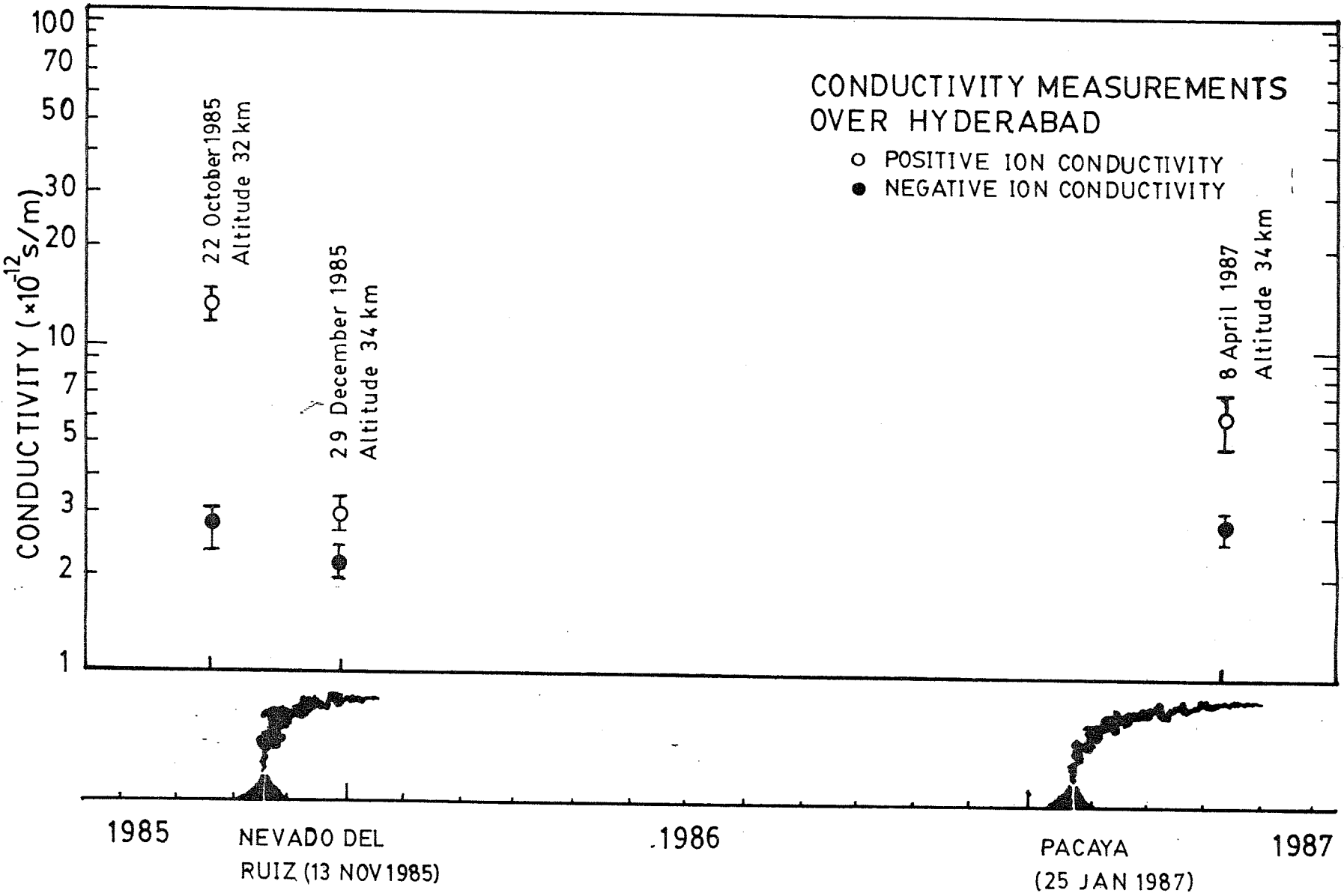

FIG 5.4 CONDUCTIVITY MEASUREMENTS BEFORE AND AFTER VOLCANIC ERUPTIONS

in a latitude range of $\pm 15^{\circ}$ with respect to the site of eruption. The balloon launching station at Hyderabad (18°N) lies within this range of dust coverage. A balloon flight (IMAP-7) was conducted on 29th December 1985. Conductivity and electric field measurements were carried out at float altitude of 34 km. By this time $1\frac{1}{2}$ months had elapsed since the volcanic eruption [Gupta and Narayan, 1987].

We observed that the positive ion conductivity had decreased by roughly a factor of five while the negative ion conductivity had decreased by a factor of about 1.7. (Note that the IMAP-9 measurement was done at 32 km, and the present measurement was done at 34 km, so we have normalised these values to 34 km altitude.) The results show that the volcanic dust affects the positive ion conductivity more than the negative ion conductivity.

After this measurement we waited for another volcanic eruption. A major volcano in Central America at Pacaya (Lat. 15°N, Long. 90°E) in Gautemala erupted on 25 January 1987. The interval between the eruption of the volcano and our balloon measurement was $2\frac{1}{2}$ months. The positive ion conductivity during this measurement had decreased about two and half times while the negative ion conductivity had decreased by a factor of about 1.3. Thus in this flight also there was a clear evidence of a decrease in the positive ion conductivity.

On both the occasions when we made conductivity measurements after volcanic eruptions, we have observed a decrease in conductivity. Such a decrease in conductivity

has been observed earlier[Rosen, 1969] and has been attributed to the increase in aerosol number density. No direct measurements of enhancement in aerosol density have been done after the Ruiz eruption over the Indian zone to the best knowledge of the author. In the case of Pacaya eruption, an increased amount of aerosol over India has been observed by Satyanarayan et al.[1987] using Lidar technique. An increase in the number density of aerosols will increase loss of ions from the atmosphere through attachment process. Under such circumstances, the attachment term in equation 1.1, βN_a becomes comparable to the recombination term and an appreciable decrease in the number density of ions can occur. Kondo et al.[1982B] have calculated ion loss terms on the basis of comparison between pre-volcanic and post-volcanic values of positive conductivity. In the present work, βNa has been calculated for the two flights, IMAP-7 and IMAP-C2. The results are tabulated in table 5.5. In both the cases $(\beta N_a)_+$ comes out to be much larger than $(\beta N_a)_-$.

The attachment coefficient is a function of collision frequency between the aerosol and the respective ions. It is thus dependent on the nature of ions. But its dependence is not very strong in the sense that it goes as the negative sixth root of size(~mass) and the 2/3rd power of density. If we assume that the ratio of densities of negative to positive ions is same as that of $H_2SO_4:H_2O$ then the ratio between collision frequencies of positive and negative ionic species with similar aerosols can at most be by a

Table 5.5

Calculated Attachment Factor due to Volcanic Aerosols

Altitude: 34 km

α : $2.13 \times 10^{-7} cm^3/sec$

Period	$\beta Na(pos)$ (sec^{-1})	$\beta Na(neg)$ (sec^{-1})
Dec 1985	2.5×10^{-3}	5.5×10^{-4}
Apr 1987	1.16×10^{-3}	3.97×10^{-4}

factor of 1.3 Such a difference cannot account for such a large ratio between $(\Phi N)_+$ and $(\Phi N)_-$. One must therefore conclude that after volcanic eruptions positive ions get depleted to a greater extent than negative ions. Thus the number density of positive and negative small ions, n_+ and n_- should not be assumed to be equal after volcanic eruptions. Several calculations of ΦN_A have been done on the basis of decrease in positive ion conductivity only[Kondo et al. 1982B]. If some chemical mechanism also exists for positive ion loss after volcanic activity as our observations of drastic decrease in σ_+/σ_- ratio after volcanic eruptions suggest, then the calculations of ΦNa on the basis of decrease in $\sigma+$ would be erroneous. The decrease in negative ion conductivity should also be considered while calculating ΦNa under such circumstances.

To the knowledge of the author, the present models of ion chemistry [e.g. Brasseur and Chatel, 1983, Mitra, 1984] do not have any reaction schemes which would cause a depletion in positive ions after volcanic eruptions, when the SO_2 and H_2SO_4 contents in the atmosphere increases. In order to explain this behaviour some new mechanism has to be invoked.

5.6 Air-earth current measurement

Electric field measurements are important because of their role in understanding the global electric circuit. The air-earth current at any place can be determined by measuring conductivity and electric field. During the IMAP-7

flight(29 December 1985), measurement of conductivity and electric field was done during the balloon float period. Due to a limited float duration, measurement could be carried out only between 6.15 a.m. and 8.30 a.m. Measurement of electric field before 6.15 a.m. are believed to be contaminated due to a large floating potential acquired by the gondola and are not shown. Fig 4.6 shows the measured conductivity while Fig 4.10 shows the electric field measured during this period.

The air-earth current is given by Iae = V/A. Alternately it is given by the following equation:

$$Iae = \sigma E \qquad ..(5.6)$$

Knowing the conductivity and the electic field, one can thus get the air earth current. Fig 5.5 shows the air earth current for IMAP-7. The smoothed electric field profile has been used for the sake of this calculation. The duation of the present observation was not long enough for the characteristic diurnal beaviour of the global air earth current[Israel, 1973] to be observed.

The present measurement of air earth current was done at the time when the conductivity of air was an appreciable 4.6 times lower than the normally existing conductivity value at that altitude. This was due to the presence of volcanic dust in the stratosphere. Such a condition of the stratosphere does not alter the air-earth current by a great deal. This is because the air earth current is directly dependant on columnar resistance. More than 90 percent of the total columnar resistance is contributed by

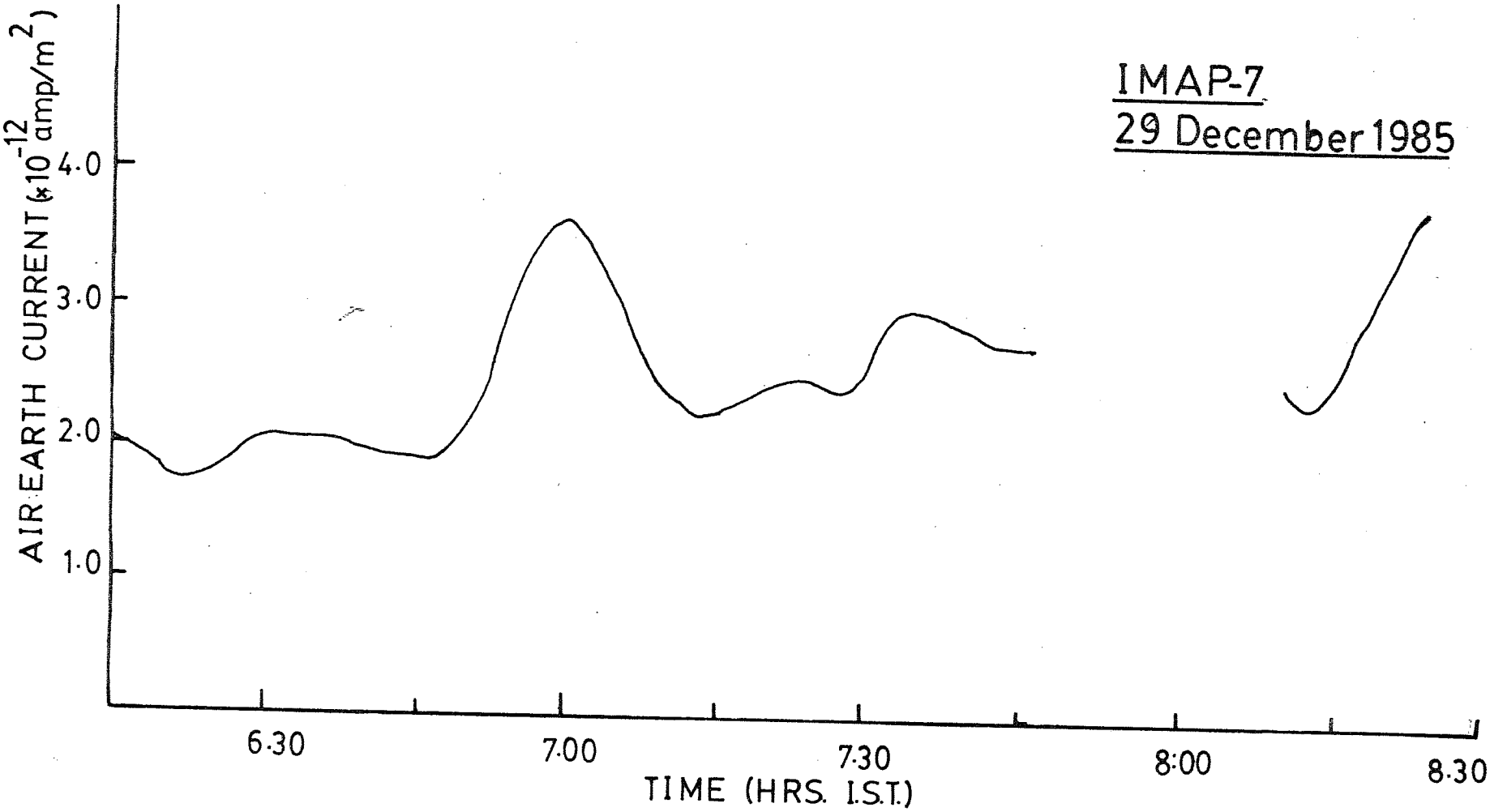

FIG 5.5 AIR EARTH CURRENT MEASUREMENTS DURING IMAP-7 FLIGHT

the lowermost 12 km of the air column in the atmosphere[Muhleson, 1977]. Since the volcanic dust resides mainly in the stratosphere, where conductivity is relatively high, even a factor of 4 to 5 change in the conductivity at stratospheric altitudes(above 15 km) will not cause more than one and half times increase in λ. In response to the decrease in conductivity what actually happens is that the ambient electric field increases. This appears to be the main reason that while the expected electric field at 35 km altitude is 0.08 V/m, we observed an electric field of 04 V/m.

5.7 Conductivity in the Middle atmosphere

Conductivity measurements spanning the full range of the middle atmosphere have been done at high latitudes by co-ordinated use of several instruments[York et al., 1982, Maynard et al., 1984]. But no such efforts have been undertaken at low latitudes.

The author was involved in conducting several balloon flights for making conductivity measurements. Apart from these, conductivity values in the mesosphere have been obtained by the author from Langmuir probe data as described in chapter 2(section 2.6.1). In the present section, all these measurements are presented in an attempt to obtain a consolidated picture of the middle atmosphere.

Fig 5.2 depicts the positive conductivity measured by Langmuir probe between 60 km and 90 km altitudes. For comparison, the measurements of Maynard et al.[1984] have

also been shown. It is seen that the conductivity increases almost exponentially with altitude in the middle atmosphere. The scale height is 6.4 km.

The diagram also shows our balloon measurements of conductivity. The IMAP-4 and IMAP-9 values of positive conductivity are consistent with the picture of the conductivity increasing with altitude in an exponential fashion. In this diagram, the higher one of the IMAP-4 values has been given because the lower values in Fig 4.2 are believed to be caused by some local source of ion depletion.

The other three balloon measurements shown are post-volcanic eruption values and they show an appreciable decrease in the positive ion conductivity.

Thus this diagram gives some idea of how the conductivity is expected to behave at various altitudes in the middle atmosphere. Also, the low latitude values seem to be similar to the high latitude ones. (Here one should keep in mind the fact that the techniques are different and apart from the expected statistical errors, these instruments might also be displaying characteristic patterns of behaviour during measurement.) To get a more complete picture therefore, more measurements are required, and if possible, intercompaisons should be done between the different techniques to check their relliability.

Such measurements can help in the understanding of other phenomena also. The sunrise effect has been observed by Mitchell et al. [1976]. They have observed the positive ion conductivity to increase between 30 km and 55 km

altitudes during morning hours and shown this increase in conductivity to be related with solar zenith angle. There are other observations also which could be verified. A large number of observations made by Maynard et al.[1984] have shown that the conductivity in the mesosphere at high latitudes displays a large variability which can be as large as by a factor of ten. Although such variations are not expected at low latitudes, one has to see wheher it is so or not. Only one set of measurements so far is available (given in Fig 5.2). This can only give an idea of the kind of conductivity values to expect in the mesosphere at low latitudes at various altitudes.

5.8 Rocket body potential in the mesosphere

During several rocket flights, the floating potential of the rocket body has been observed to display a characteristic behaviour at altitudes around 80 km. This behaviour has been discussed earlier in chapter 2 (section 2.6.4). In that section, the ratio of Langmuir probe current to electron density measured during two occasions were given. During these flights, the ratios displayed peaks at 83 km and 87 km altitudes respectively. Such a peak can be attributed to a change in the floating potential of the return electrode. In section 2.6.4, it was hypothesised that the presence of ambient electric field can bring about such a change. It has been shown [Subbaraya et al. 1983] that a drastic change in probe performance is taking place below

100 km altitude in which the ratio Ip/Ne changes by a factor of 2. This has been attributed to a shift of the ambient plasma behaviour from collision dominated regime to collisionless regime which takes place at these altitudes. Tzur and Roble[1984] have proposed a theoretical model which predicts the existence of a local vertical electric field based on difference in ion and electron mobilities in the 50 - 100 km altitude region. Such an electric fields can be upto two orders in magnitude larger than the downward mapped ionospheic fields according to Tzur and Roble.

Very careful measurements have been conducted by Maynard[1980] which have shown the presence of electric fields in the mesosphere having volts per meter magnitude during several occasions. These have been discussed by Kelley[1983]. Experimental observations of such high electric fields have also been reported by Hale et al.[1981], Maynard et al.[1984] and others.

The Langmuir probe measuements discussed in section 2.6.4 also point out to a possible existance of an electric field in middle atmosphere, although these evidences are not direct.

There are other measuements also, essentially similar in content. Gupta[1970] has reported measurement of floating potential of rocket body during two occasions when similar experiments were being performed. The rocket-probe configuation was the same as shown in Fig 2.11. Subbaaya et al.[1983] have reported another instance in which a characteristic negative peak in the floating potential was

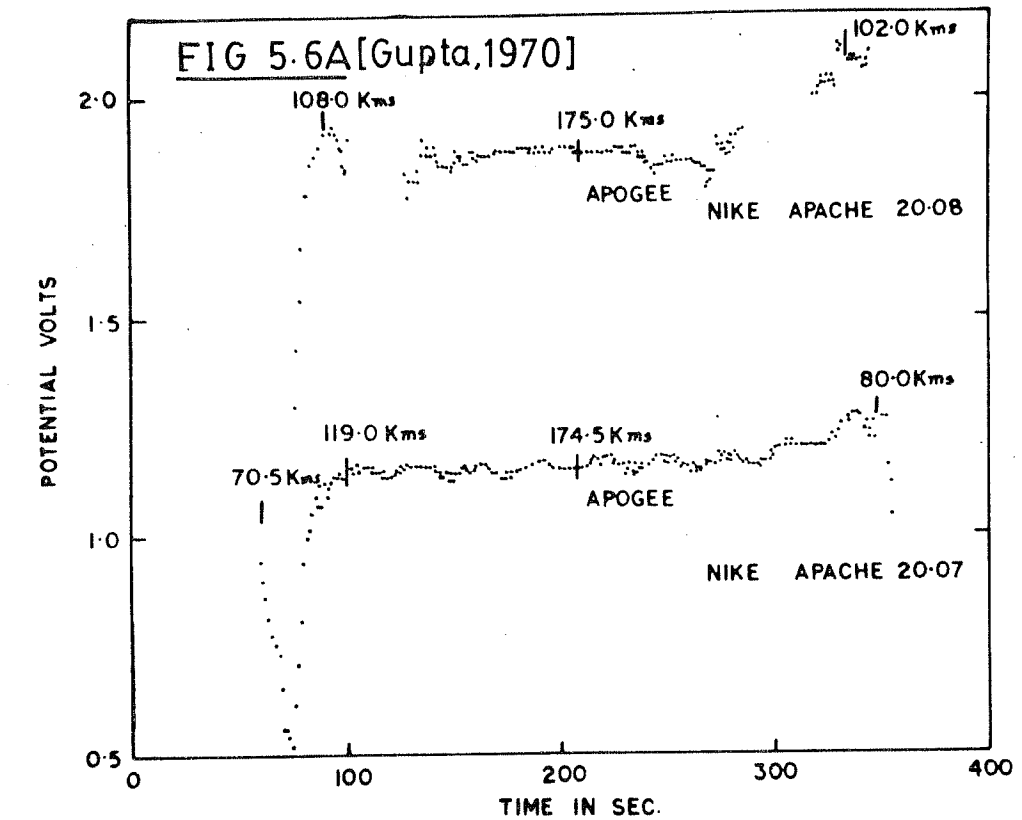

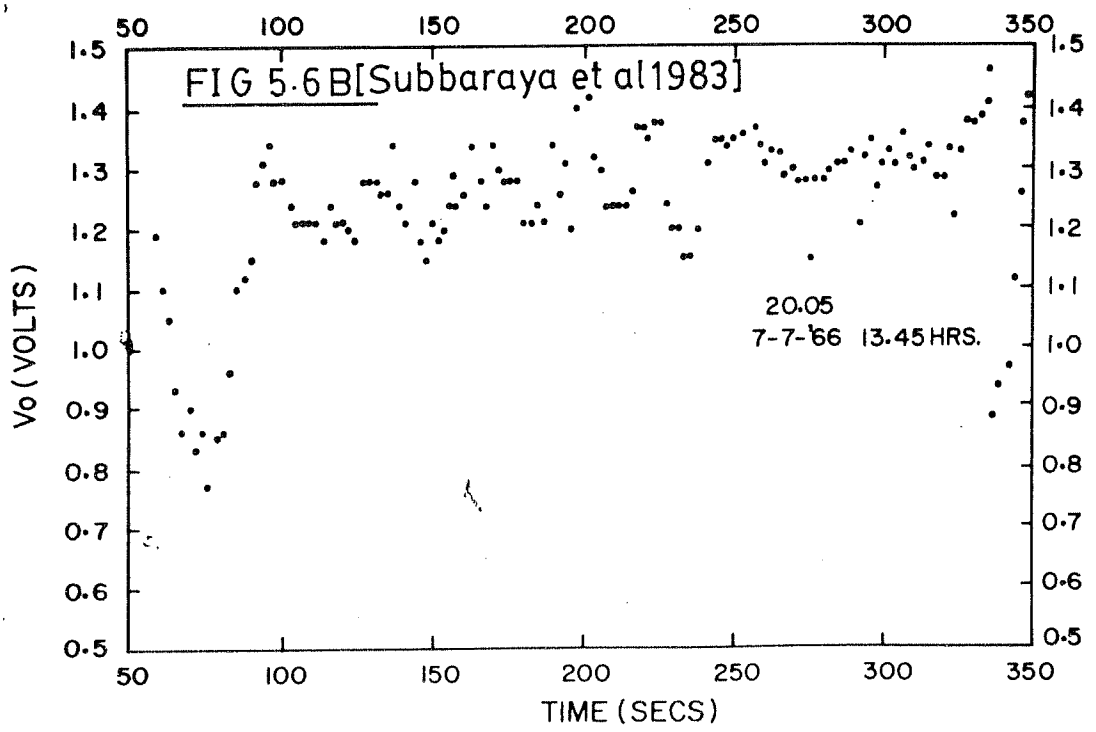

FIG 5.6 EXAMPLES OF VARIATION OF ROCKET BODY POTENTIAL IN MESOSPHERE

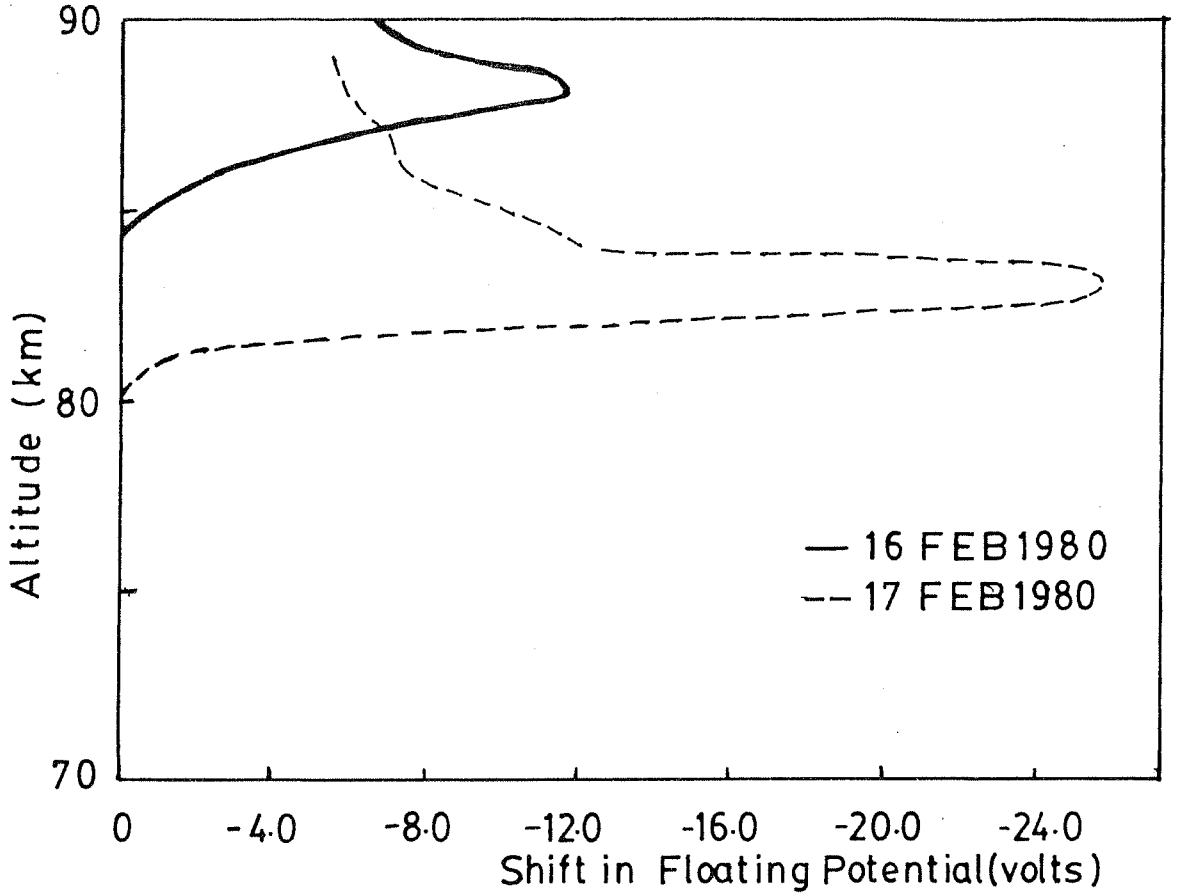

FIG 5.7 Rocket body Potential in Mesosphere

observed at around 80 km altitude. These three measurements shown in Fig 5.6A and 5.6B show sharp peaks in rocket body potential corresponding to the Langmuir Probe measurements shown in Fig 4.12.

From these observations one can say that at the altitude around 80 km, some phenomenon is occuring which changes the floating potential of the rocket body. This change is in negative direction as one can see in Fig 5.6 and 5.7 where the rocket body potential has decreased during these peaks. This situation coresponds to an upward electric field. Most of the measurements however at high latitudes by Maynard et al.[1984] or Hale et al.[1981] point to a downward directed electric field.

Thus although the observation of large shift in rocket body potential in the mesosphere appears to be a fact, its nature as well as its cause is not yet established. In order to pinpoint the cause, firstly, it has to be established whether electric field of the kind mentioned above is present or not at the time when the Langmuir probe displays anomalous current. Also, a better theoretical understanding of the rocket probe behaviour is required.

CHAPTER VI

SUMMARY AND CONCLUSIONS

6.1 Summary of this thesis

The present thesis consists of the work done by the author during the last six years. The present work mainly deals with balloon-borne measurements of the stratospheric conductivity and electric field over the low latitude station of Hyderabad(India). Some of the results of Rocket-borne conductivity measurement carried out at Thumba near Trivandrum (India) are also presented.

An instrument based on the relaxation method for conductivity measurement and double probe method for electric field measurement was developed by the author. Four balloon flights were successfully conducted from Hyderabad during the period 1984 to 1987.

The first balloon flight was conducted on 18th April

1984. We obtained the conductivity data at the ceiling altitude from 9.15 am to 12.00 am. The main observations were as follows: (1) The positive ion conductivity values obtained were between 7×10^{-12} s/m and 2.2×10^{-11} s/m. (2) The negative ion conductivity values varied between 2×10^{-12} s/m and 6×10^{-12} s/m. The positive ion conductivity was three to five times higher than the negative ion conductivity. (3) There was a large variation in the magnitudes of the two conductivities. The variations of the two polar conductivities were in phase.

The second balloon was launched on 28 October 1985. The measured positive ion conductivity was about 1.2×10^{-11} s/m while the negative ion conductivity was about 2.8×10^{-12} s/m. Thus the positive ion conductivity was about four and half times higher than the negative ion conductivity. The result is similar to that of the previous flight, except that large fluctuations in the conductivity values were not observed during this flight.

The third balloon was launched on 29th December 1985. This time the positive ion conductivity was measured to be around 3.0×10^{-12} s/m while the negative ion conductivity was around 2.2×10^{-12} s/m. The ratio between the two ionic conductivities was thus about 1.3 instead of 4.5 as in the case of the two previous flights. Compared to the October 1985 values, the observed positive ion conductivity was smaller by a factor of 4. The negative ion conductivity values were less by a factor of 1.2 only.

The fourth balloon was launched on 8th April 1987.

Conductivity measurement was done at two altitudes, 34 km and 29 km. At 34 km altitude, the positive ion conductivity was observed to be around 6 X 10^{-12} s/m, while the negative ion conductivity was about 2.8 X 10^{-12} s/m. The conductivity values at several places were observed to be lower than the mean value by almost a factor of three. The two polar conductivities measured at 29 km altitude showed large fluctuations. The average conductivity values at this altitude were 2.4 X 10^{-12} s/m for σ_+ and 1.9 X 10^{-12} s/m for σ_-.

The balloons launched on 29 December 1985 and 8 April 1987 carried electric field probes also. During December 1985 flight, the vertical electric field was measured to be of the order of 0.4 to 0.5 volts per meter. The electric field was downward and the measured values showed a variation with time. They varied between around 0.6 to 0.7 volts per meter at 7.00 am. and 0.4 to 0.5 volts per meter at 8.30 am.

The vertical electric field measured on 8 April 1987 was found to be reversed (upwards) and its magnitude was higher than 10 volts per meter. Such a condition is indicative of disturbed weather below the balloon trajectory. Since this electric field was larger than the signal handling capacity of the telemetry encoder, no measurements could be done.

Studies in mesospheric electrodynamics were also done by the author. Data from rocket borne measurements of electron and ion density from Thumba, Trivandrum (dip $\simeq 0.6^{\circ}$S)

by Langmuir Probe technique was used to calculate the electron and positive ion conductivities in the altitude range between 60 and 100 km. A comparative study of stratospheric and mesospheric conductivities was done in order to get a consolidated picture.

The main conclusions derived from this study are given below.

1. A study of probe behaviour under in-situ conditions was done which showed that it is very little likely that the conductivity measurements are getting affected by photoelectron emissions from the probe.

2. At the balloon ceiling altitudes of around 32-35 km we obtained the ratio of the two polar conductivities, σ_+/σ_- as roughly 4.5. Prior to this there had been no observations of this kind at this altitude. This ratio of 4.5 between the two polar conductivities implies that the average mobility of the positive ions is roughly four and half times higher than that of the negative ions under normal conditions in the altitude range of 30 to 35 km.

3. In the premonsoon period we have found large fluctuations in the conductivity values.

4. A comparison of the conductivity values measured in October 1985 with those measured in December 1985 shows a drastic decrease in the December 1985 value. This is expected because of the injection of a large

number of aerosol particles in the stratosphere by the volcanic eruption in Colombia. The decrease in the positive ion conductivity is about four times more than the decrease in the negative ion conductivity. A similar decrease was observed in April 1987 measurement of conductivity. Compared to the October 1985 value, the positive ion conductivity was smaller by a factor of 2. The negative ion conductivity was only marginally smaller.

5. The stratospheric conductivity is lower by a factor of 4 in the December 1985 flight, and the electric field is higher by roughly the same factor. It appears that the presence of aerosol in the stratosphere does not affect the air earth current significantly.

6. The two polar conductivities observed during 8 April 1987 flight show a ratio of $\sigma_+/\sigma_- \simeq 1.25$ at 29 km altitude and $\simeq 2.35$ at 34 km altitude. Thus the ratio of the polar conductivities was found to be altitude dependant.

7. The vertical electric field was observed to be upwards during thunderstorm period on 8 April 1987. Its magnitude was more than 10 volts per meter. During fair weather, the electric field is in the downward direction.

8. Rocket borne measurements in the mesosphere show that at 60 km altitude the positive ion conductivity is of

the order of 1.1×10^{-9} s/m. This is higher than the stratospheric conductivity values at 30 km altitude by a factor of 10^2.

9. It was observed that the balloon-borne gondola gets positively charged during the balloon ascent. Te potential developed on the gondola was measured. It was found that during ascent, the gondola acquires potentials of the order of a hundred volts.

10. It was observed that rocket bodies acquire floating potentials of the order of a few volts when they pass through the mesosphere. This phenomenon has been observed at altitudes around 80 km and exists over a narrow altitude range of about 5 km.

6.2 Suggestions for follow-up actions

The present work, while it gave a number of new and good results, it also exposed some of the areas where more work is required, either in the form of understanding the measurement process, or in the form of follow-up action based on the results obtained during the present work.

The behaviour of the charging of the gondola is one of those aspects of instrumentation which deserves a serious study. In the present experiment, we could not get ascent-time data due to this problem. The gondola potential was measured during two of the balloon flights and was

found to be of the order of a hundred volts. The cause of this large potential developing on the gondola has not been properly understood. This problem is a serious one and it should be investigated thoroughly as it affects the balloon-borne measurements of conductivity related parameters. Its cause has to be understood and methods aimed at rectifying this problem have to be developed, so that one can obtain relliable conductivity data both during ascent as well as during float periods.

Another point which emerged during the present work is that although there have been some attempts of modelling the probe behaviour in the past, the actual measurement environment is more complex than what these models have considered. Several aspects of the probe behaviour are still to be understood. For example, the effects of photoemission on probe current is not understood properly. It has been shown through simple calculation of the solar ultravoilet flux at the balloon altitudes that one should expect very large probe currents during daytime, several orders of magnitude higher than the conductivity currents measured by the probes. Yet it is not so in practice. The question of why the photoemission from the probe surface is not as high as the theoretically expected value is indeed interesting. Another interesting problem to be looked into is the current collection by a probe in flowing medium. The author has investigated this problem to a certain extent, but a rigorous numerical modelling of the probe behaviour under typical measurement conditions remains to be done.

The author feels that it is important to study the temporal and spatial variation of conductivity and electric fields in the stratosphere. Although long duration measurements have not been conducted from Hyderabad due to several constraints, the author feels that measurements spanning over a period of one full day conducted in different seasons will provide answers to a number of questions which have arisen during the present work. At the same time, such a work will help in a better understanding of the global electric circuit.

The large fluctuations measured in conductivity during April 1984 appears to be related to some yet unknown phenomenon. This observation merits a systematic follow-up action in the form of observation of stratospheric conductivity together with in-situ measurements of water vapour and particulate matter concentration.

The changes in polar conductivity values observed before and after volcanic eruptions poses an interesting problem for theoretical modelling. As an input to such a model, measurements are required of conductivity and number density of ions. The author feels that a simultaneous measurement of several parameters like conductivity, ion density and aerosol concentration will be more useful for studying the volcanic effects.

In view of the observations of rocket body potential in the mesosphere, the author feels that investigations as to whether these potentials are a manifestation of the mesospheric electric fields or due to some other cause

should be done.

In the above paragraphs, some of the questions and unsolved problems that came up during the present work are described. Apart from it, it was felt that the electrodynamics of the middle atmosphere at low latitudes offers a number of interesting problems to be solved. The intimate relation between the stratospheric electricity and chemistry should be investigated. Future experiments should be planned towards measurement of ion composition together with electrical parameters in the low latitudes.

LIST OF PUBLICATIONS

1. S. P. Gupta and **A.Narayan** (1984) Meteorological effects observed in the D region of the equatorial Ionosphere. Adv.Space Res. 4,pp167-169.

2. S. P. Gupta and **A. Narayan** (1987) Balloon-Borne Measurements of Ion Conductivity over Low Latitude Stratosphere.Planet.Space Sci. 35,pp439-443.

3. **A. Narayan** and S. P. Gupta (1987) Ion Conductivity Measurements by Balloon-borne probes over Low Latitude Stratosphere.Adv.Space Res. 7,(In Press)

List of References

1. Aikin A.C. (1981)
Meteoric Compounds in the Stratosphere
Nature **291**,638

2. Albritton D.L. (1978)
Ion-neutral reaction rate constants measured in Flow Reactors through 1977
At.Data & Nucl.Tables **22**,1-101

3. Alge E.,N.G.Adams,D.Smith (1983)
Measurements of the Dissociative Recombination coefficients of 02+, NO+, and NH4+ in the temperature range 200-600 K
J.Phys.B:At.Mol.Phys **16**,1433-1444

4. Arijs E. (1983)
Positive and Negative ions in the Stratosphere
Annales Geophysicae 1,149-160

5. Arijs E. et al. (1983)
Positive Ion Composition Measurements between 33 and 20 km altitude
Annales Geophysicae **1**,161-166

6. Arijs E. et al. (1985)
Recent Stratospheric Negative Ion Composition Measurements between 22 and 45 km altitude
J.Geophys.Res. **90**,5891-5896

7. Arijs E. and G.Brasseur (1986)
Acetonitrile in the stratosphere and implications for positive ion composition
J.Geophys.Res. **91**,4003-4016

8. Arnold F. et al. (1982)
Implications for Trace Gases and Aerosols of Large Negative Ion Clusters in the Stratosphere
Nature **297**,371-376

9. Arnold F. (1982)
Ion nucleation-a potential source for stratospheric aerosols
Nature **299**,134-137

10. Ashok N.M. et al. (1982)
Twilight IR Brightening over India due to El Chichon's Eruption in Mexico

Nature **300**,620-621

11. Banerjee A. et al. (1984)
Balloon-Borne Langmuir Probe measurements of Stratospheric Ions in Low Latitudes
Ind.J.Rad.Spa.Phys. **13**,176-179

12. Batchelor G.K. (1967)
Introduction to Fluid Dynamics
(Cambridge University Press)

13. Bates D.R. (1982)
Recombination of Small Ions in the Troposphere and the Lower Stratosphere
Planet.Spa.Sci. **30**,1275-1282

14. Bates D.R. (1985)
Ion-Ion Recombination in an ambient Gas
Adv.At.Mol.Phys. **20**,1-39

15. Beig G. and D.K.Chakravarty (1987)
A Theoretical model of the stratospheric positive ions
Ind.J.Rad.Spa.Phys. **16**,313-317

16. Bering E.A. et al. (1980)
Electric Field, Electron Precipitation and VLF Radiation during a simultaneous Magnetic substorm and Atmospheric Thunderstorm
J.Geophys.Res. **85**,55-72

17. Boyd R.L.F. and A.P.Willmore (1963)
A Method of studying the Energy Distributions of Ionospheric Ions and Electrons
Space Research (COSPAR) **3**,1168

18. Brasseur G. and A.Chatel (1983)
Modelling of Stratospheric Ions:a first attempt
Annales Geophysicae **1**,173-185

19. Cadle R.D. and G.W.Grams (1975)
Stratospheric Aerosol Particles and their Optical Properties
Rev.Spa.Phys.Geophys. **13.4**,475

20. Cadle R.D.,C.S.Kiang and J.F.Louis (1976)
The Global Scale Dispersion of the Eruption Clouds from Major Volcanic Eruptions
J.Geophys.Res. **81**,3125-3132

21. Cadle R.D. and C.S.Kiang (1977)
Stratospheric Aitken Particles
Rev.Geophys.Spa.Phys. **15**,195-202

22. Chalmers J.Alan and E.W.R.Little (1960)
The electricity of Continuous Rain

Terrest.Mag.Atmos.Elec 45,451-462

23. Chang J.S. and K.Kodera (1985)
Theory of Electric Conductivity Measurements by an Electrostatic Probe in an Atmospheric Low Density Continuum Ionized Gas
Jour.Geophys.Res. **90**,5897-5900

24. Cole R.K.Jr. and E.T.Pierce (1965)
Electrification in the Earth's Atmosphere for Altitudes between 0 and 100 Kilometers
J.Geophys.Res. **70**,2735-2749

25. Croskey C.L.,L.C.Hale and S.C.Leiden (1976)
Results of Ionisation measurements in the Middle Atmosphere
Space Res. (COSPAR) **XVII**,191-197

26. Damle S.V. et al. (1981)
Telemetry/Telecommand Ground Station at Balloon Facility Hyderabad
TIFR Technical Note (CIBA-01-81)

27. Datta J. et al. (1984)
Cosmic Ray Ion Production Rates in the Middle Atmosphere
ISRO Scientific Report (ISRO-IMAP-SR-16-84)

28. Datta J. et al. (1987A)
A model for the Cosmic Ray produced Ionisation in the Middle Atmosphere
Ind.J.Radio Spa.Phys. **16**,257-266

29. Datta J. et al. (1987B)
Influence of Aerosols on Middle Atmospheric Conductivities
Physica Scripta **36**,(In Press)

30. Derberwick G.F. et al. (1974)
Experimental Techniques in Visible and Ultravoilet Photoemission
in "Methods of Experimental Physics,Vol 11"(Ed.R.V. Coleman) 67-122

31. Deshpande S.D.,A.P.Mitra (1983)
Solar Spectral Irradiance, Photoabsorption Cross sections, Photochemical,Chemical Ion-chemical Reactions and Reaction Rate Constants
ISRO Scientific Report (ISRO-IMAP-SR-11-83)

32. Dotan I. et al. (1976)
Mobilities of (CO2)+ (N2H)+ (H3O)+ (H3O)+.H2O, and (H3O)+.(H2O)2 ions in N2
J.Chem.Phys. 65,5028-5030

33. Fahleson U. (1967)
Theory of Electric Field Measurements conducted in the Magnetosphere with Electric Probes.
Spa.Sci.Rev. 7,238-262

34. Fergusen E.E.,F.C.Fehsenfeld and D.L.Albritton (1979)
(Ed.M.T.Bowers) Ion Chemistry in the Earth's Atmosphere
(in "Gas Phase Ion Chemistry" Ed.M.T.Bowers),45-82

35. Feuerbacher B. and B.Fitton (1972)
Experimental Investigation of Photoemission from Satellite Surface Materials
J.Appl.Phys. **43**,1563-1572

36. Gish O.H. (1944)
Terr.Magn. **49**,159

37. Gish O.H. and G.R.Wait (1950)
Thunderstorms and the Earth's General Electrification
J.Geophys.Res. **55**,473-484

38. Gokhale G.S.,M.G.K.Menon and R.T.Redkar (1966)
Stratospheric Flights over Tropical Latitudes with Polyethylene Balloons of Large Volume
Proc.Ind.Acad.Sci. **LXIV**,57-72

39. Goldberg R.A. (1984)
Middle Atmospheric Electrodynamics:Status and Future
J.Atmos.Terrest.Phys. **46**,1083-1101

40. Goldberg R.A. et al. (1984)
Nighttime Auroral Energy Deposition in the Middle Atmosphere
J.Geophys.Res. **89**,5581

41. Gringel W.,K.H.Kaselau and R.Muhleisen (1978)
Recombination Rates of Small Ions and their Attachment to Aerosol Particles
PAGEOPH **116**,1101-1113

42. Gruenberg E.L. (Ed.) (1967)
Handbook of Telemetry and Remote Control
(McGraw Hill)

43. Gupta S.P. (1970)
The Study of the Lower Ionosphere at Low Latitudes
Ph.D. Thesis:Gujarat University,Ahmedabad India

44. Gupta S.P. and A.Narayan (1984)
Meteorological Effects observed in the D Region of the Equatorial Ionosphere
Adv.Space Res. **4**,167-169

45. Gupta S.P. and A.Narayan (1987)
Balloon-Borne Measurements of Ion Conductivity over Low Latitude Stratosphere
Planet.Spa.Sci. **35**,439-443

46. Gupta S.P. (1987)
Report on Balloon-borne Gondola Charging Mechanism
PRL Internal Report(September 1987)

47. Hake R.D.Jr.,E.T.Pierce and W.Viezee (1973)
Stratospheric Electricity
(Scientific Report,Stanford Res.Inst.Project No.1724)

48. Hale L.C. et al. (1981)
Measurement of Middle Atmospheric Electric Fields and related conductivities
Geophys.Res.Lett. **8**,927-930

49. Hays P.B. and R.G.Roble (1979)
A Quasi-static Model of Global Atmospheric Electricity 1 The Lower Atmosphere
J.Geophys.Res. **84**,3291-3305

50. Heaps M.G. (1978)
Parametrization of the Cosmic Ray Ion Production Rate above 18 km
Planet.Spa.Sci. **26**,513-517

51. Hill R.D. (1971)
Spherical Capacitor Hypothesis of the Earth's Electric Field
PAGEOPH **84**,67

52. Hofmann D.J. and J.M.Rosen (1982)
Stratoapheric condensation nuclei variations may relate to solar activity
Nature **297**,120-124

53. Hofmann D.J. and J.M.Rosen (1983)
Condensation Nuclei events at 30 km and possible influences of solar cosmic rays
Nature **302**,511-514

54. Holzworth R.H. (1981)
High Latitude Stratoapheric Electrical Measurements in Fair and Foul weather under various solar conditions
J.Atmos.Terrest.Phys **43**,1115-1125

55. Holzworth R.H. and Y.T.Chiu (1982)
Sferics in the Stratosphere
(CRC Hndbook of Atmospherics,Vol.II,1-19)

56. Holzworth R.H. et al. (1984)

Planetary scale variability of the fair weather Vertical Electric Field in the Stratosphere
Phys.Rev.Lett. 53,1398-1401

57. Holzworth R.H. et al. (1986)
Stratospheric Conductivity variations over Thunderstorms
J.Geophys.Res. **91**,13257-13263

58. Huertas M.L. et al. (1974)
On the nature of Positive Ions of Tropospheric interest and on the effect of polluting Organic Vapors
J.Geophys.Res. 79,1737-1743

59. Hunten D.M. (1975)
Residence Times of Aerosols and Gases in the Stratosphere
Geophys.Res.Lett. 2,26-28

60. Ichimaya T. et al. (1960)
A Probe for Measuring Ion Density in the Ionosphere
Space Research (COSPAR) 1,397-416

61. Ingels J.,et al. (1987)
Acetonotrile and Sulfuric Acid Concentrations derived from Ion Composition Measurements during the MAP/GLOBUS 1983 campaign
Planet.Spa.Sci. 35,685-691

62. Iribarne J.V. and H.R.Cho (1980)
Atmospheric Physics
(D Riedel Pub.Company)

63. Israel H. (1970)
Atmospheric Electricity
(Israel Program for Scientific Translations,Jerusalem)

64. Israel H. (1973)
Atmospheric Electricity
(Israel Program for Scientific Translations,Jerusalem)

65. Kasemir H.W. (1977)
Theoretical Problems of the Global Atmospheric Electric Circuit
(in "Electrical Processes in Atmosphere" Ed. D. Dolezalek and R.Reiter 423-439)

66. Kelley M.C. et al. (1983)
Middle Atmospheric Electric Fields:Fact or Fiction?
Geophys.Res.Lett. 10,733-736

67. Kelley M.C. (1983)
Middle Atmospheric Electrodynamics
Rev.Geophys.Spa.Phys 21,273-275

68. Kilpatric W.D. (1971)
An experimental mass-mobility relation for Ions in air at atmospheric pressure
Proc.Ann.Conf.Mass Sp. **19**,320-325

69. Kirchoff R.(1985)
Potential Flows (Marcel Dekker Inc.N.Y.)

70. Kondo Y. et al. (1982A)
Stratospheric Aerosol inferred from Electrical Conductivity during a Volcanically Quiescent Period
PAGEOPH **120**,1-10

71. Kondo Y.,R.Reiter,H.Jager,M.Takagi (1982B)
The effect of Mount St.Helens Erruption on Tropospheric and Stratospheric Ions
PAGEOPH **120**,11-16

72. Kraakevick J.H. (1958)
The Airborne Measurement of Atmospheric Conductivity
J.Geophys.Res. **88**,3894-3896

73. Landau L.,E.M.Lifshitz (1969)
Fluid Mechanics
(Pergammon Press)

74. Lange's Handbook of Chemistry (11th Edition,1973)
(Ed. J.A.Dean) McGraw Hill Book Company

75. Leiden S. (1976)
Positive Ion Densities and Mobilities in the Upper Stratosphere and Mesosphere
(Pennsylvania State University Scientific Report No. 446)

76. Levin Z.et al. (1977)
Modelling of Thunderstorm Electrification
(in "Electrical Processes in Atmosphere" Ed. D. Dolezalek and R.Reiter 394-401)

77. Lichfield E.W. and N.E.Carlson (1967)
Temperature Control of Balloon Packages
National Centre for Atmospheric Research Technical Note (TN32),1-38

78. Markson R. (1975)
Atmospheric Electrical Detection of Organized Convection
Science **188**,1171-1177

79. Maynard N.C, et al. (1981)
Measurement of Volt/Meter Vertical Electric Fields in the Middle Atmosphere

Geophys.Res.Lett. 8,923-926

80. Maynard N.C. et al. (1984)
Electrical structure in the High-Latitude middle Atmosphere
J.Atmos.Terrest.Phys. 46,807-817

81. Meyerott R.E.,J.B.Reagan and R.G.Joiner (1980)
The Mobility and Concentration of Ions and the Ionic Conductivity in the Lower Stratosphere
J.Geophys.Res. 85,1273-1278

82. Mitchell J.D.,R.S.Sagar and R.O.Olsen (1976)
Positive Ions in the Middle Atmosphere during Sunrise Conditions
Space Res. (COSPAR) XVII,199-204

83. Mitra A.P. (1981)
Chemistry of Middle Atmospheric Ionization-A Review
J.Atmos.Terrest.Phys. 43,737-752

84. Mitra S.K. (1952)
Upper Atmosphere
(Asiatic Press)

85. Moore C.B. (1977)
An Assessment of Thunderstorm Electrification Mechanism (in "Electrical Processes in Atmosphere" Ed. D.Dolezalek and R.Reiter 333-352)

86. Morita Y. (1983)
Recent Measurements of Electrical Conductivity and Ion Production Rate and the Ion-Ion Recombination coefficients derived from them in the Lower Stratosphere
J.Geomag.Geoelectr. 35,29-38

87. Mott Smith H.M. and I.Langmuir (1926)
The Theory of Collectors in Gaseous Discharges
Phys.Rev. 28,727

88. Mozer F.S. and R.Serlin (1969)
Magnetospheric Electric Field measurements with Balloons
J.Geophys.Res. 74,4739-4754

89. Muhleson R. (1977)
The Global Circuit and Its Parameters
(in "Electrical Processes in Atmosphere" Ed. D. Dolezalek and R.Reiter 467-476)

90. Murali Das S.,V.Sasikumar and S.Sampath (1987)
Measurement of Electrical Conductivities,Ion Densities & Mobilities in the Middle Atmosphere over India
Ind.Jour.Rad.Spa.Phys. 16,215-220

91. Neher H.V. (1967)
Cosmic Rays that changed from 1954 to 1965
J.Geophys.Res. **72**,1527-1539

92. Nevejans et al. (1985)
Measurement and Identification of Stratospheric Ions with Balloon-borne Instruments
in MAP Handbook **15** Balloon Techniques (Ed.Murcray D.G.) 124-138

93. Norville K. and R.H.Holzworth (1987)
Global Circuit Variability from Multiple Stratospheric Electric Measurements
J.Geophys.Res. **92**,5685-5695

94. Ogawa T.,M.Yasuhara and A.Huzita (1975)
Stratospheric Horizontal Fields over Mountains
J.Atmos.Terrest.Phys **37**,841-844

95. Orville R.E. and D.W. Spencer (1979)
Global Lightning Flash Frequency
Mon.Weather Rev. **107**,934-943

96. Paltridge G.W. (1965)
Experimental Measurements of the Small Ion Density and Electrical Conductivity in the Stratosphere
J.Geophys.Res. **70**,2751-2761

97. Pomerantz M.A. (1971)
Cosmic Rays
(Van Nostrand)

98. Prakash S. and B. H.Subbaraya (1967)
Langmuir Probe for Measuremen of Electron Density and Electron Temperature in the Ionosphere
Rev.Sci.Instr. **38**,1132-1136

99. Prakash S. et al. (1974)
Some Features of the Equatorial D Region as revealed by the Langmuir Probe Experiments conducted at Thumba
in "Methods of Measurements and Results of Lower Ionosphere Structure" Ed.K.Rawer.Akademic Verlag. 259

100. Raja J. et al. (1981)
Measurement of Electrostatic Charge Build-up on Rockets
ESA Journal **5**,65-68

101. Rampino M.R. and S.Self (1984)
The Atmospheric Effects of El Chichon
Scientific American **250**,34-43

102. Redkar R.T. (1977)

Scientific Ballooning in India
Space Research (COSPAR) **XVII**,779-793

103. Reif F. (1965)
Fundamentals of Statistical and Thermal Physics.
(McGraw Hill)

104. Reiter R. (1972)
Case Study concerning the Impact of Solar Activity upon Potential Gradients and Air-Earth Currents in the Lower Troposphere
PAGEOPH **94**,218

105. Rishbeth H. and O.K.Garriott (1969)
Introduction to Ionosphere Physics
(Academic Press)

106. Rosen J.M. (1969)
Stratospheric Dust and its Relationship to Meteoric Influx
Space Sci.Rev. **9**,58-59

107. Rosen J.M. and D.J.Hofmann (1981A)
Balloon-Borne measurements of Electrical Conductivity, Mobility and the Recombination Coefficient
J.Geophys.Res. **86**,7406-7410

108. Rosen J.M. and D.J.Hofmann (1981B)
Balloon-Borne Measurements of the Small Ion Concentration
J.Geophys.Res. **86**,7399-7405

109. Rosen J.M. et al. (1982)
Results of an International Workshop on Atmospheric Measurements
J.Geophys.Res. **87**,1219-1227

110. Rosen J.M.,D.J.Hofmann and W.Gringel (1985)
Measurement of Ion Mobility to 30 km
J.Geophys.Res. **90**,5876-5884

111. Sasi M.N. and K.Sengupta (1979)
A model Equatorial Atmosphere over the Indian Zone from 0 to 80 km
ISRO Scientific Report (ISRO-VSSC-SR-19-79)

112. Satyanarayana M.et al. (1987)
Study of Altitude Profiles of Atmospheric Extinction using a Pulsed Lidar
NSSS-87 Abstracts (Paper MAR-2) 234-235

113. Schlager H. and F.Arnold (1987)
Balloon-Borne Composition Measurements of Stratospheric Negative Ions and Inferred Sulfuric Acid Vapor Abundances during the MAP/GLOBUS 1983 Campaign

Planet.Spa.Sci. 35,693-701

114. Slamanig H. (1981)
Messung Elektrischer Felder in der Stratosphare
University of Graz Technical Note (INW-8017)

115. Smith D. and M.J.Church (1977)
Ion-ion recombinationrates in the Earth's Atmosphere
Planet.Space Sci. 25,433-439

116. Smith D. et al. (1981)
Ion-Ion Mutual Neutralization and Ion-Neutral Switching Reactions of some Stratospheric Ions
Planet.Spa.Sci. 29,449-454

117. Smith D. and N.G.Adams (1982)
Ionic Recombination in the Stratosphere
Geophys.Res.Lett. 9,1085-1087

118. Smith L.G. (1969)
Langmuir Probes in the Ionosphere
Small Rockets Instrumentation Techniques 1-15

119. Somayajulu Y.V. et al. (1971)
Some preliminary results of rocket sounding of the D region at the geomagnetic equator
Space Res. (COSPAR) XI,1131-1137

120. Somayajulu Y.V. et al. (1982)
D Region electron loss coefficients during Solar Eclipse of 16 February 1980
Proc.Ind.Nat.Sci.Acad. 48A,511-517

121. Son Jamie S. and T.J.Hanratty (1969)
Numerical Solution for the flow around a cylinder at Reynold's Numbers 40,200 and 500
J.Fluid Mech. 35,369-386

122. Spencer N.W. et al. (1962)
Electron Temperature Evidence for Non-Thermal Equilibrium in the Ionosphere
J.Geophys.Res. 67,157-175

123. Stergis C.G.,G.C.Rein and T.Kangas (1957)
Electric Field Measurements above Thunderstorms
J.Atmos.Terrest.Phys. 11,83-90

124. Subbaraya B.H.,S.Prakash and S.P.Gupta (1983)
Electron Densities in the equatorial lower ionosphere from the Langmuir Probe experiments conducted at Thumba during the year 1966-1978
ISRO Scientific Report (ISRO-PRL-SR-15-83)

125. Subbaraya B.H.,S.Prakash and S.P.Gupta (1985)
Structure of the equatorial Lower Ionosphere from the

Thumba Langmuir Probe experiments
Adv.Spa.Res. 5.7,35-38

126. Subbaraya B.H. and A.Jayraman (1987)
The Vertical Distribution of Ozone in the Equatorial Zone
Adv.Space Res. 7,(In Press)

127. Takagi M. and Y.Morita (1980)
Evaluation of Aerosol effect on electrical conductivity in the lower stratosphere
J.Geomag.Geoelectr. **32**,671-681

128. Turco R.P.,R.C.Whitten and O.B.Toon (1982)
Stratospheric Aerosols:Observation and theory
Rev.Geophys.Spa.Phys. **20**,233-279

129. Twomey S. (1977)
Atmospheric Aerosols

130. Tzur I. and R.G.Roble (1984)
Ambipolar Diffusion in the Middle Atmosphere
J.Geophys.Res. **89**,338-344

131. U.S.Standard Atmosphere (1962)

132. Velinov P. (1968)
On Ionisation in the Ionospheric D Region by Galactic and Solar Cosmic Rays
J.Atmos.Terrest.Phys. 30,1891-1905

133. Verma S.D. and Bhatnagar S.P. (1987)
Flux and Energy Spectrum of Relativistic Albedo Electrons at Balloon Altitude and their contribution to Ion Production Rate
20th ICRC (Mosco)Abstr. ,253-254

134. Verma S.D. and Kothari (1987)
Flux and Energy Spectrum of Albedo Protons in Low Latitude Region and the Ion Production rate in the Middle Atmosphere
20th ICRC (Mosco)Abstr. ,251-252

135. Viggiano et al. (1982)
Stratospheric negative ion reaction rates with H2S04
J.Geophys.Res. **87**,7340-7342

136. Volland H. (1984)
Atmospheric Electrodynamics
(Springer Verlag)

137. Whipple F.J. (1929)
Quart.J.Roy.Meteor.Soc 55,1

138. Whitten R.C. and I.G.Popoff (1965)

Physics of the Lower Ionosphere
(Prentice Hall)

139. Wigand A. (1914)
Measurement of the Electrical Conductivity in the Free Atmosphere upto 9000 meters in height
Terrest.Magn.Atmos.El. **19**,93-101

140. Wilson C.T.R. (1920)
Investigations on Lightning Discharges and on Electric field of Thunderstorms
Phil.Trans.Roy.Soc.Lon **A221**,73-125

141. Woessner R.H.,W.E.Cobb and Ross Gunn (1958)
Simultaneous Measurements of the Positive and Negative Light Ion Conductivities to 26 km
J.Geophys.Res. 63,171-180

142. York T.M. et al. (1982)
Evaluation of Electron and Ion Densities in the Middle Atmosphere from Rocket Borne Blunt Probes
J.Atmos.Terrest.Phys **44**,257-266